

NASA-CR-194865

FINAL REPORT
Covering the Period February 1, 1990 to January 31, 1994
NASA Grant NAG6-1

Theory, Image Simulation and Data Analysis
of Chemical Release Experiments

by

Eugene M. Wescott, Principal Investigator
Geophysical Institute
University of Alaska Fairbanks
Fairbanks AK, 99775-7320

April 26, 1994

Prepared for

Goddard Space Flight Center
Wallops Flight Facility
Wallops Island, Virginia 23337

(NASA-CR-194865) THEORY, IMAGE
SIMULATION, AND DATA ANALYSIS OF
CHEMICAL RELEASE EXPERIMENTS Final
Report, 1 Feb. 1990 - 31 Jan. 1994
(Alaska Univ.) 70 p

N94-31101
--THRU--
N94-31102
Unclas

G3/93 0004571

ORIGINAL CONTAINS
COLOR ILLUSTRATIONS

ABSTRACT

The final phase of Grant NAG6-1 involved analysis of physics of chemical releases in the upper atmosphere and analysis of data obtained on previous NASA sponsored chemical release rocket experiments. Several lines of investigation of past chemical release experiments and computer simulations have been proceeding in parallel.

This report summarizes the work performed and the resulting publications.

PAPER: SR 90, STRONTIUM SHAPED-CHARGE CRITICAL IONIZATION VELOCITY EXPERIMENT BY E. M. WESCOTT, H. C. STENBAEK-NIELSEN, D. W. SWIFT AND A. VALENZUELA.

This paper on the results of the strontium shaped charge experiment (TNT 38.008UE) carried out from Wallops Island May 13, 1986, was revised to meet comments of reviewers. The paper was accepted and was published in the Journal of Geophysical Research December 1, 1990. Due to the optical imaging equipment limitations, we could only observe Sr ions due to solar UV ionization in the slow part of the jet. However, the recent (September 10, 1990) successful Sr critical velocity experiment we carried out from the CRRES satellite verified CIV ionization from fast neutral Sr gas in the darkness.

ANALYSIS OF 1987 GREENLAND ROCKET EXPERIMENTS

The analysis of the optical results from Terrier Malemute 29.025 UE flight from Greenland is now complete. The three Ba releases occurred in the central polar cap in conjunction with the AFGL payload A21.428 to investigate the electric fields parallel and perpendicular to sub-visual, sun-aligned polar cap auroral arcs. The Terrier-Malemute flew high and short, and did not overfly the intended target. However, it did release Ba in sub-visual auroral patch.

The AFGL rocket which flew a few minutes after 29.025 UE did not fly over the intended aurora either, but we have made some comparisons with some of the instrumented data on that flight.

The analysis of the motion of the three Ba ion streak shows some very interesting results. The motion of the ions up the field lines showed evidence for down-directed parallel to B electric fields on two of the three plasma jets of 5 and 8 micro volts/m, on the second and third release respectively. The first release which was furthest from the sub-visual arc showed no evidence of a parallel field. We have not been able to obtain any interplanetary magnetic field data to correlate these electric fields with the typical average parallel current patterns inferred from satellite measurements by Lijima and others. We have contacted Russian colleagues also, and have come to the conclusion that no data exist.

The convection of the three streaks proceeded SW across the polar cap almost directly anti-sunward until they neared the auroral oval, where vortex-like motion was observed.

Essentially, all of the analysis has been completed and figures drafted. We intended to publish what we have, but a very extensive analysis was also done at Rice University by L. Weiss which included the cross field convection as analyzed by I.S. Mikkelsen. We decided to join in that paper which was published in 1993 as part of an AGU Geophysical Monograph 80.

The second University of Alaska Greenland rocket Terrier-Malemute 29.026 UE, also with three Ba shaped charges, was flown in conjunction with TNT 38.01 UE, an instrumented rocket (Baker). Due to moonrise at the planned dusk side launch window, the rockets were dawn side launches, where it is very difficult to distinguish sun-aligned polar arcs from the auroral oval. The Ba streaks convected into an intense auroral breakup, and therefore, was not really a polar cap experiment. Only very preliminary analysis was done on these data which do not seem to warrant publication.

CALCULATED EMISSIONS RATES FOR BARIUM, STRONTIUM AND CALCIUM

Theoretical emissions rates for barium were calculated by Stenbaek-Nielsen (*Planetary Space Science*, 37, 1441, 1989). The solar spectrum has deep Fraunhofer absorption lines at the barium ion resonances, and therefore a velocity component towards or away from the sun may Doppler shift the emission lines out of the solar absorption lines. The result is that the emission rates are highly velocity-dependent. It was proposed to extend this work in preparation for CRRES to also cover strontium and calcium, and to investigate the effects near the release when the cloud is optically thick.

In principle, the calculation for strontium and calcium is straightforward following the methods used for the barium calculation. However, while the transitions involved are known, the relevant spectroscopic parameters needed for the calculation are not. An extensive literature search has been performed with largely negative results. It may be possible to calculate theoretical transition parameters, but the uncertainty of such numbers are very large and the result may be little better than the emissions rates presently in use. The emission rates were of high importance for the analysis of the CRRES releases (where we did observe both strontium and calcium ions). Based upon spectrograph measurements of barium releases from CRRES we did further analysis of the Ba⁺ emission rates, and published the results: Stenbaek-Nielsen, H.C., E.M. Wescott, and T.J. Hallinan, Observed barium emission rates, *J. Geophys. Res.*, 98(A10) 17,501-17,516, 1993.

One of our two graduate students, Don Hampton, is doing a Ph.D. thesis based in part upon the rocket and CRRES results.

COLLISIONAL IONIZATION CROSS SECTION FOR BARIUM

The CRIT-I critical velocity ionization experiment (BBX 35.014UE) took place from Wallops Island, at dawn on May 13, 1986. Ions were observed, but during the subsequent analysis it became apparent that these ions all could be explained as resulting from collisions between barium atoms in the fast jet and the neutral atmosphere. A manuscript, describing the results, was submitted to the *Journal of Geophysical Research* in 1989. We proposed, as part of the work on this grant, to refine the cross section for collisional ionization of barium. This was to be accomplished, in part, by an improved analysis of the CRIT-I images and, in part, by searching the literature for relevant information.

This proposed effort was done and the JGR manuscript was updated accordingly before it appeared in print in June 1990 (H. C. Stenbaek-Nielsen, E. M. Wescott, D. Rees, A. Valenzuela and N. Brenning, Non-solar UV produced ions observed optically from the "CRIT-I" critical velocity ionization experiment, *J. Geophys. Res.*, 95, 7749, 1990). The effort consisted of the development of a more realistic model of the solar illumination near the terminator and a more complete literature search. In the improved model, the illumination of the ion cloud is calculated assuming a 0.5 degree solar disk shining through the 1965 U.S. Standard Atmosphere with an extinction rate of 0.28 at 4554A. The cross section derived and the modelling were used for the analysis of the images from CRIT-II (BBX 35.019 UE). We also participated in another CRIT-I paper by Brenning et al. 1991. See Appendix d.

CRIT-II

The CRIT-II experiment, (BBX 35.019 UE) was carried out from Wallops at dusk on May 4, 1989. The experiment was released into an ionosphere with a background ionization of $5 \times 10^5/\text{cm}^3$ in contrast to the CRIT-I experiment in which the background ionization was very low, and a well defined ion cloud was observed. The maximum brightness of the ion cloud was 750R. Analysis of the images obtained indicate an ionization rate of 0.8% per second (125 second ionization time constant) which is larger than what can be accounted for by collisional ionization. We concluded that the ionization is due to the presence of a critical ionization velocity (CIV)

process. The ionization falls off with increasing distance along the neutral jet reaching levels expected from ionization due to collisions with the ambient atmosphere about 50 km from the release. Thus, the CIV process is present over a distance of about 50 km which is significantly greater than allowed for by current theories. A paper, "Optical Observations on the CRIT-II Critical Ionization Velocity Experiment," by H. C. Stenbaek-Nielsen, E. M. Wescott, G. Haerendel and A. Valenzuela, outlines the analysis. It appeared in the September 1990 issue of Geophysical Research Letters.

The CRIT-II release was about 100 km below the terminator and thus, there should be no solar UV ionization or solar fluorescence. Consequently, we did not expect to see anything in the release region. However, ion emissions were detected from the region of the fast neutral jet. Emissions were also seen from the slow (v less than critical) barium cloud which would indicate that the emissions may not be from ions created directly by the CIV process. There must, nevertheless, be a connection since we did not see a similar signature in the CRIT-I releases. We also saw emissions in the dark below the solar terminator from the CRRES CIV releases of Ba, Sr, and Ca in the south Pacific. The analysis of the CRRES experiments published in the *J. Geophysical Research*, 99(A2), 2145-2158, 1994 also explains the CRIT II results.

CALIBRATION OF IMAGES USING BACKGROUND STARS

Although our imagers are intensity-calibrated in the laboratory, we often are observing under less than ideal conditions. Haze or cirrus clouds may be present which will degrade the images. To help in assessing the degree to which atmospheric conditions affect the data, we are using the stars in the background to provide a calibration. Each star in the image is identified and the spectral type can be associated with a temperature (for example, Allen, Astrophysical Quantities). Given the stellar magnitude and temperature, the photon flux available to the camera can be calculated (assuming black body radiation) and the comparison with the observed signal provides the calibration. Since the starlight has the same path through the atmosphere and the optics as the light from the release clouds, this intensity calibration will automatically correct for atmospheric absorption.

We have used this method for several years, but with varying success. While the ratio of observed to calculated star fluxes in some images is nearly constant, thus providing a very well defined calibration, that is not always the case. There have been images in which the ratios would vary by more than a factor of 10, making the method useless. We are uncertain of the cause of the problem.

We do note that there are many stars for which the spectra are well known and thus, could be used. However, they are rarely in the field-of-view, and since atmospheric transmission can vary significantly in time and across the sky, it may not be all that useful to observe a given star at the start of the observations. We would like use the star field in the actual image under analysis.

During 1990, a student employed for the summer worked on the problem. A star catalog with high resolution spectra on the main types of stars was installed on the computer and used to calculate photon fluxes. The result was a significant improvement in the scatter on the derived calibration. We had planned to continue the work using a larger catalog which has color indices for 248,000 stars (covering essentially all the stars we would normally observe), but the student left before this could be accomplished. It is highly desirable to continue this work, especially in light of the data expected from the CRRES mission. We continued the work to refine intensity calibration methods using the stars present in the observed images. The 248,000 star catalog with color indices was installed in the computer and used for calibration. This establishes a reliable method for calibrating images using the stars.

RAPID RAY MOTIONS IN IONOSPHERIC BARIUM PLASMA CLOUDS

Barium plasma clouds released at high latitudes characteristically become striated with many field-aligned rays. The rays which often resemble auroral features usually drift as a whole with the $E \times B/B^2$ drift of the cloud and alter position only slowly (order of tens of seconds). On

two evenings in 1968, in releases from Andøya, Norway, anomalous field-aligned brightenings or emission enhancements of up to 3x were observed to move rapidly (10-20 km/sec) through three different Ba⁺ clouds. Similar effects were observed in Ba⁺ clouds released from rockets launched from Poker Flat, Alaska: On Mar 21, 1973 in two Ba thermite releases and on Mar. 22, 1980 in the Ba shaped charge experiment "Miss Peggy". On these occasions, auroras on or near the Ba⁺ L shell, also exhibited active rapid ray motions. This leads us to the assumption that the two phenomena are related and the expectation that an explanation of the rapid ray motions in the Ba⁺ clouds would lead to a better understanding of the physics of auroral ray motions and the auroral ionosphere.

Seven possible mechanisms to produce the observed moving emission enhancements are discussed. Direct excitation by energetic electron bombardment is ruled out on the basis of energy fluxes required for realistic cross sections. Direct motion of an isolated Ba⁺ ray past the other rays by $E \times B/B^2$ motion seems very unlikely due to the observed variations in the enhancements and the large E field required (> 500 mV/m). Compressional waves do not seem to be of sufficient amplitude or velocity. Formation of folds or curls in a sheet beam instability require moving radial fields of 500 mV/m, but would explain the auroral features as well as the Ba⁺ by the same mechanism. Qualitatively the redistribution of Ba ions as a flux tube encounters a higher electron density in the ionosphere may result in enhancements. Absorption or radiation of Doppler shifted Ba⁺ emissions by ions gyrating or moving at a few km/s seems to be the most promising mechanism for producing the enhancements. The observations provide compelling evidence for the existence of transient electric fields of order 100 mV/m at altitudes as low as 200 km during active aurora with rapid ray motions. The affected regions have dimensions of order a few km across-B and move eastward at 10-20 km/sec.

We completed the analysis and published a paper: Wescott, E.M., T.J. Hallinan, H.C. Stenbaek-Nielsen, D.W. Swift and D.D. Wallis, Rapid ray motions in barium plasma clouds and auroras, *J. Geophys. Res.*, 98(A3), 3711-3724, 1993.

35.019 UE, NOONCUSP EXPERIMENTS: ELECTRODYNAMICS, AURORAS, PARTICLE PRECIPITATION AND FIELDS IN THE POLAR CUSP NEAR SVALBARD

One magnetospheric feature of growing scientific interest in solar-terrestrial relationships is the magnetospheric cusp/clefts. There is one in each hemisphere on the sunward side, where field lines forming the boundary regions separate. Those forming the boundary of the magnetospheric tail go in the anti-solar direction over the poles, while those forming the sunward magnetospheric boundary close on the dayside. Solar wind particle and field transport to the ionosphere is thought to be essentially direct in the cusp region. The low-altitude region where the cusp/cleft field lines intersect the ionosphere, though of limited spatial extent, is perhaps among the more intriguing places in the solar wind-magnetosphere-ionosphere system, since there a host of plasma-physics problems awaits solution.

There has been much controversy over the definition and use of the terms cleft and cusp. Heikkila (1985) has provided a definition based on the consensus of a Cusp NATO Advanced workshop, at Lillehammer, Norway.

"The cleft is the low altitude region around noon of about 100 eV electron precipitation associated with 6300Å emission, but containing also structured features of higher energy. The cusp is a more localized region near noon within the cleft characterized by low energy precipitation only, having no discrete auroral arcs, but often displaying regular behavior, presumably associated with the magnetic cusp."

Holtet and Egeland (1985) suggest "that the upper atmosphere at high latitudes is called the Earth's window to outer space." Through various electrodynamic coupling processes as well as through direct transfer of particles, many geophysical effects displayed there are direct manifestations of phenomena occurring in deep space. The cleft/cusp region connects to a vast portion of the earth's magnetic field envelope. The electrons from the magnetosheath have direct access to the upper atmosphere in the limited cusp region. The electrons precipitating just equatorward of the direct access electrons have some characteristics in common with electrons

observed in the boundary layer of the low latitude magnetopause but also show the signature of acceleration, probably occurring at low altitudes (Johnstone, 1985).

Because the cleft regions occur on the dayside of the polar cap, the visual optical emissions associated with precipitating particles can only be observed from the ground or aircraft in the appropriate winter season, and from appropriate geophysical locations. Due to the separation of the geographic and geomagnetic poles, the sites where the cleft regions can be viewed in maximum solar depression angle conditions are at the South Pole Station, Antarctica, and at Svalbard, Norway. Eather (1985) has reviewed data sets of cusp position (latitude) vs. AE index and Bz, and found support for the view that the position is most closely related to AE with little dependence on Bz.

There are several optical observatories in Svalbard: Ny Ålesund, Longyearbyen, Barentsburg and Hornsund, which can observe the auroral emissions for 24 hours in mid-winter to determine the time, spatial, and wavelength variations of the high latitude auroras. The general pattern of auroral emission agrees in general with the particle emissions. Near local noon 6300Å emissions from soft electrons are enhanced and other auroral emissions from hard electrons are reduced with respect to the rest of the auroral oval. The actual small cusp region may be very much reduced in hard electron emissions. Meridian scanning photometers have shown evidence of auroral bands "breaking off" from the cleft region and convecting polewards into the polar cap, which have been cited as evidence of FTEs (Sandholt et al., 1986). Typically, these emissions last for only 5-10 minutes. Such features are practically ready-made for sounding rocket observations as such flights are typically of 5-10 minutes in duration.

Lockwood et al. (1989) have combined optical measurements from Svalbard with EISCAT radar convection measurements to show that the "midday-auroral breakup" phenomenon is associated with major increases in ionospheric flow. Optical structures move westward (under positive Bz) before moving polewards. "The potentials observed across the radar field of view are comparable with that expected across the entire polar cap."

Another feature of the cusp/cleft region is the inferred flow of O⁺ ions from the ionosphere into the mantle. The morphology of upward ion jets (beams) and conics has been well covered by the work on data from ISIS2, DE-1 and other "high" altitude satellites (Gheilmetti et al., 1978; Greenwald, 1982; Kaufman, 1984; Kinter et al., 1979; Klumper, 1979; Lockwood and Titheridge, 1982; Sharp et al., 1977; Horwitz et al., 1985; Horwitz and Lockwood, 1985; and Lockwood et al., 1985).

The cusp region, in recent years, has been the subject of a number of studies from satellites (Menietti and Burch, 1988; Newell and Meng, 1988). However, the detailed observations afforded by sounding rockets have been few. Instrumentation has made great strides over the past decade and consequently the level of fine detail that can be resolved has also greatly improved. This is especially true of sounding rockets, which, due to much lower velocities than satellites, afford the opportunity to study, in depth, the space plasma physics of the regions they traverse. The cusp, with its great variety of phenomena ranging from ion injection signatures to "turbulent" convection electric field regions, is an ideal region for such sounding rocket studies.

Barium plasma injection experiments in the polar cleft/cusp region can offer some advantages over other measurements of electric field and convection. The upfield traveling plasma jet, and ion debris cloud drifting at ionospheric heights, can be tracked for tens of minutes to give E_⊥ and E_∥ out to tens of thousands of km over that time.

In past campaigns we have launched barium plasma injection payloads from Cape Parry, N.W.T., and recently from Sondrestrom fjord, Greenland, and Andenes, Norway, to study the electric fields in the cleft and polar cap regions. Cape Parry is not an ideal site because in December-January the maximum solar depression angle is only near 6° at the time of the cleft passage. Despite the difficulty in making optical observations of auroral emissions, significant scientific results were obtained from two experiments, TORDO I AND 11 (Jeffries et al., 1975 and Wescott et al., 1978). The location of the cleft was determined primarily from a pair of ionosondes operated by us at Cape Parry and Sachs Harbor, N.W.T. Wescott et al. (1978) reported on the TORDO 1 experiment in which the barium was immediately convected away from the cleft in an

anti-sunward direction clear across the polar cap to near the nightside auroral oval. An interesting field-aligned acceleration was also observed; it apparently was not related to any discrete aurora beneath. The barium was observed out to near 50,000 km altitude, with an energy gain of probably several hundred eV. Haerendel et al. (1976) have reported electrostatic acceleration of barium plasma in the polar cap, and Heppner (1979) reported that the four Cameo barium releases from satellite orbit in the polar cap, two experienced anomalous acceleration upwards. Heppner proposed that such parallel electric fields are characteristics of the polar cap.

On December 17, 1988 we carried out several experiments called NOONCUSP from Black Brant X rocket 35.024UE launched from Andøya, Norway, over the vicinity of Svalbard. The concept was to detonate three barium shaped charges: one south of the cusp; one polewards of the cusp; and the third in the cusp by ground command when Don McEwen's on board low energy particle spectrometer indicated the payload was in the cusp. The particles and field experiments carried were: Don McEwen's, University of Saskatchewan, low energy spectrometer; three axis magnetometer by Fritz Primdahl of the Danish Space Research Institute and Aarne Ranta of the Geophysical Observatory Sodankylä, Finland; high energy particle and x-ray detectors by Johan Stadsnes and Finn Søråas, University of Bergen, Norway.

Because of weight limitations, and the requirement to place the shaped charges straddling the cusp at minimum 450 km altitude, a number of compromises had to be made: 1) There was no attitude control system, so the nominal axis of the Ba jets would be close to 45° to the magnetic field; 2) The detonation of the ground command shaped charge destroyed the instrumental payload since it was not possible to separate it from the payload; 3) We could not afford the weight of E-field booms; and 4) finally in the late stages of payload construction, we had to remove one shaped charge to achieve a satisfactory trajectory.

The decision to launch 34.024 UE was based primarily on meridian scanning photometer data from our observatory at Longyearbyen. December 17 was almost the last day of the window, and optical coverage was limited to Longyearbyen, Svalbard, and the USSR station at Barentsburg, Svalbard. The auroral conditions were unusual in that the cusp and a discrete red aurora were very far south, Kp was 5 and there was 1400 nT negative bay in H at College. Fig. 2 shows the meridian scanning photometer plots (180° scans vs. time) from Longyearbyen, with the ratio of $6300\text{\AA}/5577\text{\AA}$. The red arc shows clearly at $20\text{-}21^\circ$ elevation angle near the south horizon.

McEwen's suprathermal electron analyser (SEA 1-430 eV) was turned on at T + 130 sec, but no electron fluxes were observed until about 168 sec when the edge of the cusp was encountered. From 168 sec until 175 sec, electrons of ~ 100 eV were detected, which probably corresponds to the red aurora recorded by the MSP. (Figure 3), as projecting around on 68° corrected magnetic latitude comes near the electron precipitation region. A second 10 s period of energetic electrons up to and beyond 400 eV was detected from T + 168 to T + 175.

The first shaped charge, ALPHA, attached to the payload, was protected from premature detonation by a timer enable switch set for T+308 sec. This would normally have been far south of the cusp. In order to have the detonation in the cusp when it was so far south on the 17th, we raised the launcher setting of 73 QE to 76 QE, and moved the azimuth toward the east to enable us to intercept the red aurora at the detonate enable time. However, the actual flight was lower than the original nominal at 72 QE. As a result the first detonation was polewards of the cusp in the polar cap even though at T + 324 sec the soft particle spectrometer was still measuring soft electron fluxes of about 50 eV suggesting that the shaped charge was still in the cusp. Also, because of the low trajectory the angle between the jet and B was about 50° . Consequently, the ion jet was diffuse and only visible for a few minutes. No jet at all was observed from the second detonation which was near 426 km altitude, and perhaps at a greater angle to B.

Analysis of the motion of the barium shows anti-sunward convection across the polar cap, with an average velocity of 480 m/sec.

From 0 UT to 6 UT the IMF from IMP-8 had a north Bz and negative By. At 06 the field changed to south Bz and positive By, which was the situation until 12 when another transition to north Bz occurred.

The NOONCUSP payload contained a supra thermal electron analyser (SEA) provided by

D. McEwen of Saskatoon. It had two functions:

- To examine in detail the low energy electron flux across the mid-day cusp.
- To monitor in real time the progress of the rocket across the cusp and to remotely command the detonation of the first barium release in the region of precipitation.

The SEA scanned an energy range from 0.5 to 430 eV in 64 steps with an energy resolution of 0.13 and at a rate of 8 scans/s. Its field of view was $10 \times 60^\circ$. Its orientation on the payload covered magnetic pitch angles from approximately 0 to 90° in the course of each spin.

Data were obtained from T+130s, when the high voltage was turned on, to T+324s when the Ba shaped charge on board was detonated. We measured integrated electron flux (0-430 eV) from high voltage turn on at 1103:10 to 1105:23 UT in ergs/cm²s. Each point is the average of five successive electron spectra, and thus integrated over 0 to 90° pitch angle. A soft photoelectron flux was recorded until 1103:50 when the rocket appeared to cross the equatorward boundary of the cusp and more energetic electrons were observed. There was a major burst of electrons around 1105 UT (73.5° latitude, 70.5° Λ) near the poleward edge of the cusp where the total electron flux reached 0.88 ergs/cm²s. At about 1105: (74^o lat.) more energetic electrons were observed. This is interpreted as polar rain within the polar cap.

This paper is still in preparation as contributions and correlations between the Svalbard meridian scanning photometer and the particle precipitation data are needed to make a publishable paper. The experiment occurred during an active substorm period, and the integrated analysis of all the data will hopefully be published in the near future.

GRADUATE STUDENT STUDIES

Two graduate students have been supported in part by NASA Grant NAG6-1. Mr. Don Hampton finished his MS degree thesis based upon observations made during the NOONCUSP experiment 35.019 UE. His thesis is listed below. He is continuing towards a Ph.D. degree involving critical velocity ionization. Mr. Peter Delamere is also working towards a Ph.D. with a thesis topic involving chemical release effects.

PUBLISHED PAPERS

Stenbaek-Nielsen, H. C., E.M. Wescott, D. Rees, A. Valenzuela, and N. Brenning, Non-solar produced ions observed optically from the CRIT I critical velocity ionization experiment, *J. Geophys. Res.*, 95(A6), 7749-7757, 1990. Appendix a.

Wescott, E. M., H.C. Stenbaek-Nielsen, D.W. Swift, A. Valenzuela and D. Rees, Sr90, Strontium shaped-charge critical ionization velocity experiment, *J. Geophys. Res.*, 95(A6), 21,069-21,075, 1990. Appendix b.

Stenbaek-Nielsen, H. C., E.M. Wescott, G. Haerendel and A. Valenzuela, Optical observations on the CRIT-II critical ionization velocity experiment, *Geophys. Res. Lett.*, 17(10), 1601-1604, 1990. Appendix c.

Brenning, N., C.-G. Fälthammar, G. Haerendel, M.C. Kelley, G. Marklund, R. Pfaff, J. Providakes, H.C. Stenbaek-Nielsen, C. Swenson, R. Torbert, and E.M. Wescott, Interpretation of the electric fields measured in an ionospheric critical ionization velocity experiment, *J. Geophys. Res.*, 96(A6), 9719-9733, 1991. Appendix d.

Stenbaek-Nielsen, H.C. and E.M. Wescott, Resonance fluorescence of barium releases, Proceedings from the 19th Annual European Optical Meeting (A. Steen, ed.), Swedish Institute of Space Physics, Kiruna, Sweden, 1992, *IRF Scientific Report 209*, pp 292-297, November 1992 (Invited paper).

Wescott, E.M., T.J. Hallinan, H.C. Stenbaek-Nielsen, D.W. Swift and D.D. Wallis, Rapid ray motions in barium plasma clouds and auroras, *J. Geophys. Res.*, 98(A3), 3711-3724, 1993. Appendix e.

Weiss, L.A., E.J. Weber, P.H. Reiff, J.R. Sharber, J.D. Winningham, F. Primdahl, I.S. Mikkelsen, C. Seifring and E.M. Wescott, Convection and electrodynamic signatures in the vicinity of a sun-aligned arc: Results from the Polar Acceleration Regions and Convection Study (Polar ARCS), Auroral Plasma Dynamics, *Geophysical Monograph 80*, Published by the American Geophysical Union, p 69-80, 1993. Appendix f.

THESIS

D.L. Hampton, M.S. Thesis: A Search for Upflowing O^+ Using an Imaging Fabry-Perot Interferometer, 65 pages, December 1990.

Non-Solar UV Produced Ions Observed Optically From the "CRIT I" Critical Velocity Ionization Experiment

H. C. STENBAEK-NIELSEN,¹ E. M. WESCOTT,¹ D. REES,² A. VALENZUELA,³ AND N. BRENNING⁴

A critical velocity ionization experiment was carried out with a heavily instrumented rocket launched from Wallops Island at dawn on May 13, 1986. Two neutral barium beams were created by explosive shaped charges released from the rocket and detonated at 48° to B at altitudes near 400 km and below the solar UV cutoff. Critical velocity ionization was expected to form a detectable ion jet along the release field line, but instead an ion cloud of fairly uniform intensity was observed stretching from the release field line across to where the neutral barium jet reached sunlight. The process creating these ions must have been present from the time of the release and the efficiency is estimated to be equivalent to an ionization time constant of 1800 s. This ionization is most likely from collisions between the neutral barium jet and the ambient atmospheric oxygen, and if so, the cross section for collisional ionization is 9×10^{-18} cm². A critical velocity ionization process may have been present during the first few tenths of a second after release, but its efficiency cannot have exceeded an equivalent ionization time constant of about 1800 s.

INTRODUCTION

During the last years a number of experiments have been performed both in the laboratory and in space to explore the concept of a critical ionization velocity (CIV) proposed by *Alfvén* [1954] and *Alfvén and Arrhenius* [1975] as part of a theory for the formation of planetary systems. Recent reviews have been given by *Newell* [1985], *Lai and Murad* [1989], *Torbert* [1988 and 1990], and *Piel* [1990]. The ionization takes place through collective plasma processes with the energy provided by the neutrals moving across a magnetic field embedded in the background plasma. For the ionization process to take place the velocity of the neutrals must exceed the critical ionization velocity determined by the kinetic energy in the velocity component perpendicular to the magnetic field being equal to the ionization potential of the neutrals.

In this paper we report on the results of the optical observations from a CIV experiment with two barium shaped charge releases carried out before dawn on May 13, 1986, from Wallops Island. The experiment was a continuation of earlier CIV experiments [*Wescott et al.*, 1986a,b], but with much improved diagnostics on the rocket and the ejected subpayload. The barium vapor was created below the solar terminator to prevent photoionization. The *Alfvén* critical velocity ionization process was expected to ionize a fraction of the neutral barium, and those ions would be observed as they rose up the field lines into the sunlight about 40 to 50 km above the detonations.

First, the general geometry of the releases is given based on the optical observations and the instrumentation on the rocket. The remaining part of the paper covers the analysis of the optical data and the search for evidence of CIV ionization. The

experiment was designed with the expectation that ions would be created near the release by a relatively short lived critical velocity ionization process to form a field aligned jet along the release field line similar to the "Porcupine" experiment [*Haerendel*, 1982]. The "Porcupine" barium shaped charge experiment was carried out from Esrange, Sweden, on March 19, 1979, with injection about 100 km below the terminator and at a 28° angle to B. An approximately 15 km wide ion cloud was observed near the release field line. The source of these ions created below the terminator was attributed to a CIV process, and a recent reevaluation of the data indicates that the CIV ion cloud contained about 20% of the neutrals with velocities in excess of the critical ionization velocity [*G. Haerendel*, private communication, 1989].

However, in the experiment described here, no such ion jet was observed. Instead, an ion cloud of relatively uniform and low brightness, less than 100 R, was observed in the region above the solar terminator and between the release field line and the neutral barium jet. Since the neutral jet in this region was well below the terminator, these ions must have been produced by a process other than ionization by solar UV; further, the process must have been present continuously from the release.

To investigate the nature of this non-solar UV ion cloud, we present a computer simulation of the observations which shows that the number of ions produced followed:

$$N_i = N_{\text{neutral}} \times (1 - \exp^{-t/\tau})$$

with an ionization time constant, τ , of about 1800 s. The analysis can place an upper limit on the ion production rate from a CIV process in this experiment. Various sources for these ions are considered, and collisions between the neutral barium and the ambient atmosphere appears to be the most likely process, although a CIV process may be present near the release point. Assuming collisional ionization the analysis allows the ionization cross section to be calculated, which is an important piece of information for future release experiments.

OPTICAL OBSERVATIONS AND RELEASE GEOMETRY

The primary purpose for the optical observations was to obtain an inventory of both ions and neutrals in each barium injection and to obtain a differential velocity function of the CIV ions produced. To accomplish these goals three optical sites were located at Wallops Island, Virginia (37.861N, -75.457E), which is about 2 km from the launcher; Duck, North Carolina,

¹Geophysical Institute, University of Alaska Fairbanks.

²University College London.

³Max Planck Institute for Extraterrestrial Physics, Garching, FRG.

⁴Royal Institute of Technology, Stockholm, Sweden.

Copyright 1990 by the American Geophysical Union.

Paper number 90JA00107.
0148-0227/90/90JA-00107\$05.00

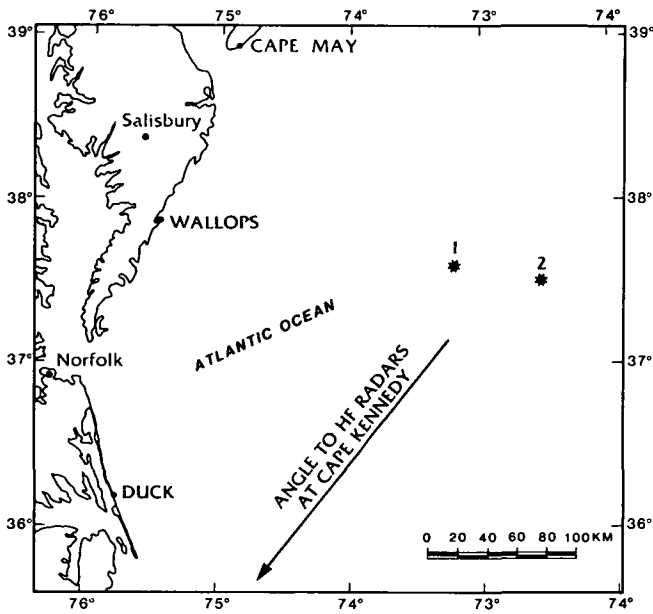


Fig. 1. Geographical positions of releases and main optical sites.

(36.182N, -75.751E); and Cape May, New Jersey (38.945N, -74.883E). At Wallops Island the University of Alaska and University College London operated 2 imaging photon detector (IPD) systems observing at the 5535 Å neutral barium and at the 4554 Å barium ion emission lines respectively. These lines are the dominant ion and neutral solar fluorescent emission lines. At Duck the University of Alaska operated an unfiltered intensified silicon intensifier target (ISIT) TV system and an intensified film camera observing in the 4554 Å barium ion line.

At Cape May the Max Planck Institute had a 1.8° field of view intensified secondary electron conduction (SEC) TV system filtered at 4554 Å and 5535 Å, a 5.6° field of view intensified change injection device (CID) TV system filtered at 4554 Å, and a larger field of view unfiltered TV system. In addition, Technologies Incorporated operated an ISIT TV camera and film cameras at the Air Force Geophysics Laboratory, Bedford, Massachusetts (42.45N, 71.27W). The location of the two barium releases and the three main optical sites are shown in Figure 1.

The experimental configuration chosen for the releases was detonation of the shaped charges upwards at an angle of 45° to the magnetic field direction and that the direction of the neutral jets be in the plane containing the magnetic field line and an HF radar site at Cape Kennedy and that the jet be directed away from the radar. The results of these requirements were neutral jets intended at an azimuth of 15° and an elevation of 64°.

One somewhat unfortunate consequence of this release geometry is that the neutral jet will go up, reaching sunlight at about the same time that the CIV ions would become visible. Figure 2 shows the look angles to the two releases from the three sites to illustrate this point. The heavy lines indicate the distance covered by neutrals and CIV ions at about 4 s when the neutral jet reaches the 19 km screening height above which the barium becomes optically detectable [Stenbaek-Nielsen *et al.*, 1984]. The screening height for the ionizing solar UV radiation (calculated below) is at about 34 km. When the neutral jet reaches this altitude it will ionize rapidly creating a bright ion cloud which might interfere with the observations of the CIV ions. To avoid interference, the intent was to keep this ion cloud outside the field of view of sensitive imagers, in particular the IPD observing in the ion line. A computer program using real time tracking radar data provided updates of look angles to the

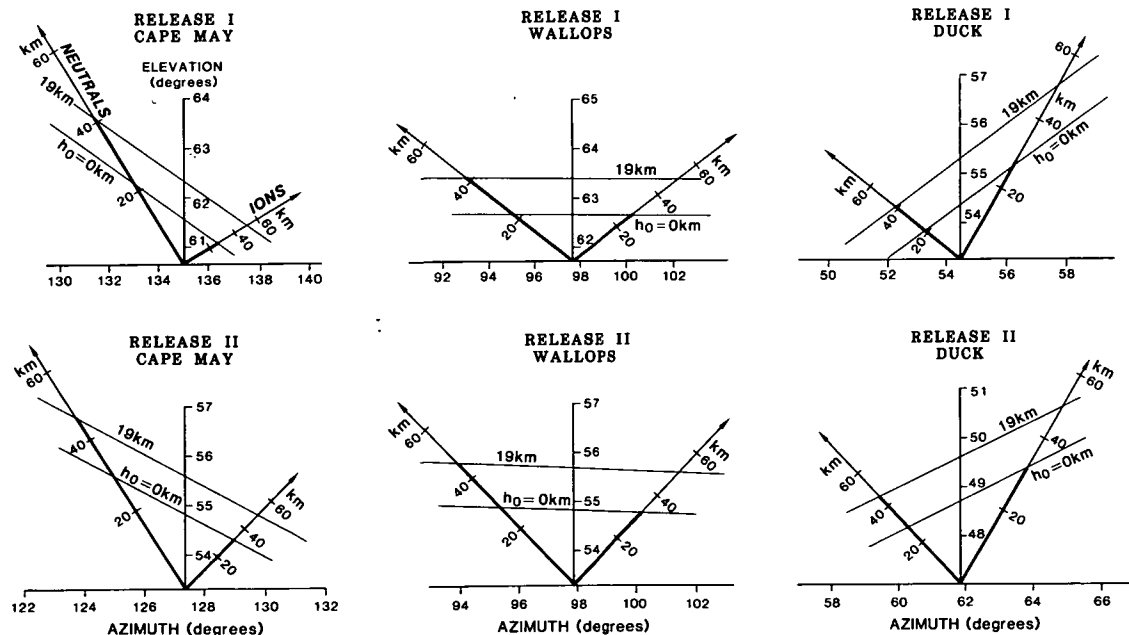


Fig. 2. Look angles to the two releases from the three optical sites. The neutral jet is going up towards the left and the magnetic field line to the right. The location of the geometrical terminator and the terminator corresponding to a screening height of 19 km above which the barium may be observed optically are shown. The heavy lines indicate that when the neutral jet reaches the 19 km screening height and becomes visible, ions created near the release will barely be at the geometric screening height.

releases. However, this was not entirely successful and only the ISIT TV cameras recorded both releases fully.

Various release parameters are listed in Table 1. These data are based on a best fit of the optical data and information from radar and telemetry. The magnetic field was calculated from the 1985 International Geomagnetic Reference Field [IGRF85] model of the Earth's internal field updated to the epoch of the experiment. The direction of the neutral jet was derived by triangulation and the direction is estimated to be accurate to within about a degree. The main payload was located a few km in front of the release and very near the center axis of the neutral jet. The subpayload was above and outside the jet, but the edge of the jet at cone angles of 15.8° of and 11.5° respectively for the two releases, cut across the field line through the payload about 1 km from the release and ions created there would reach the payload.

We assessed the performance of the two shaped charges. Since the releases were below the terminator, the data are not ideal for this assessment, but there is nothing in the optical data which indicates that the yield and jet velocities differed between the two releases. Further, the velocity distribution function and yield appear to be similar to that observed for the SR90 release (E. M. Wescott et al., SR90, strontium shaped-charge critical ionization velocity experiment, submitted to *Journal of Geophysical Research*, 1989) and reproduced here as Figure 3. The angular

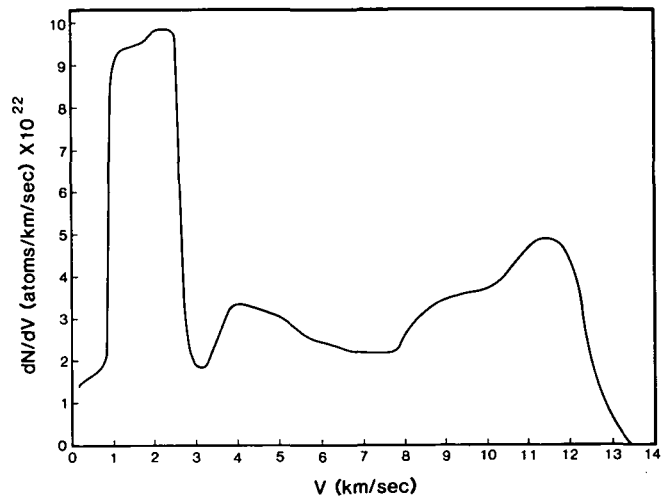


Fig. 3. Differential velocity distribution function as observed in the SR90 release (E. M. Wescott et al., SR90, strontium shaped-charge critical ionization velocity experiment, submitted to *Journal of Geophysical Research*, 1989). The ordinate scale is derived from the assumption that 15% of the barium liner is vaporized.

TABLE 1. Release Geometry for CRIT I Launched From Wallops Island on May 13, 1986

	Release 1	Release 2
Time (UT)	07:46:00	07:47:25
Latitude (N)	37.5983	37.5037
Longitude (E)	-73.2113	-72.5554
Altitude (km)	398.965	373.057
Magnetic field:		
B (nT)	43976.	44397.
Azimuth (°)	349.1	348.6
Elevation (°)	-66.8	-66.6
Direction to Sun:		
Azimuth (°)	44.9	45.8
Elevation (°)	-20.3	-19.8
Screening height (km)	-21.6	-25.5
Direction of neutral jet:		
Azimuth (°)	14.7	14.0
Elevation (°)	64.2	64.2
Direction of ion jet (-B):		
Azimuth (°)	169.1	168.6
Elevation (°)	66.8	66.6
Angle (°) between:		
Neutr. jet and ion jet	47.8	47.9
Neutr. jet and dir sun	87.7	87.5
Ion jet and dir Sun	148.2	149.1
Location of payloads:		
Main		
Latitude (N)	37.6051	37.5185
Longitude (E)	-73.2093	-72.5515
Altitude (km)	400.768	377.021
Dist. from burst (km)	1.987	4.344
Angle to jet (°)	1.2	1.7
Sub		
Latitude (N)	37.5962	37.5062
Longitude (E)	-73.2125	-72.5565
Altitude (km)	402.766	379.833
Dist. from burst (km)	3.811	6.783
Angle to jet (°)	29.7	23.4

Distances to sunlight are given in Figure 2.

distribution is nearly Gaussian with the half width, half maximum cone angle 6.6° for velocities above 7.0 km/s, 10-11° for velocities between 7.0 and 3.5 km/s, and 21-24° at the lowest velocities. The details of the distribution functions for the barium jet may differ from that of the SR90 release, but the observations of the major features (tip and peaks) in the barium jet are consistent with the SR90 release to better than a few tenths of km/s.

ATMOSPHERIC TRANSMISSION

For planning of the experiment and for data analysis it is important to know the brightness and the spectral content of the sunlight in the region of the releases. Above the geometric shadow height sunlight travels through varying parts of the atmosphere to the region of the release. The path may be characterized by the screening height defined as the height (km) of the lowest point on the ray path. The corresponding optical depth for a given wavelength can be calculated given the absorption cross section and an atmospheric model. For ionizing light (wavelengths shorter than 3266 Å) the effects of ozone, which strongly absorbs UV radiation, must also be included. Using the atmospheric model given in the U.S. Standard Atmosphere Supplements, U.S. Government Printing Office [1966], and atmospheric extinction rates [Guttman, 1968] plus ozone densities and absorption cross sections given by Banks and Kockarts [1973], attenuation as function of screening height was calculated for the dominant barium neutral and ion emission lines at 5535 Å and 4554 Å respectively, and for ionizing light at wavelengths less than 3265 Å. It should be noted that the ozone content of the atmosphere is highly varying and the extent to which the chosen model reflects the actual conditions at the time of the releases is uncertain.

Figure 4 shows the calculated relative intensities of the ionizing UV radiation, the 4554 Å barium ion emission and the 5535 Å barium neutral emission versus screening height. Considering only the absorption due to ozone, the maximum UV screening occurs at 18 km. Below 18 km absorption by the regular air-

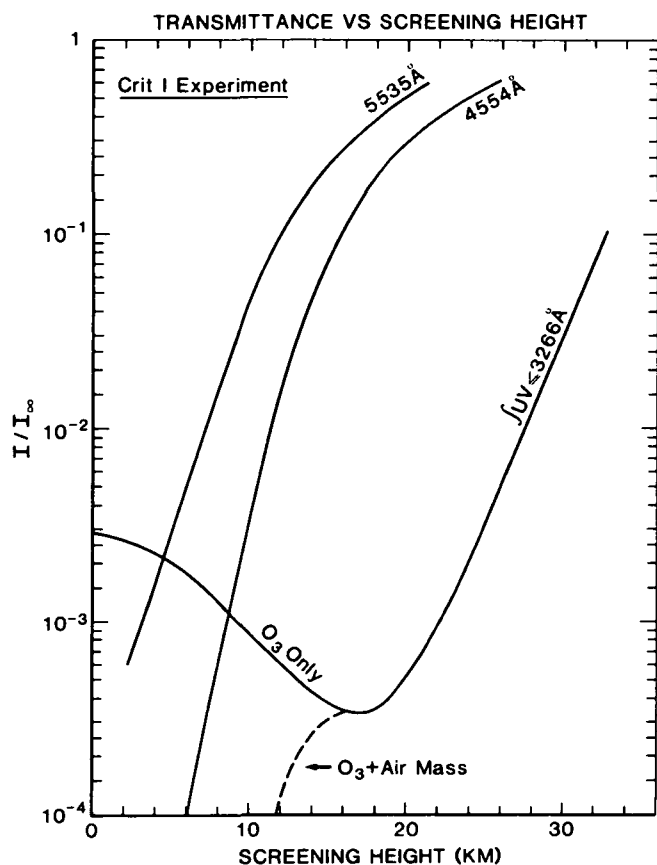


Fig. 4. Relative intensities of solar illumination at the releases at relevant wavelengths calculated as function of screening height.

mass dominates. The absorption of light at 4554 Å and at 5535 Å is much less than the absorption of the UV ionizing light. The limiting screening height depends on the brightness of the streak, but based on data from previous release experiments we can detect a barium streak above a screening height of about 19 km [Stenbaek-Nielsen *et al.*, 1984].

ISIT TV OBSERVATIONS

The ISIT TV system operated at Duck, North Carolina, observed both releases. It was operated unfiltered to obtain the best possible images from which the release position and the direction of the neutral jet and, if observable, the critical velocity ions. Even with the application of various image enhancing techniques there was no evidence of an ion streak along the burst field line.

The ISIT provided data with high time resolution throughout the experiment, and although the camera is less sensitive than the IPD which only provided data for 10 s on the first release, it was well pointed to observe ions along the release field line. An estimate of the sensitivity of the camera was made using the stars present in the data. The limiting star magnitude was about 8.0 which together with the spectral response function of the detector and the barium emission rates calculated by Stenbaek-Nielsen [1989] results in a minimum line of sight integrated (column) barium ion density of $5 \times 10^9/\text{cm}^2$. If the column density had been larger, the ion jet would have been observable in the ISIT TV camera images.

IPD ION OBSERVATIONS

The primary data for the analysis were obtained by an imaging photon detector system observing in the dominant barium ion line at 4554 Å and operated at a site near the launching complex at Wallops Island. The filter width was 28.8° FWHM with 60% peak transmission, sufficient to observe the emission line across the entire 10° field of view. The images were recorded digitally on a Compaq computer with 5 s integration time. The IPD processes the detected photons serially and the image is built up in computer memory. The upper limit on the number of photons that can be processed per second is near 100,000. At higher rates the detector may be damaged and an electronic switch turns the IPD off. We intended to position the cameras for optimum view of the release field line above the terminator. But real time update information about the trajectory was not received and the bright ion cloud created by photoionization when the neutral jet came up over the UV terminator appeared in the field of view. Two complete 5 s images were obtained before the detector turned off, but as luck would have it, the "wrong" pointing direction was almost perfect for the unexpected non-solar UV produced ion cloud that appeared.

The second release was observed from Wallops to take place embedded in a large diffuse ion cloud from the first release which effectively precluded the IPD from making useful observations.

The two IPD ion images obtained on the first release are of critical importance to the present study. The thermal emissions from the explosion were detected in the frame covering the release, but nothing else was seen in this frame, which covered the time period -2.0 s to +3.0 s from the release. In the next image, covering the time period 5.0 to 10.0 s from release, ions are present, but not as a well defined field aligned streak, as would have been expected from an efficient ionization process active during the first second or so after the release.

Since the burst frame did not show any barium ions it was used as representative of the sky background present and by subtracting that from the following image the background, including the stars, was eliminated. The resulting image, filtered to reduce the high frequency spatial noise, is shown in Figure 5.

To help in the interpretation of the image various lines have been inserted. The release location is identified by the cross at the bottom of the frame. The magnetic field line (IGRF85 updated to the epoch of the experiment) extends up to the right from the release point while the direction of the neutral jet is towards the upper left. The points along B and the neutral direction are at 10 km intervals. The top is delineated by the maximum distance a neutral or ion at 13.5 km/s, the tip of the jet, can reach in 10 s, and the bottom by the terminator at 19 km screening height.

The ions are in two parts: The very bright circular cloud in the left center part of the image is the cloud produced by photoionization and is of no interest to the present study. The second part is the faint cloud of fairly uniform intensity in the center of the image and within the shown delimiters. This cloud must have been produced from the neutral jet below the UV terminator. (The tendency of the ion cloud to be wider than indicated by the delimiters towards the left in the image is due to aspect: the ion cloud is viewed at an elevation angle of 67°, i.e. essentially from the underside. The delimiters are drawn in the plane of B and the jet, but the ions extend out to both sides of this plane because of the finite jet cone angle.)

The image was intensity calibrated based on the signal in the stars present and the measured characteristics of the interference

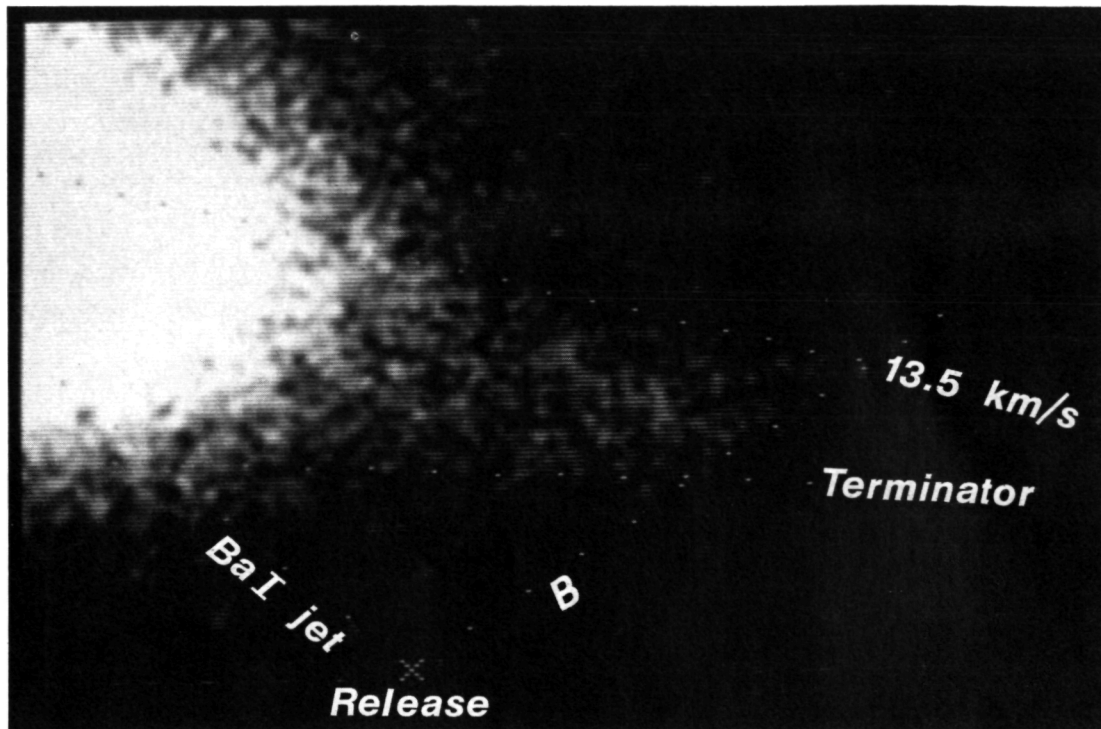


Fig. 5. IPD image of the first release observed in the 4554 Å barium ion line emission. The image is a 5 s exposure covering the time 5 to 10 s after release. The background has been subtracted and high frequency noise eliminated. The location of the release is at the bottom center of the image. The neutral jet was directed up towards the left and the direction of the magnetic field is up towards the right (marks at 10 km increments). The top delimiter is the maximum distance barium at 13.5 km/s can reach in 10 s, and the bottom is the terminator. The bright circular cloud dominating the image is from ions produced by solar UV illumination of the neutral jet. The faint cloud stretching right and slightly downwards from the bright ion cloud is from ions which must have been produced below the 19 km screening height terminator.

filter. Magnitudes and spectral types of the stars were obtained from the Smithsonian star catalog. Since the starlight and the emissions from the barium ion cloud has the same optical path to the detector, the use of the star background for calibration offers the advantage of automatically correcting for effects of atmospheric absorption and the possible presence of haze or thin clouds. The calibration of the image agrees well with the known characteristics of the detector and estimates of losses in the optics and in the atmosphere.

The cloud appears to be of relatively uniform intensity. It is doubtful that the apparent finer structure in the ion cloud has significance since there are only a few counts in each pixel. The average brightness of the brightest regions in the non-UV produced ion cloud is about 100 R, corresponding to a column density of $6 \times 10^7 \text{ cm}^{-2}$ if all ions are in full sunlight.

SYNTHETIC IMAGE CALCULATION

A computer program was written to simulate the observed IPD image. The program is in effect similar to that described in E. M. Wescott et al. (SR90, Strontium shaped-charge critical ionization velocity experiment, submitted to *Journal of Geophysical Research*, 1989) but employs a different computational path in order to include atmospheric absorption of the sunlight illuminating the ion cloud. This is an important part of the simulation since the lower altitude edge of the ion cloud is defined by the terminator. The program assumes no special physical process but only that the production of ions can be described by an ionization time constant. The effective ioniza-

tion time constant was determined by matching the synthetic images with the observed image (Figure 5). To avoid potential problems with the illumination near the terminator the match was made near the top of the cloud, and the best match was found for an ionization time constant of 1800 s. The resulting synthetic image is shown in Figure 6 and is seen to give the essential feature of the observed image: A broad relatively uniform ion cloud stretching left from the injection field line.

The image shown in Figure 6 is an average of a number of synthetic images covering the 5.0 to 10.0 s time interval of the observed image. Each individual image is calculated for a given time using the actual release geometry and the same aspect geometry as the observed image. The velocity distribution function of the neutral barium was given in Figure 3; the angular distribution is Gaussian with a HWHM angle of 6.6° for the fast part of the jet (the slower material does not reach above the terminator before after +10 s). The ion cloud is assumed to be optically thin, and the emission rates for resonance of sunlight, given by Stenbaek-Nielsen [1989], include the velocity dependence due to the Doppler shift of the resonance lines relative to the deep Fraunhofer absorption lines in the solar spectrum at the main ion resonances. The emission rate is further adjusted for atmospheric absorption at 4554 Å as given in Figure 4. Finally, the effects of the barium ion gyromotion is neglected since it is small compared to the size of an image element.

The brightness of each picture element is calculated by numerical integration of the ion brightness along the line of sight. At each step in this integration, the ions would have been

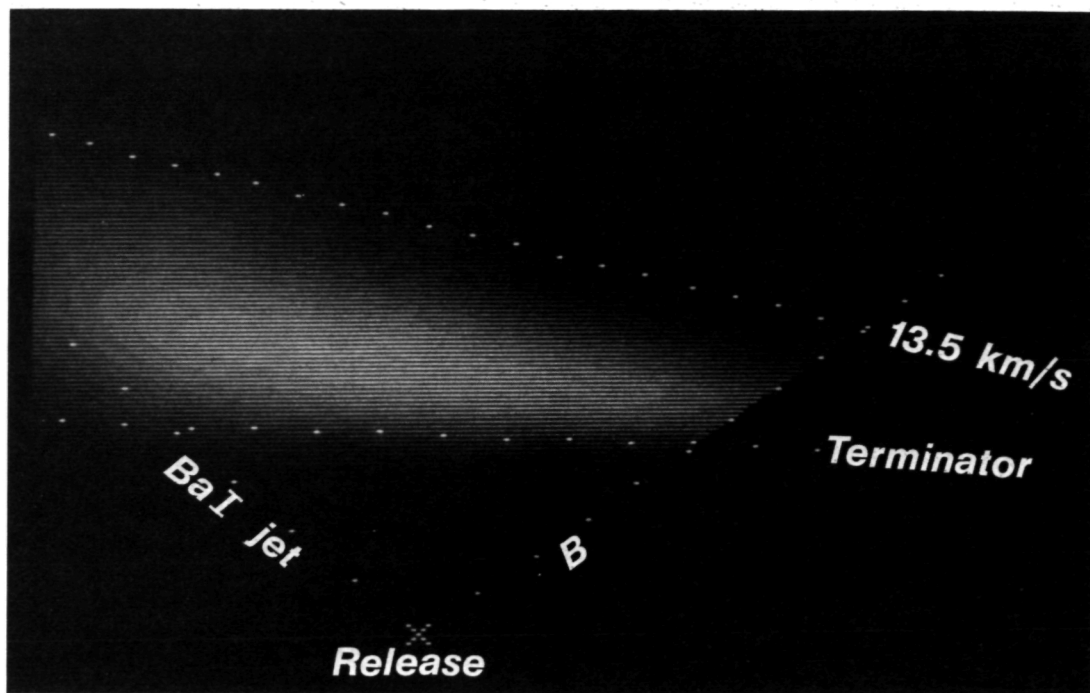


Fig. 6. Synthetic image calculated to simulate the observed IPD image in Figure 5. The 1800 s ionization time constant used in the simulation was selected to best match the observed intensity near the top of the ion cloud where full solar illumination can be assumed. The delimiters are the same as in Figure 5.

created along B and within the neutral beam below (all ions will go up given the injection geometry), and the total contribution to the brightness is evaluated through another numerical integration along B. The distances and angles involved from release to the point of ionization and then up along B to the line of sight, are defined, and for each selected point along B only atoms with one initial velocity will reach the line of sight at the time for which the image is calculated.

The model allows neutral and ion densities to be calculated at the location of the two payloads (neutral barium would only be present in significant amounts at the main payload—cf. Table 1). Figure 7 shows the results under two ionization scenarios both using the 1800 s ionization time constant determined from the optical observations. The solid line assumes ionization of all velocities. The dashed line represents the case of ionization due to collisions with the ambient atmosphere; in this case energy considerations require the neutral barium to have a velocity of at least 8.4 km/s relative to the ambient atmospheric oxygen atoms to ionize.

While the energy spectrum of the neutrals at any given time is a delta function, more velocities will be present in the ions because more than one path would lead to the position of the main payload. As a consequence, the ion densities are less structured than the neutral densities.

The model does not include the effects of a finite barium ion gyroradius. This is a reasonable assumption for the image calculation, but less so for the calculation of ion densities at the instrumented payloads located only a few km from the releases. The gyroradius of the fast jet is of the order of 200 m and the ions can therefore be displaced up to 400 m. This could affect the ion density considerably compared to the case where the ions remain on the field line of creation. The effect should be minor for the main payload since it is located near

the center axis of the jet. However, the subpayload is encountering ions created near the edge of the neutral beam, and the calculated values would then be an underestimate.

SOURCES FOR ION PRODUCTION

Most barium releases rely on solar UV radiation for ionization. This is a fairly efficient process with an effective time constant of about 28 s [Carlsten, 1975; Hallinan, 1988] and thus much faster than the 1800 s estimated for the process in question here. (The difference in efficiencies is clearly illustrated by the relative brightness of the solar UV produced ion cloud in the upper left and the ion cloud in the center of Figure 5.) In the absence of direct sunlight there are several processes in addition to CIV ionization which can contribute to the ionization of the neutral barium jet: (1) photoionization by scattered UV light and (2) collisional ionization. There may also be ionization from the explosion process itself, but the temperature of the explosive products is substantially lower than the 5.21 eV required for ionization and more importantly, the explosive vapor cools as $1/\text{time}$. An evaluation based on the Saha equation shows that any thermally produced ionization must be produced within the first few tens of microseconds in a very small volume at the release. Hence, the ionization would be expected to be confined to near the release field line which contrasts with the observed uniform ionization extending tens of km beyond with no discernible enhancement near the release field line. Consequently, we can disregard this process as contributing to the observed ionization.

Photoionization

Photoionization requires the presence of light of wavelengths less than 3265 Å. The primary source appears to be sunlight reaching the barium jet through scattering in the atmosphere.

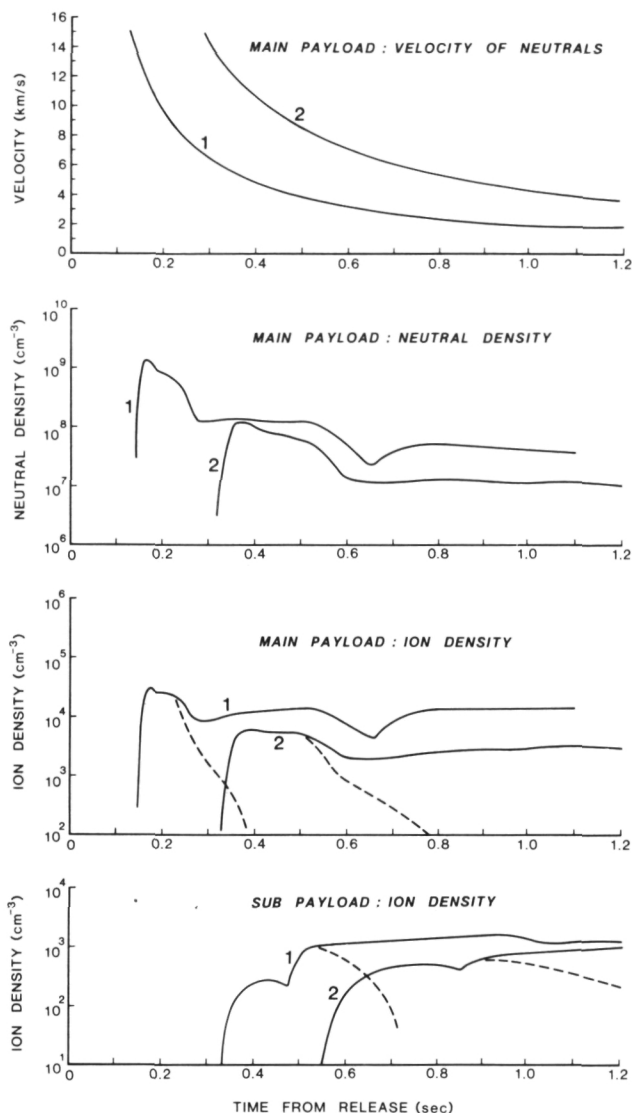


Fig. 7. Barium release parameters calculated at the positions of the two instrumented payloads. The top panel shows the velocity of the neutral barium passing the main payload as function of time after release. The center panels show the corresponding barium neutral and ion densities, and the bottom panel shows the ion density at the subpayload. The solid line gives the ion densities if we assume a constant ionization rate independent of velocity. If the ions are produced by collisions with ionospheric oxygen, there is an energy threshold at 8.4 km/s, below which no ionization occur. The resulting densities are given by the dashed line.

The moon was not visible from the release region and therefore need not be considered. Light from stars and the interstellar background, thermal radiation from the atmosphere and the Earth, and radiation from chemical processes in the atmosphere are estimated to be insignificant.

To estimate the flux of UV photons from scattered sunlight, we assume the scattering process to be Rayleigh scattering, that singly scattered photons dominate at the release, that the atmosphere above the UV terminator is optically thin and below optically thick, and that refraction can be neglected. Thus the problem is reduced to calculate the flux scattered towards the release from all parts of the sunlit atmosphere visible from the release.

For a given direction from the release the brightness in Rayleigh of the sky is

$$(4\pi \times 10^{-6})(3/16\pi)(1 + \cos(\theta)) \times \int n(h)dl \times \int I(\lambda) \times \sigma(\lambda)d\lambda$$

In this equation the terms in front of the integrals are the scaling factor for the unit Rayleigh (4π to give equivalent isotropic flux) and the normalized angular scattering function for Rayleigh scattering (in units per steradian). The first integral is the column density (cm^{-2}) of the sunlit atmosphere along the line of sight; for an evaluation we used the model given in the U.S. Standard Atmosphere Supplements, U.S. Government Printing Office [1966]. The last integral gives the total number of photons scattered per atmospheric nucleus; using the solar flux given by *Banks and Kockarts* [1973] and the Rayleigh scattering cross sections given by *Bates* [1984] its value for wavelengths less than 3266 \AA is 3.5×10^{-10} photons/s.

A computer program was written to perform the detailed calculation using the actual release geometry. At the point on the UV horizon closest to the Sun we find a sky brightness of 2400 MR. The brightness falls rapidly off above this point reflecting the rapidly decreasing column density and is down by three orders of magnitude in only 1.5° of elevation. The decrease is less dramatic along the horizon where the same decrease in brightness requires 60° in azimuth.

The total omnidirectional UV photon flux at the release is 1.2×10^{13} photons $\text{cm}^{-2} \text{ s}^{-1}$ or only 0.02% of the full solar UV flux. The ionization time constant for this flux would be about 120,000 s, wholly insufficient to explain the observed ions, and it is unlikely that a more refined calculation would alter this conclusion.

Collisional Ionization

The neutral barium is streaming in the background atmosphere and some ionization may occur due to collisions. Two types of ionization processes can be envisioned: charge exchanges with ambient ions and collisions with ambient neutrals.

Charge exchange with ambient ions has a cross section of $2 \times 10^{-16} \text{ cm}^2$ [*R. Torbert*, private communication, 1989]. The ambient ion density at the releases, as measured by the Millstone incoherent radar, was $6 \times 10^4 \text{ cm}^{-3}$ which results in an ionization rate of $1.4 \times 10^{-5} \text{ s}^{-1}$ corresponding to a time constant of 70,000 s. Thus, the contribution from this process towards the observed ionization would be insignificant.

For collisional ionization (or stripping) to be possible the barium must have an energy in excess of 5.21 eV (the ionization energy for barium) in the center of mass reference frame. At the altitude of the release the dominant constituent is atomic oxygen which, assuming the oxygen at rest, leads to a minimum velocity of the barium of 8.4 km/s. Therefore only the fastest part of the neutral jet will be able to ionize by atmospheric collisions.

Assuming the density of the neutral barium beam to be much less than that of the ambient atmosphere, the ionization rate per neutral barium atom for a given cross section, σ , is

$$I = n(h) \times \sigma \times v$$

where $n(h)$ is the atmospheric density and v is the velocity of the barium atom relative to the target. At the release altitude of 400 km MSIS-86 [*Hedin*, 1987] gives $n = 5 \times 10^7/\text{cm}^3$ and with $v = 12 \text{ km/s}$, the velocity of the peak in the velocity distribution function, and an ionization rate of 1/1800 per second, the ionization cross sections would be $9 \times 10^{-18} \text{ cm}^2$.

We are not aware of any laboratory data with which a direct comparison can be made. *Firsov* [1959] made a theoretical

analysis which for the velocity range of interest here, 8-13 km/s, yields cross sections in the range $5 \times 10^{-17} - 8 \times 10^{-17} \text{ cm}^2$. This is considerably above our cross section of $9 \times 10^{-18} \text{ cm}^2$. *Fleischmann et al.* [1972] compared Firsov's formula to more than 100 neutral-neutral ionization experiments including Ba, but all at energies several orders of magnitude above the beam energy in our experiment. They derived a semiempirical formula claimed to fit 80% of the cross sections to within a factor of about 2. Applying this formula we obtain cross sections in the range 2×10^{-18} to $3.5 \times 10^{-18} \text{ cm}^2$ for barium neutrals between 8 and 13 km/s. Our cross section of $9 \times 10^{-18} \text{ cm}^2$ is 2.5 times the Fleischmann et al. cross section for 13 km/s barium neutrals. Both Firsov and Fleischmann et al. concentrated on energies considerably above threshold which is clearly demonstrated by the fact that both formulas give finite cross sections below a barium neutral velocity of 8.4 km/s where the ionization process is energetically impossible. On the other hand, from measurements by *Maier and Murad* [1971] of stripping of molecular nitrogen near the energy threshold, *Lai and Murad* [1989] estimate that the cross section may be as large as 10^{-16} cm^2 , which is 10 times the cross section we have inferred.

Our cross section is based on the 1800 s ionization time constant determined by matching the simulated and observed image. To avoid potential problems with atmospheric absorption the match was made near the top of the image farthest above the terminator. This part of the image would be from the fastest part of the neutral jet, and therefore, the cross section must be associated with velocities near 13 km/s. For velocities near threshold the cross section should fall off reaching 0 at 8.4 km/s. The effect in the image (in which ions from neutrals with velocities near 8.4 km/s are just appearing above the terminator) would be that the part of the ion cloud near the terminator would be less bright than predicted by the simulation. Although the observed image tends to support this, the calculation of the terminator in the model is at present too uncertain to warrant any definite claim. In Figure 7 the effect would be that the densities at the payloads would fall off more rapidly than the dashed line calculated using a constant ionization rate for all velocities above 8.4 km/s.

CONCLUSIONS

The optical observations on the first of the two releases revealed an ion cloud stretching from the release field line to the neutral jet (Figure 5). These ions were produced below the solar terminator and therefore must have resulted from an ionizing process other than direct photoionization by solar UV radiation. The process must have been present continuously from the time of release. A computer simulation of the image (Figure 6) has shown that the efficiency must have been nearly constant in time and equivalent to an ionization time constant of about 1800 s.

The probable source of this ionization is collisions with the ambient atmospheric oxygen. The observed image is almost exclusively due to ions with initial neutral velocities above the threshold of 8.4 km/s for collisional ionization, and the cross section required to match the observations is of order 10^{-17} cm^2 , which is not an entirely unreasonable cross section. Model calculations [*Torbert*, 1988] indicate that the CIV effect should produce most of the ionization within 5 km from the release. A definite distance limit is set by excitation of ambient neutral oxygen, which will cool the electrons and damp the CIV effect when the barium density falls below 1/8 of the neutral oxygen density [*Newell and Torbert*, 1985]. In CRIT I, this would hap-

pen at distances exceeding 11 km from the explosion, while the observed ionization extended to at least 40 km.

Assuming that the source of the ionization is collisions with the ambient atmosphere, it is clear that this constitutes an important source that must be taken into account in future release experiments, notably the upcoming ionospheric releases from the Combined Release and Radiation Effects Satellite (CRRES), which will take place at an orbital velocity near 10 km/s. It would therefore be important to acquire more information about the ionization cross section near threshold in the 8 to 12 km/s velocity range.

When estimating the collision cross section it was implicitly assumed that the beam density is much lower than that of the ambient atmosphere. This is not the case immediately after release. Using the distribution function inferred from the SR90 release and an atmospheric density of $5 \times 10^7 \text{ cm}^{-3}$ [*Hedin*, 1987] the maximum beam density along the axis of the neutral jet will not be below the atmospheric density before 6 km, or 0.5 s, from the release. There is in the observed image a clear indication that the ions start to form essentially at the time of release (Figure 5) leaving open the possibility that collisional ionization only becomes important at a later time and that the ions observed near the release could be critical velocity ionization with similar efficiency. We must therefore conclude, that if a CIV process is present immediately after release, its ionization time constant cannot be smaller than 1800 s corresponding to a maximum ionization rate of 1/1800 or 0.06% per second.

Lai et al. [1988] have argued, based on observations made from the space shuttle, that CIV is less likely to occur as the ambient density decreases and they give an altitude limit of about 240 km. Although this might agree with the observations reported here, it would not explain the ionization observed in the "Porcupine" experiment at an altitude of 450 km. A comparison of the many CIV rocket experiments carried out by our team have now led us to believe that the critical parameter for CIV is the background electron density. In "Porcupine" the background electron density was $2 \times 10^5 \text{ cm}^{-3}$ [*Torbert*, 1988], much higher than in any of the other experiments conducted until CRIT II, carried out May 4, 1989, from Wallops Island. In this experiment the ambient electron density was $6 \times 10^5 \text{ cm}^{-3}$, and preliminary analysis of the observational data indicates that, indeed, CIV took place [*Torbert*, 1989; *Stenbaek-Nielsen et al.*, 1989].

Acknowledgments. We thank W. Boquist, Technologies Inc., for optical data; J. Foster, Millstone Hill, for the electron densities; D. Bostow and B. McKibben, University of Alaska, for experimental support; and the U.S. Army Corps of Engineers for use of their Coastal Environmental Research Station at Duck, North Carolina. We also thank the members of the CRIT I team for many discussions during the preparation of this paper. Support for the Geophysical Institute, University of Alaska Fairbanks was provided by NASA grants NAG6-1 and NAGW-269. D. Rees acknowledges the support of the U.K. Science and Engineering Research Council. A. Valenzuela acknowledges the support of the Max Planck Institute for Extraterrestrial Physics. N. Brenning acknowledges the Swedish Board of Space Sciences for support.

The Editor thanks E. Murad and another referee for their assistance in evaluating this paper.

REFERENCES

- Alfvén, H., *On the Origin of the Solar System*, Oxford University Press, New York, 1954.
- Alfvén, H., and G. Arrhenius, *Structure and Evolutionary History of the Solar System*, D. Reidel, Hingham, Mass., 1975.
- Banks, P.M., and G. Kockarts, *Aeronomy*, Academic, San Diego, Calif., 1973.

- Bates, D.R., Rayleigh scattering by air, *Planet. Space Sci.*, 32, 785, 1984.
- Carlsten, J.L., Photoionization of barium clouds via the 3D metastable levels, *Planet. Space Sci.*, 23, 53-60, 1975.
- Firsov, O.B., A qualitative interpretation of the mean electron excitation energy in atomic collisions, *Zh. Exp. Teor. Fiz.*, 36, 1517, 1959. (*Sov. Phys. JETP*, Engl. Transl., 9, 1076, 1959).
- Fleischmann, H.H., R.C. Dehmelt, and S.K. Lee, Direct-transition features in stripping collisions of heavy neutral atoms and ions, *Phys. Rev. A*, 5, 1784, 1972.
- Guttman, A., Extinction coefficient measurements on clear atmosphere and thin cirrus clouds, *Appl. Opt.*, 7, pp. 2377-2381, 1968.
- Haerendel, G., Alfvén's critical effect tested in space, *Z. Naturforsch. A*, 37, 1042, 1982.
- Hallinan, T.J., Observed rate of ionization in barium shaped-charge releases in the ionosphere, *J. Geophys. Res.*, 93, 8705, 1988.
- Hedin, A.E., MSIS-86 thermospheric model, *J. Geophys. Res.*, 92, 4649, 1987.
- Lai, S.T., and E. Murad, Critical ionizations velocity experiments in space, *Planet. Space Sci.*, 37, 865, 1989.
- Lai, S., W.F., Denig, E. Murad, and W.J. McNeil, The Role of Plasma processing in the space shuttle environment, *Planet. Space Sci.*, 36, 841, 1988.
- Maier, W.B., II, and E. Murad, Study of collision between low energy N^+ and N_2 : Reaction cross section, isotopic compositions, and kinetic energies of the products, *J. Chem. Phys.*, 55, 2308, 1971.
- Newell, P.T., Review of critical ionization velocity in space, *Rev. Geophys.*, 23, 93, 1985.
- Newell, P.T., and R.B. Torbert, Competing atomic processes in Ba and Sr injection critical velocity experiments, *Geophys. Res. Lett.* 12, 835, 1985.
- Piel, A., Review of laboratory experiments on Alfvén's critical ionization velocity, *Adv. Space Res.*, 10, nr7, 47, 1990.
- Stenbaek-Nielsen, H.C., Calculated emission rates for barium releases in space, *Planet. Space Sci.*, 37, 1441, 1989.
- Stenbaek-Nielsen, H.C., T.J. Hallinan, E.M. Wescott, and H. Foepl, Acceleration of barium ions near 8000 km above an aurora, *J. Geophys. Res.*, 89, 10788, 1984.
- Stenbaek-Nielsen, H.C., E.M. Wescott, G. Haerendel and A. Valenzuela, CRIT II: Optical observations of critical velocity ionization ions, *Trans. Am. Geophys. Un.*, 70, 1277, 1989.
- Torbert, R.B., Critical velocity experiments in space, *Adv. Space Res.*, 8, 39, 1988.
- Torbert, R.B., Review of ionospheric CIV experiments, *Adv. Space Res.*, 10, nr7, 7, 1990.
- Torbert, R.B., An overview of the CRIT-II experiment, *Trans. Am. Geophys. Un.*, 70, 1277, 1989.
- Wescott, E.M., H.C. Stenbaek-Nielsen, T. Hallinan, H. Foepl, and A. Valenzuela, Star of Lima: Overview and optical diagnostics of a barium Alfvén critical velocity experiment, *J. Geophys. Res.*, 91, 9923, 1986a.
- Wescott, E.M., H.C. Stenbaek-Nielsen, T. Hallinan, H. Foepl, and A. Valenzuela, Star of Condor: A strontium critical velocity experiment, *J. Geophys. Res.*, 91, 9933, 1986b.
- N. Brenning, Royal Institute of Technology, Stockholm, Sweden.
- D. Rees, University College London, London, U.K.
- H.C. Stenbaek-Nielsen, Geophysical Institute, University of Alaska Fairbanks, Fairbanks, Alaska 99775-0800, U.S.A.
- A. Valenzuela, Max Planck Institute for Extraterrestrial Physics, Garching, FRG.
- E.M. Wescott, Geophysical Institute, University of Alaska Fairbanks, Fairbanks, Alaska 99775-0800, U.S.A.

(Received July 18, 1989;
revised December 27, 1989;
accepted December 29, 1989.)

Page Intentionally Left Blank

SR90, Strontium Shaped-Charge Critical Ionization Velocity Experiment

EUGENE M. WESCOTT, HANS STENBAEK-NIELSEN, AND DANIEL W. SWIFT

Geophysical Institute, University of Alaska Fairbanks

ARNOLDO VALENZUELA

Max-Planck-Institut für Extraterrestrische Physik, Garching, Federal Republic of Germany

DAVID REES

Department of Physics and Astronomy, University College, London

In May 1986 we carried out an experiment to test Alfvén's critical ionization velocity (CIV) effect in free space, using the first high-explosive shaped charge with a conical liner of strontium metal. The release, made at 540 km altitude at dawn twilight, was aimed at 48° to **B**. The background electron density was $1.5 \times 10^4 \text{ cm}^{-3}$. A faint field-aligned Sr^+ ion streak with tip velocity of 2.6 km s^{-1} was observed from two optical sites. Using two calibration methods, we calculate that between 4.5×10^{20} and 2×10^{21} ions were visible. We have calculated an ionization time constant of 1920 s for Sr from the solar UV spectrum and ionization cross section, which combined with a computer simulation of the injection predicts 1.7×10^{21} solar UV ions in the low-velocity part of the ion streak. Thus all the observed ions are from solar UV ionization of the slow (less than critical) velocity portion of the neutral jet. The observed neutral Sr velocity distribution and computer simulations indicate that 2×10^{21} solar UV ions would have been created from the fast (greater than critical) part of the jet. They would have been more diffuse and were not observed. Using this fact, we estimate that any CIV ions created were less than 10^{21} . We conclude that future Sr CIV free space experiments should be conducted below the UV shadow height and in much larger background plasma density.

INTRODUCTION

Alfvén [1954] and later Alfvén and Arrhenius [1975] proposed a theory of the formation of the solar system which provided a means of separating the elements depending upon their ionization potential. As a part of that theory it was proposed that if a neutral gas streaming through a plasma across a magnetic field exceeds a critical velocity $V_c = (2W_i/M_a)^{1/2}$ (where W_i and M_a are the ionization potential and atomic mass of the neutral gas), then the neutral gas would rapidly ionize. For a central attracting mass, Alfvén showed that the critical velocity relationship led to a critical accretion radius for each of four groups of the most abundant elements with apparently good agreement with the mean distance of several groups of satellites, such as the terrestrial and the giant planets, or the Galilean moons in the Jovian system [Möbius *et al.*, 1979].

Laboratory experiments documenting the critical velocity effect have been carried out for years and were reviewed by Danielsson [1973]. Möbius *et al.* [1979, p. 29] pointed out that

All the laboratory experiments besides scaling in dimensions are different from Alfvén's cosmogonic scenario in two basic features:

- The magnetized plasma is moving with respect to the neutral gas, caused by the external discharge voltage.
- Walls are present, making up the discharge chamber.

Several free space experiments have been made to test the critical ionization velocity (CIV) effect with more appropriate

scaling factors and without walls. For a review of theory, laboratory, and free space experiments, see Newell [1985]. The experiments have used barium and strontium vapor with critical velocities of 2.7 km s^{-1} and 3.5 km s^{-1} , respectively. Haerendel [1982] and Haerendel *et al.* [1988] observed 16–18% ionization of those neutrals that exceeded the critical velocity from a conical barium shaped charge detonated 30° to **B** well below the solar UV horizon in project Porcupine. Deehr *et al.* [1982] detected strontium ions in the sunlit detonation of a radial barium shaped charge. The strontium was present as a 1% impurity in the barium, and the analysis shows that about 50% of the strontium ionized, at a time when less than 1% ionization would be produced by solar UV. In 1983, two experiments were carried out from rockets at the magnetic equator in Peru. Star of Lima [Wescott *et al.*, 1986a; Torbert and Newell, 1986] was a barium conical shaped charge fired perpendicular to **B** in partial solar UV illumination. Optical observations indicate that 2.5 to 5×10^{20} Ba ions were produced, which could have been due to the solar UV ionization. Star of Condor [Wescott *et al.*, 1986b] was a radial shaped charge lined with strontium metal and detonated such that Sr vapor was produced at all pitch angles to **B**. The detonation produced 43% of the neutral gas with velocity component perpendicular to **B** greater than the 3.5 km s^{-1} critical velocity. Ten minutes after detonation, a field-aligned ion streak was observed; it was estimated to contain 2.4×10^{19} ions, which is 0.004% ionization of the Sr vapor. This amount can be explained by solar UV and initial Maxwellian temperature tail ionization.

In order to understand the apparent failure of the Alfvén mechanism to produce a cascade of ionization in the 1983 Peru experiments, we carried out three additional CIV

Copyright 1990 by the American Geophysical Union.

Paper number 90JA01211.
0148-0227/90/90JA-01211\$05.00



Fig. 1. TV picture of SR90 neutral jet in white light at 11.5 s from Duck, North Carolina.

experiments from rockets at Wallops Island in May 1986. CRIT I used two barium conical shaped charges detonated below the solar UV cutoff altitude at 45° to **B** at different distances from a well-instrumented mother payload [Stenbaek-Nielsen *et al.*, 1990a; Brenning *et al.*, 1990]. There was also a daughter payload several kilometers up the magnetic field line.

The third experiment, called SR90, consisted of a high-explosive conical shaped charge with a strontium metal liner on a Taurus-Nike-Tomahawk fired 9 min after the launch of the barium experiment rocket. The Sr release was in full solar UV radiation. Föppl *et al.* [1965] estimated the solar UV ionization time constant for Sr atoms to be 4545 s. Based upon this very long ionization time constant, it was assumed that the solar UV contribution to the ionization processes would be negligible compared with the Alfvén mechanism; however, we have found this to be an unwarranted assumption. This paper addresses the optical observations, computer simulations, and analysis of the SR90 experiment. There were no in situ diagnostics other than background electron densities from the Millstone Hill radar.

THE SR90 EXPERIMENT

The Taurus-Nike-Tomahawk, 38,008 UE, was launched from Wallops Island May 13, 1986, at 0756:00 UT. The payload consisted of an attitude control system, timers, and power supplies to detonate a single high-explosive conical shaped charge aimed forward and coaxial with the rocket. The shaped charge consisted of 7.4 kg of 75/25 Octol high explosive, with a tapered 30° conical liner of Sr metal

weighing 0.57 kg. The two-axis attitude control system was set to nominally align the shaped charge at 45° to **B**, but the azimuth was undetermined; detonation could occur anywhere on a 45° cone about **B**.

The detonation occurred at 0801:29 UT, at 539.6 km altitude, 37.72°N , -74.72°E . By triangulation the axis of the neutral strontium jet was upward at a geodetic elevation angle of 26° and azimuth of 212° , giving an actual angle of 48.2° with respect to **B**. The experiment was observed from three primary optical sites using low light level imagers: Wallops V25, 37.861°N , -75.457°E , about 2 km from the launcher; Duck, North Carolina, 36.182°N , -75.751°E ; and Cape May, New Jersey, 38.945°N , -74.883°E . NASA film cameras were also operated at Wallops Island near the control center.

At Duck, observations were made using an intensified film camera and an intensified silicon intensified target (ISIT) TV system. Figure 1 shows a picture of the neutral jet taken in white light from the ISIT TV 11.5 s after detonation. The detonation azimuth and elevation were very fortunate for analysis of the neutral velocity distribution, as the viewing angle between Duck and the jet was close to 90° , allowing the best neutral velocity distribution from a shaped charge that we have ever obtained. The ISIT image (Figure 1) was digitized, and each pixel value was printed out. The corresponding distances along various angles away from the detonation point were calculated and plotted on the pixel diagram. We were able to fit Gaussian curves across the jet at various distances, and to integrate the total intensity of all neutral Sr gas in velocity intervals Δv of 0.875 km s^{-1} . The Gaussian function for axis intensity, or density dependence,

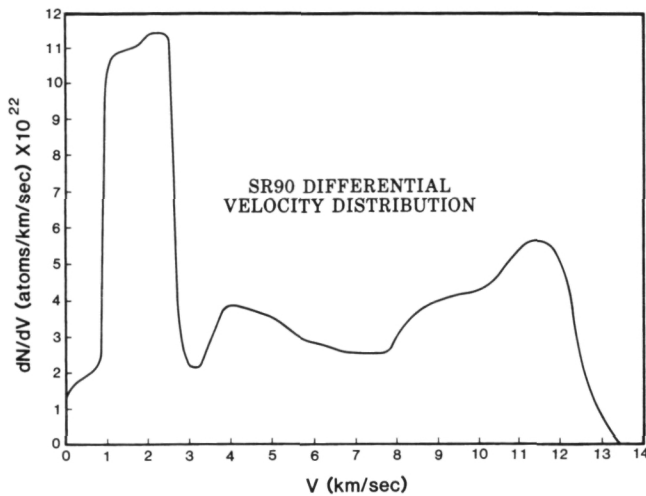


Fig. 2. Differential strontium neutral velocity function. The scale is derived from the assumption that 15% of the liner is vaporized.

for the fast portion of the jet ($v > 8 \text{ km s}^{-1}$) has a half amplitude angle of 6.6° and is given by

$$I = I_0 \exp \left[-\frac{\theta^2 \ln 2}{(6.6^\circ)^2} \right]$$

where θ is the angle from the central axis in degrees and I_0 is the intensity (or neutral density) at the center. For velocities between 3.5 and 8 km s^{-1} the half amplitude angle is near 10° , and for the very low velocity material ($v < 3.5 \text{ km s}^{-1}$) the half angle is close to 22° .

Figure 2 shows the differential velocity function derived from integrating the total pixel counts per 0.875 km s^{-1} increments. The apparent tip velocity was slightly over 13 km s^{-1} . The differential velocity distribution was normalized by assuming that 15% of the 0.556-kg Sr liner was vaporized, based on vacuum chamber experiments with small Ba and Sr shaped charges [Michel, 1969, 1974].

Föppl *et al.* [1965, pp. 98–99] estimated the ionization time constant for strontium at about 4545 s and noted “. . . which is of course highly uncertain.” We used this value in planning the experiment, but after the experiment we were able to calculate a better number. Using the newer experimental ionization cross section between 1700 and 2400 \AA of Lütjens [1973], which he estimates is good to 30%, convolved with the solar UV spectrum of Banks and Kockarts [1973], we find an ionization time constant of 1920 s ($\pm 30\%$). With 5.7×10^{23} Sr atoms available for ionization and a time constant of 1920 s , in 0.1 s there should be 3×10^{19} ions, in 1 s , 3×10^{20} ions, and in 10 s , 3×10^{21} ions produced.

Analysis of the Sr metal chips left over from machining the cone indicates that there were 2.13% Ba atoms by weight impurity, or 0.012 kg of Ba in the cone. Assuming 15% vaporization of the Ba and a solar UV ionization time constant of 28 s [Hallinan, 1988], the number of Ba ions would equal the number of Sr ions, but they would not be visible through the Sr ion filters.

OPTICAL OBSERVATIONS

At Duck, North Carolina, the Sr injection was also observed with an intensified film camera with a narrow-band

4078-\AA interference filter on the principal Sr II line. A faint field-aligned streak of Sr^+ ions was observed. Figure 3 shows a sequence of portions of six intensified camera frames which were digitized electronically. The bright oval-shaped feature in Figure 3a is the explosive debris cloud with broadband emissions coming through the 4078-\AA filter. The field-aligned streak can be seen coming upward from slightly left of center of the debris cloud at 6.6 s and progressing up the field line in successive 2-s intervals. The last frame (Figure 3f) at 63 s shows the streak visible about 85 km along the field line (distances in 20-km ticks shown along the field line).

The early time apparent velocity of the tip of the field-aligned Sr^+ jet is about 2.6 km s^{-1} . With an injection of pitch angle 48.2° to B, the corresponding neutral Sr velocity would be 3.9 km s^{-1} . This agrees well with the low-velocity peak in the differential velocity distribution (Figure 2). The low-velocity peak is estimated to contain 2.3×10^{23} atoms of Sr.

The ISIT camera at Duck in white light is less sensitive than the intensified film camera, and the bright neutral Sr cloud partially obscured the direction up the magnetic field line. No ion streak is evident, even with post factum 3-s integration, but this is consistent with the observed brightness and the sensitivity of the camera.

A pair of imaging photon detectors (IPD) observing in the ion and neutral emission lines, respectively, were operated at the Wallops V25 site in the launch complex. The neutral cloud was very bright, and about 15 s after release it became necessary to stop down the lens aperture to prevent damage to the detector. Unfortunately, the neutral detector and the ion detector were both stopped down. As a result the later ion images are very noisy and are not of as good quality as the images from Duck. No prompt ions could be identified, but a faint trail of Sr ions was detected along B above the release over a period of 2–3 min following the release. No Sr ions were seen on images at Cape May due to the geometry of the release, the brightness of the neutrals, and the sensitivity of the camera in white light.

BRIGHTNESS OF THE ION STREAK AND ION PRODUCTION ESTIMATE

An estimate of the brightness of the field-aligned streak shown in Figure 3f at 63 s after release can be made using several methods. The most direct is using the IPD data, but because the lens was stopped down, the signal to noise is low, resulting in a large uncertainty on the result. The streak is not discernible in individual IPD images but can be brought out by summing several images. The IPD employs photon counting and thus is absolutely calibrated. The brightness of the ion cloud near 63 s , as observed in the IPD images, is $100\text{--}200 \text{ R}$.

The second method combines the intensified camera data from Duck and the Wallops Island IPD data. Both data sets are observations filtered on the 4078-\AA Sr II line. The intensified film camera is not absolutely calibrated, but an estimate of the ion cloud brightness can be made using images from the IPD (prior to that instrument's being stopped down) for calibration of corresponding images from the intensified camera. Assuming the high-explosive debris cloud to be broadband emissions, the IPD images indicate its brightness at 6.6 s after release to be 40 R/\AA . The intensified

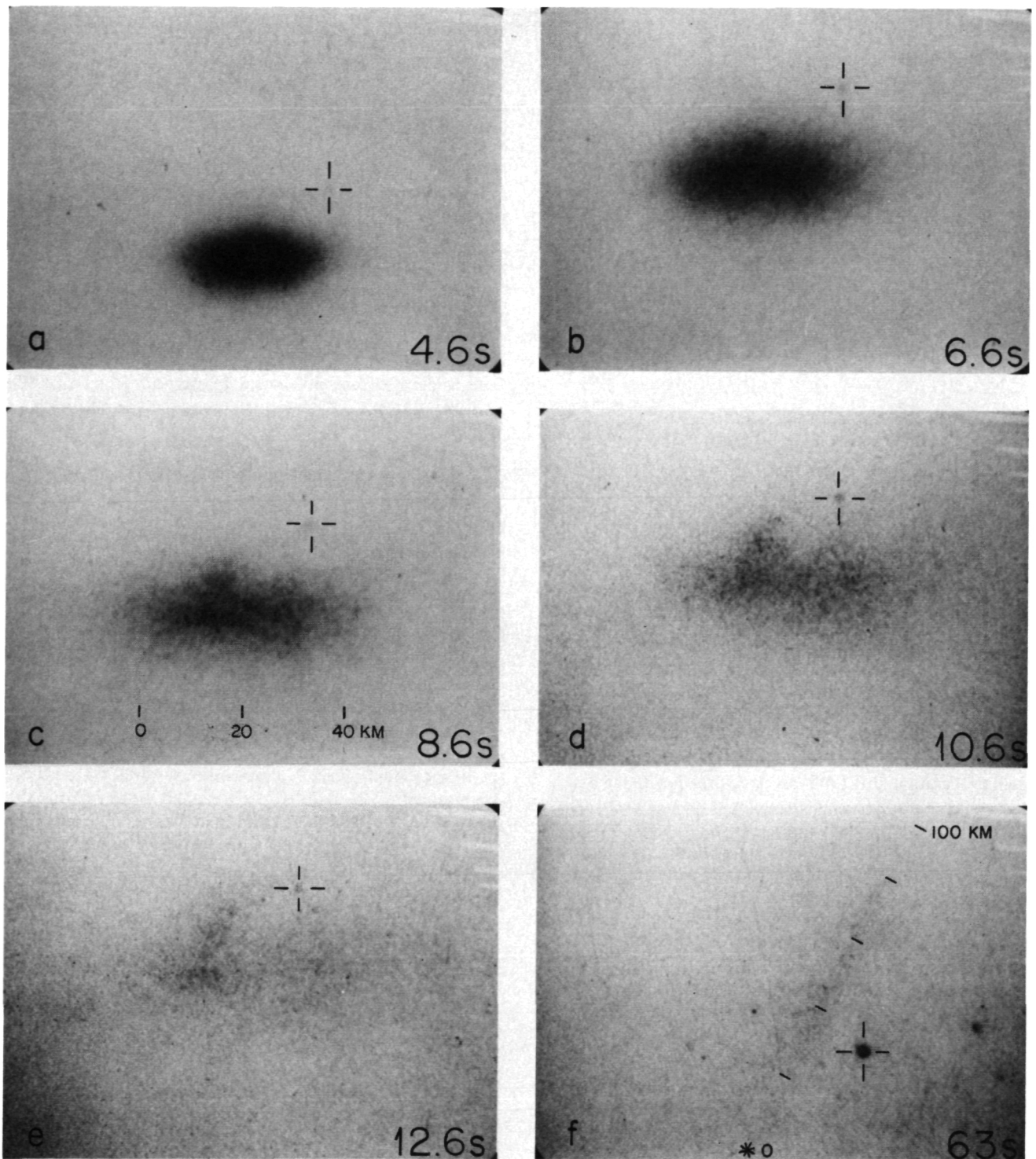


Fig. 3. TV frames from portions of digitized intensified film camera at Duck, North Carolina, showing the development of a slow ($v < 2.6 \text{ km s}^{-1}$) Sr ion streak. The brightest star, shown with a cross, is Cygnus i. The next brightest star is Cygnus θ . The distance along the magnetic field line from the burst point is shown in Figure 3f.

camera was equipped with a filter of 44 \AA full width at half maximum and 40% peak transmission.

From densitometry of the original Duck intensifier film frame and the film development characteristics we measured the ratio of ion line streak brightness to center of explosive debris (broadband emissions) brightness at 6.6 s after detonation to be 0.66. Using the IPD-based brightness of 40 R/\AA for the debris cloud, the ion cloud would have a brightness of

1200 R at 6.6 s. The brightness of the ion cloud decreases as $1/\text{time}$ because of velocity dispersion. Thus at 63 s the brightness would be 125 R, which is within the brightness range established based on the IPD data.

NUMBER OF IONS IN CLOUD

To obtain the number of ions in the cloud, the emission rate is required. For strontium in full sunlight, *Föppl et al.*

[1965] report an emission rate at 4078 Å of 0.087 photon/ion s, assuming all ions to be in the ground state. This rate was calculated assuming the depth of the solar Fraunhofer absorption line to be 2%. Newer solar spectral data [Beckers *et al.*, 1976] of the solar flux at the top of the atmosphere indicate a brighter solar continuum than that used by Föppl *et al.* and indicate that the depth of the absorption line is closer to 4%. This alone would raise the emission rate by more than a factor of 2. We have not been able to perform a detailed calculation of the strontium emission rate as for example has been done for barium by Stenbaek-Nielsen [1989], but using the newer solar data by Beckers *et al.* [1976], we calculate an emission rate of 0.2 photon/ion s.

Because of the deep Fraunhofer absorption line in the solar spectrum, a Doppler shift of the resonance line can change the emission rate drastically. However, the ions present in the ion cloud discernible at 63 s would all have low velocities ($v < 2.6 \text{ km s}^{-1}$), and the change in the resonance relative to the solar spectrum due to a velocity component in the direction of the Sun (Doppler effect) is very small and can be ignored. Therefore, for the estimate of the number of ions in the image, no Doppler connection is required to the emission rate of 0.2 photon/ion s.

We converted the film frame at 63 s to a digitized image, subtracted the background, and printed out all the pixel values. The intensity calibration of the image derived above defines the brightness in all pixels of the cloud. The triangulated distance from the station to the cloud was 600 km, and the field of view of the image was $4.9^\circ \times 5.9^\circ$. The total number of ions in the cloud observed in the image is, by integration over all pixels in the image, found to be 4.5×10^{20} ions. This value corresponds to 0.17% of the total amount of strontium at velocities less than 3.5 km s^{-1} .

MODEL TO CALCULATE SYNTHETIC IMAGES

The number of ions observed can be compared with the number of ions expected from photoionization. In order to estimate how the neutral Sr jet and field-aligned Sr ion streak would appear to optical imagers at the various sites used in the experiment, we made computer simulations of the solar ionization produced effects using a time constant of 1920 s. The synthetic images were constructed by calculating brightness at individual points across a $6^\circ \times 3.6^\circ$ image plane. We assumed the neutral and ion jets to be optically thin, so that the brightness is simply the integration of radiation over all particles along the line of sight. For the ion emission rate we used 0.2 photon/ion s.

The model calculations assumed that the neutral particles followed straight-line trajectories, traveling radially outward from the site of the shaped-charge explosion. The neutral density was calculated from the differential velocity distribution function

$$\eta = \frac{d^2F}{dv d\theta} \quad (1)$$

which is the number of particles with speeds between v and $v + dv$ and with polar angles between θ and $\theta + d\theta$, where θ is the angle between the burst direction and the radial vector. Rotational symmetry about the burst direction was assumed. Specifically, we assumed

$$\eta = \mu NF(v) \exp\left(\frac{-\theta^2 \ln 2}{(\Delta\theta)^2}\right) \quad (2)$$

where N is the total number of strontium neutrals in the beam, μ is a normalizing constant, and the angular width of the beam, $\Delta\theta$, was taken to be a function of the velocity. The velocity distribution, $F(v)$, and angular half width were inferred from TV observations from Duck as shown in Figure 2. The neutral density is given by

$$n_n = \frac{\eta(v, \theta)}{r^2 t} e^{-t/\tau} \Bigg|_{v=r/t} \quad (3)$$

where r is the distance from the burst point and τ is the photoionization lifetime of a Sr neutral, which we have calculated to be 1920 s.

The calculation of the ion density is based on the assumption that the ion, upon creation, moves parallel to the magnetic field at a velocity equal to the projection of the velocity of the parent neutral upon the magnetic field direction. The ions may be described in terms of the distribution function $f = f(\mathbf{x}, v_s, t)$, where v_s is the velocity parallel to the magnetic field. The distribution function satisfies the equation

$$\frac{\partial f}{\partial t} + v_s \mathbf{1}_b \cdot \frac{\partial f}{\partial \mathbf{x}} = \frac{1}{\tau_0} n_n(\mathbf{x}, t) \delta\left(v_s - \frac{\mathbf{x} \cdot \mathbf{1}_b}{t}\right) \quad (4)$$

where $\mathbf{1}_b$ is the unit vector in the direction of the magnetic field. This states that the total time derivative for ions with velocity v_s is given by the rate of decay of the neutrals present in a given volume element.

The solution to (4) may be evaluated by integrating the right-hand side along the ion trajectories:

$$f = \frac{1}{\tau_0} \int_0^t dt' n_n(\mathbf{x}', t') \delta\left(v_s - \frac{\mathbf{x} \cdot \mathbf{1}_b}{t'}\right) \quad (5)$$

where

$$\mathbf{x}'(t') = \mathbf{x} - \mathbf{1}_b v_s (t - t') \quad (6)$$

The ion number density is obtained by integration of f over the velocity v_s , which is easily done because of the δ function in the integral. The result is

$$n_i = \frac{1}{\tau t} \int_0^t dt' t' n_n[\mathbf{x} - (\mathbf{1}_b \cdot \mathbf{x}) \mathbf{1}_b (1 - t'/t), t'] \quad (7)$$

Upon substituting expression (3) for the neutral density,

$$n_i = \frac{1}{\tau t} \int_0^t dt' \frac{\eta(r', \theta', t')}{r'^2} e^{-t'/\tau} \quad (8)$$

where

$$r'^2 = (x - \sigma_x s)^2 + (y - \sigma_y s)^2 + (z - \sigma_z s)^2 = x'^2 + y'^2 + z'^2$$

$$\theta' = \tan^{-1} \left[\frac{(x'^2 + y'^2)^{1/2}}{z'} \right]$$

and $s = (1 - t/t')r \cos \Omega$, where Ω is the angle between the direction of \mathbf{x} and the magnetic field. The σ_s are the direction cosines of the unit vector $\mathbf{1}_b$.

The calculation of the image intensities from the volume densities is then a matter of integrating the volume densities n_n and n_i along a line of sight. The line-of-sight direction is

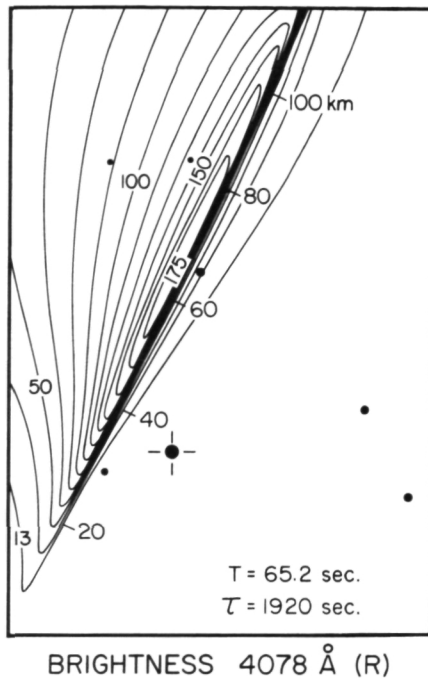


Fig. 4. Contour plot of computer simulation of Sr ions' brightness at 4078 Å at 65.2 s after detonation as viewed from Duck, North Carolina. The burst point is at lower left-hand corner, and 120 km of the field-aligned streak is shown. Tick marks show distance in kilometers along **B**. The total ion count in the $6^\circ \times 3.6^\circ$ field of view is 1.71×10^{21} ions. Only the brightest portion of the streak would be visible on the Duck intensified camera frame (Figure 3f).

specified in terms of view angles, α and β , from the observation point. The picture coordinates are $\alpha \cos \beta$ and $\alpha \sin \beta$, where α is the angle between the view direction and the line of sight to the burst and where β is an azimuthal angle about the line of sight to the burst measured from the projection of the burst direction on the plane normal to the line of sight to the burst. The details of converting the coordinates in which the density is computed to geocentric coordinates (in which the observer's position, burst location, and magnetic field direction are computed) to the picture coordinates are tedious and will not be repeated here. The results of the calculations are synthetic images projected on the image plane as viewed from the observation point.

Figure 4 shows a contour plot of the brightness of the Sr ions at 4078 Å as viewed from Duck at $t + 65.2$ s. We used the emission rate of 0.2 photon/ion s. The initiation point is at the lower left corner. The upper right end of the streak would correspond to 2.6 km s^{-1} in the neutral velocity distribution (Figure 2). Thus the streak shown is from neutrals within the low-velocity peak, all with velocities less than the critical velocity.

This simulated view can be compared with the observed streak at 63 s shown in Figure 3f. The simulation of the ion streak (Figure 4) does not correspond exactly with the observed streak (Figure 3f) because the actual ions are affected by gravity and $\mathbf{E} \times \mathbf{B}$ drift. By 63 s ions with initial velocities less than 1.5 km s^{-1} will have reached their maximum altitude and begin to fall back down along **B**.

The maximum brightness in the simulated image (Figure 4) is 175 R, which agrees well with the observed brightness of the streak (100–200 R based on the IPD images from Wal-

lops, and 125 R based on the intensified camera images from Duck). Also, the appearance of the streak in the simulation is very much as that observed in the Duck image (Figure 3f). This is a rather important point. The presence of a field-aligned streak along the release field line could be taken as evidence of a CIV process present only in the vicinity of the release, but the simulation clearly shows that the streak also can be produced by a uniform ionization rate. Thus we must conclude that the observed ions can all be accounted for by solar UV ionization.

CONCLUSIONS

We have carried out a free space CIV experiment using the first shaped charge with a conical strontium metal liner, but no CIV ions were detected. The use of a conical liner was an improvement over the "Star of Condor" Peru experiment, which used a radial shaped charge, in that a higher peak velocity and a much more dense jet were produced. The ambient plasma background density in both experiments was similar: $2 \times 10^4 \text{ cm}^{-3}$. In the Peru experiment we only detected a Sr ion streak 10 min after the injection and estimated that we could see 2.4×10^{19} ions, or 0.004% of the vaporized Sr. As the Star of Condor ion streak was first noticed 10 min after the injection, it is likely that many of the ions initially formed by solar UV were no longer dense enough to be detected, and the ion inventory was low.

In the SR90 experiment we detected a faint Sr II field-aligned streak (about 150 R) in 4078-Å light from the Duck and Wallops V25 optical sites. The tip of the streak had a velocity of 2.6 km s^{-1} , which corresponds to 3.9 km s^{-1} in the initial 48° to **B** neutral jet. From several calibrations of the brightness of the ion streak we estimate that the detectable portion contained about 10^{21} ions to an uncertainty of a factor of 2. A computer simulation using a new computation of the solar UV ionization time constant (1920 s) shows 1.7×10^{21} ions in the slow portion of the ion streak. We note that the SR90 ion streak detected is from the portion of the neutral jet with velocity perpendicular to **B** which is below the Alfvén critical velocity of 3.5 km s^{-1} .

Although no high-velocity ($v > 2.6 \text{ km s}^{-1}$) ion jet was observed, the IPD ion images available combined with model calculations allow an estimate to be made of the maximum number of CIV ions that could have been present. The release was observed from Wallops V25 near the edge of the IPD field of view where the ion filter unfortunately rapidly cuts off. Solar UV and CIV ions in a fast ($v \approx 9 \text{ km s}^{-1}$) field-aligned ion jet would have been clear of the bright explosive debris area about 5 s after release and out of the field of view about 9 s after release. We have an IPD image covering the time interval 4–10 s after release. There is a slight increase in the counts in the general area where the jet should be just at the edge of the passband of the filter. A computer simulation at 10 s indicates that the solar UV produced ions should have a brightness of 30 R, which our calibration indicates is just below the limit of detectability where the fast ion streak should be. We therefore conclude that if there were CIV ions present in numbers comparable to the solar UV produced ions we should have seen them. This sets the maximum number of CIV ions which could have been produced in the fast jet, but not detected, at less than 2×10^{21} to within a factor of 2, or less than 0.18% yield of the vaporized Sr.

Since this maximum possible CIV yield is a factor of 100 less than the Porcupine experiment in which the ambient plasma density was $6 \times 10^5 \text{ cm}^{-3}$, or 30 times greater, we conjectured that future CIV experiments should have high ambient background plasma density. This was proven to be true in the CRIT II experiment carried out on May 4, 1989, from Wallops Island. In this experiment the ambient background density was $6 \times 10^5 \text{ cm}^{-3}$, and preliminary analysis indicates about 4% CIV ionization [Torbert, 1989; Stenbaek-Nielsen et al., 1989, 1990b].

On the positive side we were able to obtain the best alkali metal shaped-charge neutral velocity distribution as a function of radial angle from the detonation point and as a differential number of neutrals per unit velocity. We also calculated a solar UV ionization time constant for Sr of 1920 s (to 30%), which agrees with the observed ion inventory. If the Sr experiment had been carried out in high ambient electron density and produced 4% CIV ionization, the solar component would be negligible, but it is clear that future Sr CIV experiments should be carried out below the solar UV height. Such an experiment is planned for August 1990 from the CRRES satellite. On the other hand, Sr vapor releases in the distant magnetosphere or in the solar wind might have advantages over faster ionizing Ba or Eu to produce larger volumes of ions.

Acknowledgments. We thank the personnel of NASA Wallops Flight Facility and, in particular, Jay Brown, the payload manager, for payload fabrication and launch support. DuWayne Bostow was instrumental in managing the high-explosive shaped-charge components and in casting and machining the strontium metal liner. Gale Weeding of the Denver Research Institute made the high-explosive shaped charge. Bruce McKibben provided technical optical preparation and optical observations. We greatly appreciate the assistance of the U.S. Army Corps of Engineers in allowing the use of the Coastal Environmental Research Station at Duck, North Carolina. Walley Boquist of Technology International Corporation kindly furnished optical observations of the neutral Sr jet which were useful in determining the burst position and orientation. We thank John C. Foster of Millstone Hill Radar for help in providing radar coverage of the experiment and reduced data on background electron densities. Support for the University of Alaska Geophysical Institute was provided by grant NAG6-1 and NAGW-269 from NASA.

The Editor thanks two referees for their assistance in evaluating this paper.

REFERENCES

- Alfvén, H., *On the Origin of the Solar System*, Oxford University Press, New York, 1954.
- Alfvén, H., and G. Arrhenius, *Structure and Evolutionary History of the Solar System*, D. Reidel, Norwell, Mass., 1975.
- Banks, P. M., and G. Kockarts, *Aeronomy*, Academic, San Diego, Calif., 1973.
- Beckers, J. M., C. A. Bridges, and L. G. Gilliam, A high resolution spectral atlas of the solar irradiance from 380 to 700 nanometers, *Rep. AFGL-TR-0126*, Air Force Geophys. Lab., Bedford, Mass., 1976.
- Brenning, N., C.-G. Fälthammar, G. Haerendel, M. Kelley, G. Marklund, R. Pfaff, J. Providakes, H. C. Stenbaek-Nielsen, C. Swenson, R. Torbert, and E. M. Wescott, Interpretation of the electric fields measured in an ionospheric critical ionization velocity experiment, *J. Geophys. Res.*, in press, 1990.
- Danielsson, L., Review of the critical velocity of gas-plasma interactions, I, Experimental observations, *Astrophys. Space Sci.*, **24**, 459–485, 1973.
- Deehr, C. S., E. M. Wescott, H. C. Stenbaek-Nielsen, G. J. Romick, T. J. Hallinan, and H. Föppl, A critical velocity interaction between fast barium and strontium atoms and the terrestrial ionospheric plasma, *Geophys. Res. Lett.*, **9**(3), 195–198, 1982.
- Föppl, H., G. Haerendel, J. Loidl, R. Lüst, F. Melzner, B. Mayer, H. Neuss, and E. Rieger, Preliminary experiments for the study of the interplanetary medium by the release of metal vapor in the upper atmosphere, *Planet. Space Sci.*, **13**, 95–114, 1965.
- Haerendel, G., Alfvén's critical velocity effect tested in space, *Z. Naturforsch. A*, **37**, 728–735, 1982.
- Haerendel, G., H. Höfner, E. Rieger, and H. Föppl, Re-evaluation of the ion yield in a critical velocity experiment in the upper ionosphere, paper presented at 27th Plenary Meeting, Comm. on Space Res., Espoo, Finland, July 18–29, 1988.
- Hallinan, T. J., Observed rate of ionization in shaped-charge releases of barium in the ionosphere, *J. Geophys. Res.*, **93**, 8705–8712, 1988.
- Lütjens, P., Messung des Photoionisationsquerschnitts von BaI und SrI im Wellenlängenbereich 1700–2400 Å, *Z. Naturforsch. A*, **28**, 260–263, 1973.
- Michel, K. W., Verhalten der Ba-Ionenstrahlen ans Hohlladungen beim Nike-Tomahawk, *Rep. MPT-PAF 19*, Max-Planck-Inst. für Phys. und Astrophys., Garching, Federal Republic of Germany, 1969.
- Michel, K. W., Fluorescent ion jets for studying the ionosphere and magnetosphere, *Acta Astronaut.*, **1**(1–2), 37–69, 1974.
- Möbius, E., R. W. Boswell, A. Piel, and P. Henry, A Spacelab experiment on the critical ionization velocity, *Geophys. Res. Lett.*, **6**, 29–31, 1979.
- Newell, P. T., Review of critical ionization velocity effect in space, *Rev. Geophys.*, **23**, 93–104, 1985.
- Stenbaek-Nielsen, H. C., Calculated emission rates for barium releases in space, *Planet. Space Sci.*, **37**(11), 1441–1452, 1989.
- Stenbaek-Nielsen, H. C., E. M. Wescott, G. Haerendel, and A. Valenzuela, CRIT II: Optical observations of critical velocity ionization ions (abstract), *Eos Trans. AGU*, **70**(43), 1277, 1989.
- Stenbaek-Nielsen, H. C., E. M. Wescott, D. Rees, A. Valenzuela, and N. Brenning, Nonsolar UV produced ions observed optically from the "CRIT I" critical velocity ionization experiment, *J. Geophys. Res.*, **95**, 7749–7757, 1990a.
- Stenbaek-Nielsen, H. C., E. M. Wescott, G. Haerendel, and A. Valenzuela, Optical observations on the CRIT-II critical ionization velocity experiment, *Geophys. Res. Lett.*, **17**(10), 1601–1604, 1990b.
- Torbert, R., An overview of the CRIT II experiment (abstract), *Eos Trans. AGU*, **70**(43), 1277, 1989.
- Torbert, R. B., and P. T. Newell, A magnetospheric critical velocity experiment: Particle results, *J. Geophys. Res.*, **91**, 9947–9955, 1986.
- Wescott, E. M., H. C. Stenbaek-Nielsen, T. Hallinan, H. Föppl, and A. Valenzuela, Star of Lima: Overview and optical diagnostics of a barium Alfvén critical velocity experiment, *J. Geophys. Res.*, **91**(A9), 9923–9931, 1986a.
- Wescott, E. M., H. C. Stenbaek-Nielsen, T. Hallinan, H. Föppl, and A. Valenzuela, Star of Condor: A strontium critical velocity experiment, Peru, 1983, *J. Geophys. Res.*, **91**(A9), 9933–9938, 1986b.

D. Rees, Department of Physics and Astronomy, University College, Gower Street, London WC1E 6BT, England.

H. Stenbaek-Nielsen, D. W. Swift, and E. M. Wescott, Geophysical Institute, University of Alaska, Fairbanks, AK 99775.

A. Valenzuela, Max-Planck-Institut für Extraterrestrische Physik, 8046 Garching, Federal Republic of Germany.

(Received July 19, 1989;
revised April 12, 1990;
accepted May 21, 1990.)

OPTICAL OBSERVATIONS ON THE CRIT-II CRITICAL IONIZATION VELOCITY EXPERIMENT.

H.C. Stenbaek-Nielsen and E.M. Wescott

Geophysical Institute, University of Alaska Fairbanks

G. Haerendel and A. Valenzuela

Max Planck Institute for Extraterrestrial Physics

Abstract. A rocket borne Critical Ionization Velocity (CIV) experiment was carried out from Wallops Island at dusk on May 4, 1989. Two barium shaped charges were released below the solar terminator (to prevent photoionization) at altitudes near 400 km. The ambient ionospheric electron density was $5 \times 10^5 \text{ cm}^{-3}$. The neutral barium jet was directed upwards and at an angle of nominally 45 degrees to B which gives approximately 3×10^{23} neutrals with super critical velocity. Ions created by a CIV process in the region of the neutral jet would travel up along B into sunlight where they can be detected optically. Well defined ion clouds (max. brightness 750 R) were observed in both releases. An ionization rate of $0.8\% \text{ s}^{-1}$ (125s ionization time constant) can account for the observed ion cloud near the release field line, but the ionization rate falls off with increasing distance from the release. It is concluded that a CIV process was present in the neutral jet out to about 50 km from the release, which is significantly further than allowed by current theories.

Introduction.

The hypothesis of ionization through plasma processes was first presented by Alfvén (1954) as part of a theory for the formation of planetary systems. The hypothesis states that if a neutral gas is streaming across a background magnetic field with the cross field kinetic energy per atom greater than its ionization potential, the gas will ionize. In the literature these processes are termed Critical Ionization Velocity (CIV) processes. Recent reviews have been given by Newell (1985); Lai and Mauk (1989); and Torbert (1990).

A barium shaped charge is ideal for the study of CIV processes. It will create a high velocity neutral jet (figure 1), and when injected at a reasonably large angle to B, roughly half of the neutral atoms in the jet will have kinetic energies in excess of the ionization energy. In sunlight, both ions and neutrals can be detected optically from the ground.

The CRIT-II CIV rocket experiment was carried out from Wallops Island at dusk on May 4, 1989. It carried 2 barium shaped charges and was a follow-on to the CRIT-I experiment (Torbert, 1990; Stenbaek-Nielsen et al., 1990).

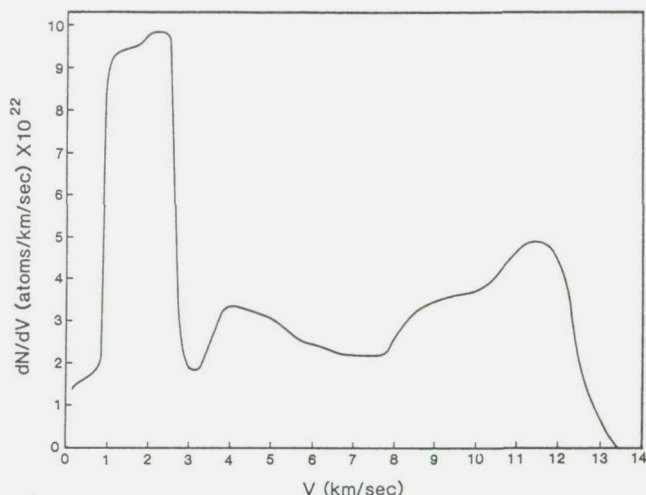


Fig 1. Differential velocity distribution for the neutral barium jet. The ordinate scale is assuming a vaporization of 15% of the barium liner in the shaped charge.

Like in the "Porcupine" experiment (Haerendel, 1982) CRIT-II was carried out in a high electron density ionosphere ($5 \times 10^5 \text{ cm}^{-3}$) and enhanced ionization resulted.

The morphology of the two CRIT-II releases was very similar. Thus, without loss of generality, the presentation can be restricted to data from the first release.

Release geometry and optical data.

The release was made below the terminator to prevent photoionization competing with the CIV process. The direction of the barium jet was towards the east at an elevation angle of about 20 degrees giving an angle to B of 57 degrees. (Due to a problem in the attitude control system the planned 45 degrees to B was not achieved). The release resulted in an estimated 3×10^{23} neutral atoms with super critical velocity. The ions formed from the neutral barium moved up along B into sunlight, where they were detected optically. The release geometry is illustrated in figure 2. The release took place at 37.162N, 73.895W and at an altitude of 422 km. The distance to the terminator was about 100 km, and the first ions would reach sunlight about 12 seconds after release.

In this letter we will concentrate on barium ion observations made at 4554A with an imaging photon detector (IPD) from Duck N.C. (36.182, 75.751W) during the first minute after the first release. Figure 3 and 4 (left column) shows a sequence of 5 second integration images.

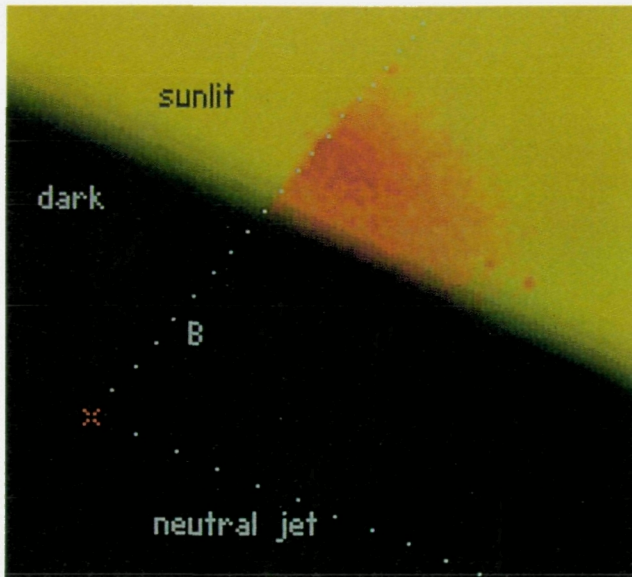


Fig 2. Release geometry as viewed from Duck, N.C.. The terminator is calculated in the plane of the jet and the magnetic field. The position of the release is shown by the cross and the directions of the neutral jet and the magnetic field are indicated with points 10 km apart. The sunlit ioncloud is red.

The view geometry is given in figure 2. The background has been subtracted from the images, and the images have been color encoded for emphasis. The observed ion cloud has a maximum brightness of 750 R, and is stretching from the release field line in the direction of the neutral jet. The number of ions contributing to the observed ion cloud is of the order of 5×10^{21} ions. Some luminosity along the path of the neutral jet below the solar terminator is present, but its origin is at present not understood.

Model image calculation.

In order to better evaluate the observations a computer program has been developed to simulate the observed images. The optical emissions from the ion cloud are from resonance scattering of sunlight. The ions are moving at velocities up to 13.5 km/s, which will Doppler shift the resonances within the narrow, deep Fraunhofer absorption lines in the solar spectrum at the main barium ion resonances. This causes the emission rates to be velocity dependent. The ion emission rates for the release have been calculated following the general evaluation of the problem by Stenbaek-Nielsen (1989) and are similar to those for the CRIT-I experiment given there.

The field aligned barium ions are first observed very close to the terminator. Therefore, in addition to the velocity dependence, the ion emission rate will also be affected by atmospheric absorption of the sunlight illuminating the ion cloud. In the model this has been quantified by calculating the relative absorption as function of screening height (the minimum altitude of ray path from the Sun). The calculation assumes a 0.5 degree solar disk shining through the 1965 US Standard Atmosphere

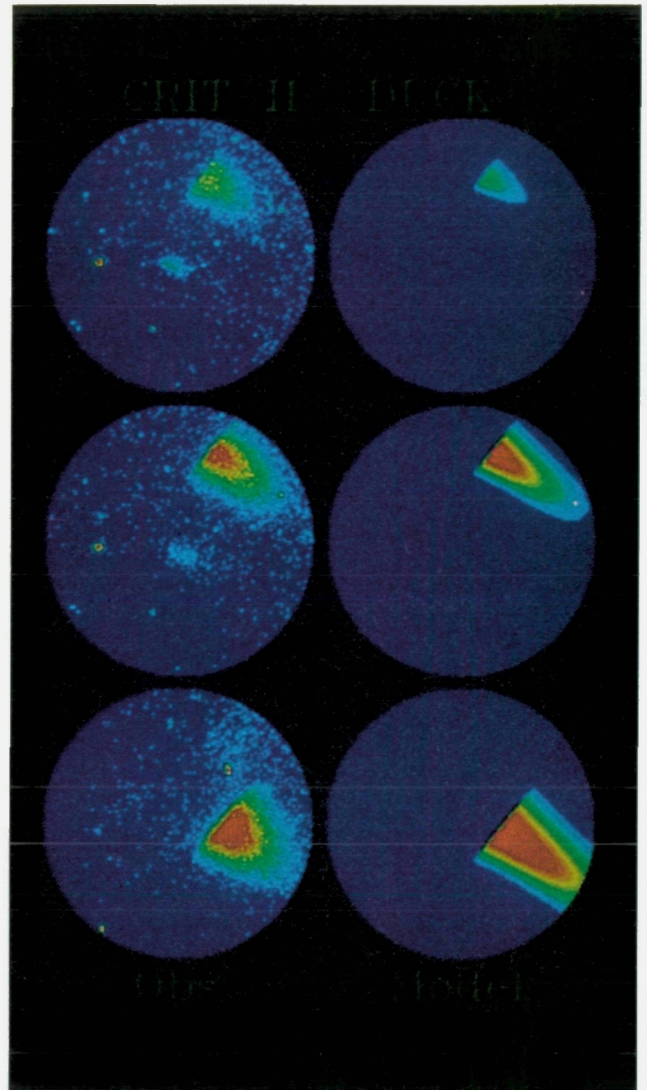


Fig 3. Comparison of observed (left) and model (right) images. Each set of images covers a 5 second period at 13-17 s, 19-23 s and, 25-29 s after release respectively. (The first ions appear above the terminator at 12 seconds after release). The model images were calculated assuming a constant ionization rate of $0.8\%s^{-1}$.

(ESSA-NASA-USAF, US Government Printing Office, Washington, D.C., 1966) over a spheroid Earth and an extinction rate at 4554A of 0.28 (Guttman, 1968).

The release point and the direction of the neutral jet was established by triangulation. The velocity and angular distribution functions for the neutral jet is given in figure 1 and by Stenbaek-Nielsen et al. (1990) and Wescott et al. (1990). The direction and magnitude of the magnetic field at the release is derived from IGRF(1985). The ionization process is assumed not to affect energy and momentum significantly; thus, the ions, when formed, will move up along B with the velocity component parallel to B. A significant simplification of the model calculations is obtained by the assumptions of no magnetic field curvature, no gravity, and no grad B effect (i.e. no mirror force). These assumptions are all quite reasonable when

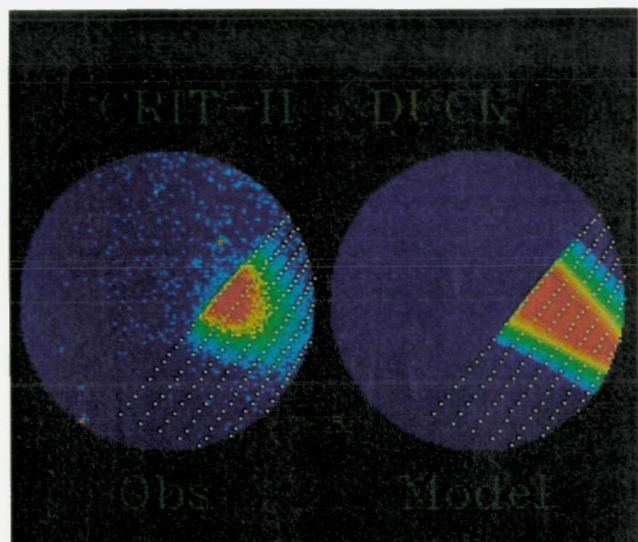


Fig 4. Observed and model images (31-35s from release) with B traced from the neutral jet tip position at 1 seconds (13.5 km) intervals.

the modelling is restricted to relatively short times and distances from the release, as is the case here.

Given an ionization rate the number of ions, their velocities and optical emissions can be calculated at any point in space and time, and by integrating along the line of sight the cloud brightness may be derived. In the model the ion cloud brightness is calculated with the 256x256 pixel image resolution of the observed IPD images. The model images are calculated for a given time, and to simulate the observed 5 second integration IPD images, images were calculated with one second resolution and then averaged.

The only free parameter in the calculation is the ionization rate, which can be determined by comparing the model images with the observations. The maximum brightness in both synthetic and observed images is along the release field line and will be equal for an ionization rate in the model of $0.8\%/s$ corresponding to an ionization time constant of 125 s (figures 3 and 4, right column).

Discussion.

The observed and simulated images agree well in the two first frames. However, in the third image (25-29 s after release) the model predicts the "tail" of the ion cloud to stretch further away from the release field line than was actually observed. While the observations were made tens of seconds after the release as the ions appeared in sunlight 100 km above the release, the ionization itself took place within seconds of the release in the neutral jet on the field line conjugate to the observations. To evaluate the time history of the ionization process we have in figure 4 inserted the field line through the tip of the neutral jet at 1 s intervals. (The tip of the neutral jet has a velocity of 13.5 km/s). It is seen that the observed ionization falls off after a few seconds; thus the ionizing process is only present in the neutral jet near the release.

To further explore the distribution of the ionization, figure 5 shows intensity traces taken across B at the

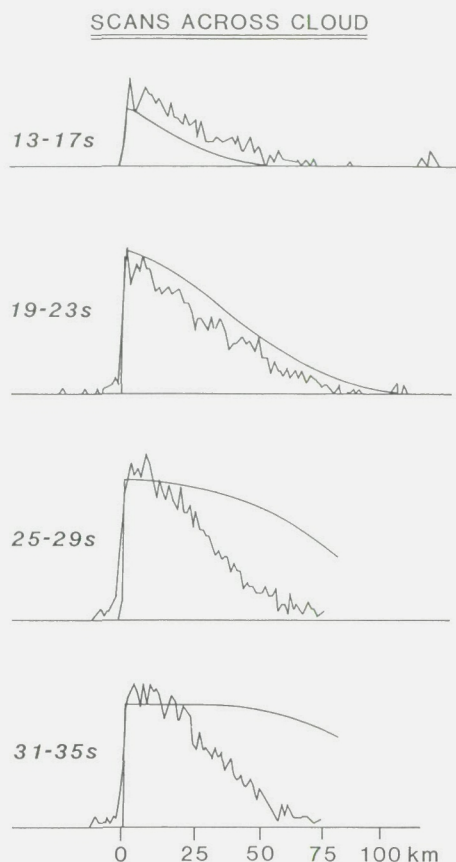


Fig 5. Relative intensities from the observed and model images shown in figures 3 and 4. The traces are taken across B nearly along the maximum intensity in the ion cloud. The smooth line is from the model images. The scale on the abscissae is the distance from the release along the neutral jet.

intensity maximum. While the traces agree for the early frames, the later frames indicate the ionization to be confined primarily to within about 75 km. The difference in amplitude between observed and model traces is primarily due to the model images being calculated to the nearest whole second and thus is not significant.

Traces along B, figure 6, show good agreement between observations and model for the scans 3 km from the release field line. Thus, the ionization process is not velocity (energy) dependant over the range of velocities present in these images. This is as expected since the ionization is assumed due to hot CIV electrons which would ionize any neutral barium atom in their path.

60 km from the release field line the observed brightness is only about 25% of the model prediction indicating a decrease in the ionization rate to $0.2\%/s$. These ions are from neutrals with velocities in excess of 8.4 km/s where ionization can take place by collisions between the neutrals and the ambient atmosphere (stripping). Data from the CRIT-I experiment (Stenbaek-Nielsen et al., 1990) indicate a stripping cross section of $9 \times 10^{-18} \text{ cm}^2$, which, with an ambient density of the order of $2 \times 10^8 \text{ cm}^{-3}$ (Hedin, 1987), results in an ionization rate of $0.2\%/s$ in good agreement with the observations.

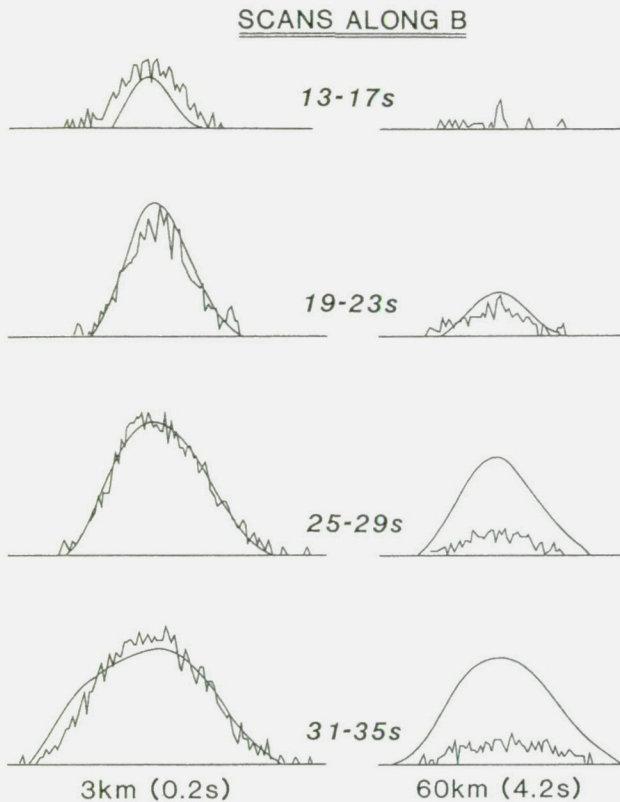


Fig 6. Relative intensities from the observed and model images shown in figures 3 and 4. The traces are taken along B at a distance of 3 km (left column) and 60 km (right column) from the release.

Conclusion.

The initial analysis of the optical data indicates that enhanced ionization took place in the neutral jet near the release. The ionization rate near the release is $0.8\%s^{-1}$, which includes collisional ionization at $0.2\%s^{-1}$, leaving $0.6\%s^{-1}$ (170 s ionization time constant) to some process other than classical collisional processes. Given the in situ observations of energetic electron fluxes (Torbert, 1989), we believe the process is a CIV process. Although current CIV theories can explain this amount of ionization (Torbert, 1988), they predict the ionization to be confined to within, at the most, 10 km of the release. Beyond this distance the densities would be so low that the hot electrons would escape without causing any ionization and therefore not able to sustain the CIV process. However, the observations clearly show CIV ionization to greater distances, as was also the case in the "Porcupine"

experiment (Haerendel, 1982), and this presents a challenge to our understanding of the process.

Acknowledgements: The Geophysical Institute, University of Alaska Fairbanks, acknowledge the support by NASA grant NAG6-1, and the US Army Corps of Engineers for the support of their Coastal Environmental Research Station at Duck, N.C.

References.

- Alfvén, H., *On the origin of the solar system*, Oxford University Press, New York, 1954.
- Guttman, A., Extinction coefficient measurements on clear atmosphere and thin cirrus clouds, *Appl. Optics*, 7, 2377, 1968.
- Haerendel, G., Alfvén's critical effect tested in space, *Z. Naturforsch. A*, 37, 1042, 1982.
- Hedin, A.E., MSIS-86 thermospheric model, *J. Geophys. Res.*, 92, 4649, 1987.
- Lai, S.T., and E. Mauk, Critical ionizations velocity experiments in space, *Planet. Space Sci.*, 37, 865, 1989.
- Newell, P.T., Review of critical ionization velocity in space, *Revs. Geophys.*, 23, 93, 1985.
- Stenbaek-Nielsen, H.C., Calculated emission rates for barium releases in space, *Planet. Space Sci.*, 37, 1441, 1989.
- Stenbaek-Nielsen, H.C., E.M. Wescott, D. Rees, A. Valenzuela, and N. Brenning, Non-solar UV produced ions observed optically from the CRIT-I critical velocity ionization experiment, *J. Geophys. Res.*, 95, 7749, 1990.
- Torbert, R.B., Critical velocity experiments in space, *Adv. Space Res.*, 8, 39, 1988.
- Torbert, R.B., An overview of the CRIT II experiment (abstract), *EOS*, 70, 1277, 1989.
- Torbert, R.B., Review of ionospheric CIV experiments, *Adv. Space Res.*, 10, 7, 1990.
- Wescott, E.M., H.C. Stenbaek-Nielsen, D.W. Swift, A. Valenzuela and D. Rees, SR90, Strontium shaped-charge critical ionization velocity experiment, *J. Geophys. Res.*, (in press) 1990.

H.C. Stenbaek-Nielsen and E.M. Wescott, Geophysical Institute, University of Alaska Fairbanks, Alaska 99775-0800, USA.

G. Haerendel and A. Valenzuela, Max Planck Institute for Extraterrestrial Physics, Garching B. Munchen, FRG.

(Received: April 17, 1990;

Accepted: May 24, 1990.)

Interpretation of the Electric Fields Measured in an Ionospheric Critical Ionization Velocity Experiment

N. BRENNING,¹ C.-G. FÄLTHAMMAR,¹ G. HAERENDEL,² M. C. KELLEY,³ G. MARKLUND,¹ R. PFAFF,⁴
 J. PROVIDAKES,⁵ H. C. STENBAEK-NIELSEN,⁶ C. SWENSON,³ R. TORBERT,⁷ AND E. M. WESCOTT⁶

This paper deals with the quasi-dc electric fields measured in the CRIT I ionospheric release experiment, which was launched from Wallops Island on May 13, 1986. The purpose of the experiment was to study the critical ionization velocity (CIV) mechanism in the ionosphere. Two identical barium shaped charges were fired from distances of 1.99 km and 4.34 km towards a main payload, which made full three-dimensional measurements of the electric field inside the streams. There was also a subpayload separated from the main payload by a couple of kilometers along the magnetic field. The relevance of earlier proposed mechanisms for electron heating in CIV is investigated in the light of the CRIT I results. It is concluded that both the "homogeneous" and the "ionizing front" models probably apply, but in different parts of the stream. It is also possible that electrons are directly accelerated by a magnetic-field-aligned component of the electric field; the quasi-dc electric field observed within the streams had a large magnetic-field-aligned component, persisting on the time scale of the passage of the streams. The coupling between the ambient ionosphere and the ionized barium stream in CRIT I was more complicated than is usually assumed in CIV theories, with strong magnetic-field-aligned electric fields and probably current limitation as important processes. One interpretation of the quasi-dc electric field data is that the internal electric fields of the streams were not greatly modified by magnetic-field-aligned currents, i.e., a state was established where the transverse currents were to a first approximation divergence-free. It is argued that this interpretation can explain both a reversal of the strong explosion-directed electric field in burst 1 and the absence of such a reversal in burst 2.

1. INTRODUCTION

The CRIT I rocket was launched from Wallops Island, Virginia, on May 13, 1986. The purpose was to study Alfvén's critical ionization velocity (CIV) phenomenon by means of injecting high-velocity streams of barium in the ionosphere. For a review of such injection experiments on CIV, see *Newell* [1985]. In CRIT I, two injections were made at about 400 km altitude, both at an angle of 46° to the magnetic field but at different distances from the main payload.

Both bursts produced strong quasi-dc electric fields (i.e., varying on the time scale of the neutral barium streams), as well as wave activity at various frequencies, most notably a band above the lower hybrid frequency of the ambient plasma and narrower peaks associated with the gyrofrequencies of H^+ , He^+ , O^+ , and Ba^+ . Other observations were those of strong magnetic field fluctuations inside the barium stream, and enhanced particle fluxes of both ions and electrons at the subpayload, which was separated from the streams by a few kilometers along the magnetic field.

Different aspects of the CRIT I experiment are treated in separate papers. We here concentrate on the interpretation of the quasi-dc electric fields, measured inside the stream, in relation to

existing theories for CIV interaction. A key problem in these theories is to identify a mechanism which can transfer ion kinetic energy to the electrons. The results from CRIT I indicate that both the "ionizing front" and the "homogeneous" models for electron heating apply, but in different phases of the interaction. However, direct acceleration of electrons by magnetic-field-aligned electric fields, which is not included in any of these models, may also be involved. Beside the "CIV problem" of electron heating and ionization there is the "electrodynamical problem" of coupling between the ionized barium stream and the ambient ionosphere. The results from CRIT I show that this coupling can take a more complicated form than is usually assumed in CIV theories; strong magnetic-field-aligned electric fields and current limitation are probably important processes.

In the discussion of the different aspects of the interaction it is useful to keep the following broader scenario in mind (see Figure 1):

1. The energy source is a relatively well known neutral barium stream in the quiet ionosphere. Seed ionization by barium collisions with ambient ions and/or neutrals triggers the process.

2. The CIV mechanism heats the electrons, which leads to electron impact ionization of the neutral barium. The differential motion between the electrons and the barium ions makes the stream act as a three-dimensional, time-varying MHD generator.

3. The electromagnetic interaction between this generator and the ionospheric load determines the spatial structure and time variation of the electric field $E(r,t)$ and current density $I(r,t)$. The electric field and current system is in turn important for the CIV process and feeds back into the generator process.

4. Associated with the process are various waves. Some are "active" in the sense that they can influence the processes described above. For example, it has been proposed that lower hybrid waves can heat the electrons at the expense of directed ion

¹ Department of Plasma Physics, Royal Institute of Technology, Stockholm, Sweden.

² Max-Planck-Institut für extraterrestrische Physik, Garching, Germany.

³ Cornell University, Ithaca, New York.

⁴ NASA Goddard Space Flight Center, Greenbelt, Maryland.

⁵ MITRE Corporation, Bedford, Massachusetts.

⁶ Geophysical Institute, University of Alaska, Fairbanks.

⁷ Space Science Center, University of New Hampshire, Durham.

Copyright 1991 by the American Geophysical Union.

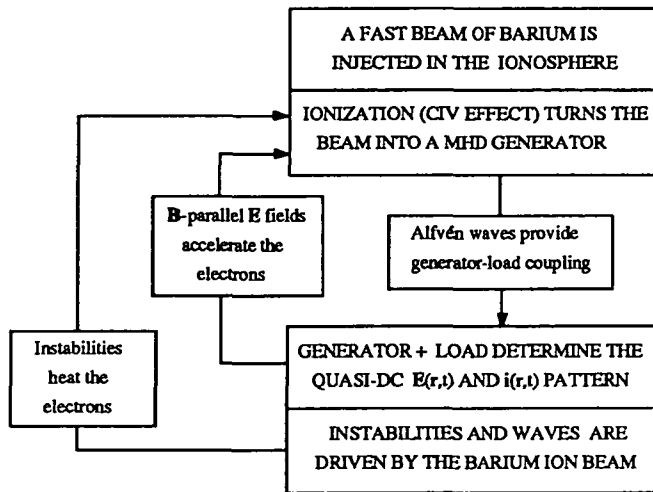


Fig. 1. Overview of the CRIT I problem complex. The interaction can be crudely split into two interlocking processes: (1) the CIV problem of electron ionization and electron impact ionization, and (2) the electrodynamic problem of coupling between the ionized barium stream "generator" and the ambient ionosphere.

energy [Raadu, 1978] and that Alfvén waves exchange momentum between the barium stream and the surrounding ionosphere [Haerendel, 1982]. Other waves are "passive" but still provide information about what is going on. For example, the observation of ion acoustic waves (R. F. Pfaff et al., Plasma waves observed at the leading edge of a heavy neutral/ion beam in the mid-latitude ionosphere, submitted to *Journal of Geophysical Research*, 1991; hereinafter Pfaff et al., submitted manuscript, 1991) indicates that the electrons are heated since these waves are damped unless $T_e > T_i$.

This paper is organized as follows. Section 2 contains the basic data and observations. Section 3 concentrates on the CIV problem: the mechanisms for electron heating and ionization. The electrodynamic problem of the electric coupling between the ionosphere and the barium stream is discussed in section 4, and section 5 contains a summary and discussion.

2. DATA PRESENTATION

Complete descriptions of the measurements are found in the companion paper by Kelley et al. [this issue], Brenning et al. [this issue], Stenbaek-Nielsen et al. [1990], Providakes et al. [1990], J. Providakes et al. (In situ and radar observations of ion cyclotron waves associated with two barium shaped charge releases, submitted to *Journal of Geophysical Research*, 1990; hereinafter Providakes et al., submitted manuscript, 1990), and Pfaff et al., submitted manuscript, 1991. The geometries of the releases are shown in Figures 2 and 3. The barium streams were produced by shaped-charge explosions, which ejected approximately 80 g of the vaporized barium in fast streams. The angle distribution was nearly Gaussian with the half width, half maximum cone angle 6.6° for velocities above 7.0 km/s, 10° - 11° for velocities between 7.0 and 3.5 km/s, and 21° - 24° for the lowest velocities. The explosions were aimed directly at the main payload, which was at a distance 1.99 kilometers from the explosion in burst 1 and 4.34 kilometers in burst 2. The subpayload was a few kilometers outside the stream along the

magnetic field and at a distance about half a kilometer from the stream across the magnetic field.

We will here mainly use electric field measurements from the main payload, which was oriented with the spin axis parallel to the barium stream, i.e., at 46° to the magnetic field. Two probe pairs measured the electric field component parallel to the spin axis, while three separate probe pairs measured the electric field perpendicular to that direction. The low-pass-filtered (500 Hz) electric fields in burst 1 are plotted in Figure 4 together with the neutral stream density and velocity. The arrows mark the time of burst, 358.51 s in flight time. The vertical dashed line marks the time 0.10 s after the burst, when a clear high-frequency band developed above the (ambient) lower hybrid frequency (Pfaff et al., submitted manuscript, 1991). During this first period of the interaction, which we call the precursor, the quasi-dc electric field was below 5 mV/m. The fastest (13 km/s) barium atoms arrived at the main payload during the precursor, at a time $L/V_{Ba} = 1.99/13 = 0.15$ s after the burst. A short time later, a large electric field directed towards the explosion rapidly grew, shown in the top panel of Figure 4. We call this the "towards pulse." In burst 1 there was also a pulse with reversed polarity, the "away pulse," with approximately the same strength and time duration as the towards pulse. Strong broadband noise was associated with the towards and away pulses, covering the frequency range from 5 Hz up to well above 1 kHz (Providakes et al., submitted manuscript, 1990). The dominating quasi-dc electric field components, in both the towards and the away pulses, fell along the direction of the stream. It is remarkable that the strong magnetic-field-aligned components $E_{||}$, which peaked at about 450 mV/m in the towards pulse and 600 mV/m in the away pulse, were not shorted out: they had a time duration of about 30 transit times, through the cloud along the magnetic field, of ambient ionospheric electrons.

The third panel in Figure 4 shows the perpendicular electric field in the $V_{Ba} \times B$ direction. The expected self-polarization field $E_p = -V_{Ba} \times B$ for a dense beam is also drawn for reference. The perpendicular field approached this value during the away pulse, but then dropped to a much lower value. In the later-arriving "slug" ($V_{Ba} < 2$ km/s, arriving later than 0.7 s after the burst), the magnetic-field-aligned component approached zero, while the perpendicular component (third panel) approached one third of the $-V_{Ba} \times B$ value 1.5 s after the burst.

The second burst is shown in Figure 5. Only the electric field component along the flow is included; both the other two components in this burst were both much smaller than the self-polarization field E_p . The burst time was 443.63 s. The vertical dashed line marks the onset of a precursor with the same frequency characteristics as in burst 1. As in the first burst, this precursor began 0.05 s before the arrival of the fastest (13 km/s) barium atoms (Pfaff et al., submitted manuscript, 1991). Also as in the first burst, a towards pulse developed at a slight delay with respect to the fastest barium atoms, and with no tendency to short-circuit along the magnetic field. There was no away pulse in burst 2.

At the time of burst 1, the CUPRI (Cornell portable radar interferometer) radar operated from Kennedy Space Center showed coherent 3-m waves located 100 km above the release along the same magnetic field line. This is interpreted

CRIT I May 13 1986
Magnetic Field Plane Projection
 Distances and angles to scale

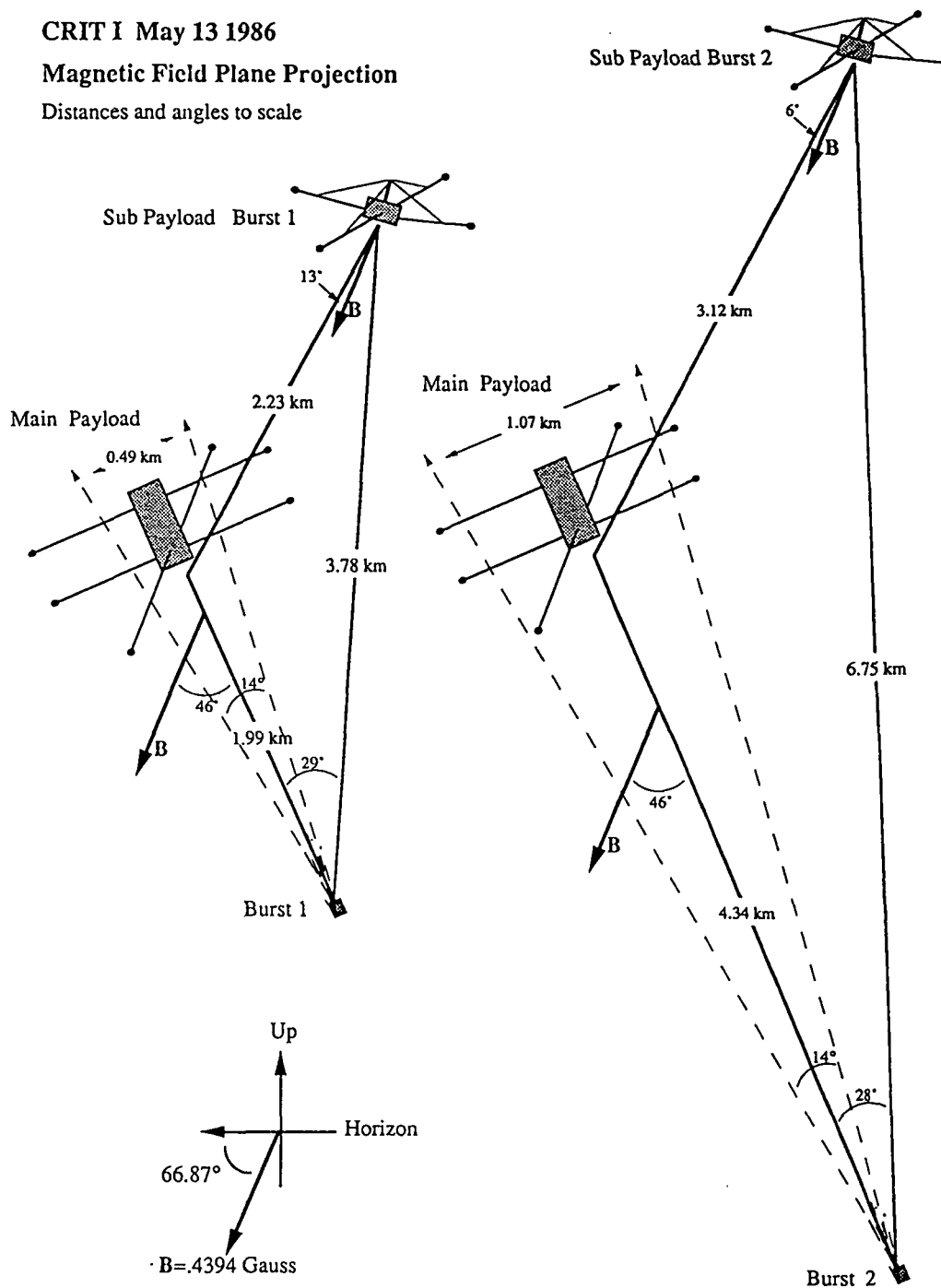


Fig. 2. The relative positions of the burst, the main payload, and the sub payload projected on the plane of the magnetic field and the burst direction.

[Providakes *et al.*, 1990] as electrostatic ion cyclotron (EIC) waves excited by magnetic-field-aligned currents. In burst 2 no such waves were observed, in spite of the fact that the shaped charges were intended to be identical.

The barium stream densities in Figures 4 and 5 were not measured directly in CRIT I but are taken from a similar shaped-charge explosion [Wescott *et al.*, 1990]. At a distance z from the explosion, the maximum density is reached approximately at a time $t_{\max} = 8 \times 10^{-5} z$ (in MKSA units). The value of this maximum decreases quickly with z :

$$n_{Ba, \max} = 9 \times 10^{24} z^{-3} \quad (1)$$

The neutral barium velocities in Figures 4 and 5 were calculated from the time of flight from the explosion point. This gives an accurate value of the velocity because the mean free path for neutral barium, for momentum loss in the ambient neutral gas, is several hundred km; consequently, the neutral barium streams expanded as into vacuum.

Ground-based TV cameras saw an extended cloud of ionized barium, produced below the solar UV terminator, which came up

CRIT I May 13 1986
 Perpendicular Magnetic Field Projection
 Distances to Scale

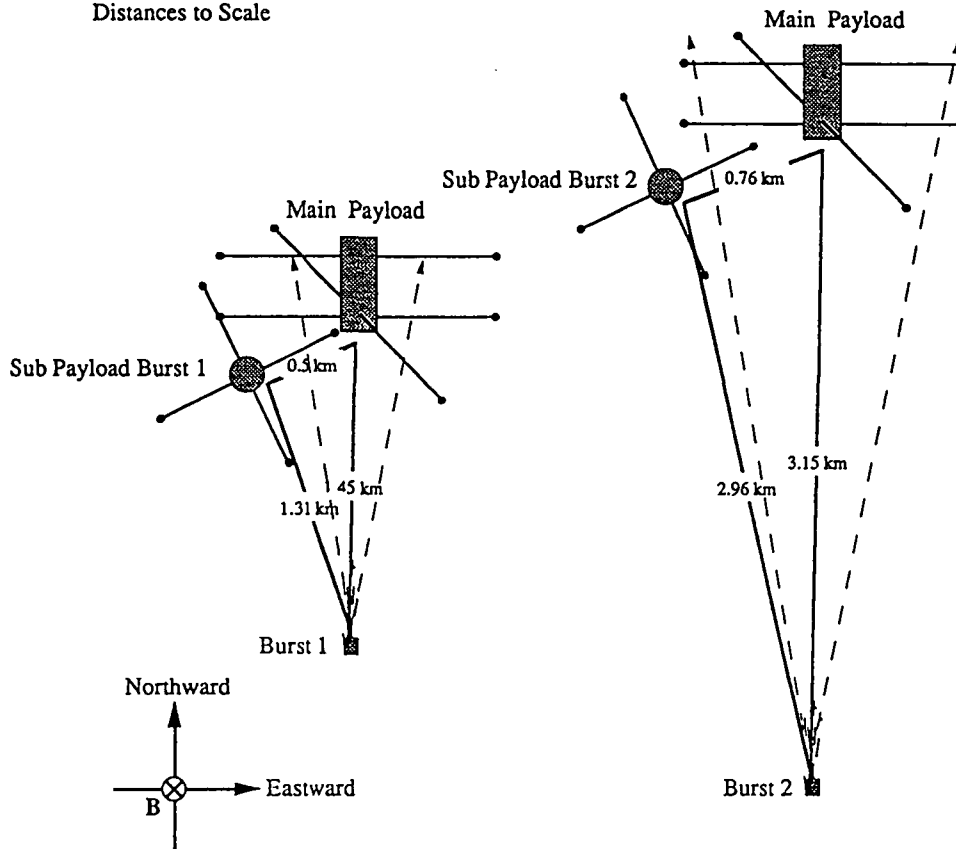


Fig. 3. The relative positions of the burst, the main payload, and the sub payload projected on the plane perpendicular to the magnetic field.

into the sunlight 5-10 s after the burst [Stenbaek-Nielsen *et al.*, 1990]. There was no prominent streak of ions along the field lines closest to the burst. Instead the observations could be well reproduced by a model which used a constant ionization time of 1800 s (an ionization rate of 0.06% per second). The total ionization of the fast jet (7-13 km/s) below the solar UV terminator would, using this constant ionization rate, be 0.2 - 0.3%. This places CRIT I in the category of low-yield CIV experiments, together with for example Star of Lima [Torbert and Newell, 1986].

Table 1 summarizes the parameters for the experiment. The magnetic field at Wallops Island, at 400 km altitude, is 0.44×10^{-4} T, and the dip angle is 67° . The ambient neutrals at 400 km are mainly atomic oxygen. For CRIT I, a density $n_n = 4 \times 10^{13} \text{ m}^{-3}$ has been calculated using a neutral model of A. Hedin. The plasma density is somewhat uncertain. The Millstone Hill incoherent scatter radar gave $n_e = 6 \times 10^{10} \text{ m}^{-3}$, while the on-board instrument gave a lower value, $n_e = 3 \times 10^{10} \text{ m}^{-3}$. The on-board instrument, however, did not give a measurement until a time 1.5 s after the second burst. We will here use the radar value, because that measurement gave the plasma density both at the burst and 100 km above the burst. Both these values will be used below, and the radar is therefore preferable for internal consistency. The electron impact ionization rates in Table 1 are

calculated from the cross section measured by Vainshtein *et al.* [1972].

3. THE CIV PROBLEM: ELECTRON HEATING AND IONIZATION

Two different models have earlier been proposed [Haerendel, 1982] for ionospheric CIV experiments, the homogeneous model and the ionizing front model. The homogeneous model builds on a theory by Sherman [1969] and Raadu [1978] for laboratory CIV experiments. The electrons are heated by the modified two-stream instability (MTSI), which is driven by the relative motion, across the magnetic field, between the electrons and the newly ionized neutrals. The efficiency of the process is denoted by the energy transfer factor η , which is the fraction of the new ion's kinetic energy $m_n v^2/2$ that goes to the electrons. Different theoretical estimates of η [Raadu, 1978; Galeev and Sagdeev, 1983; McBride *et al.*, 1972] put η somewhere in the range 0.25 - 0.67.

If the η value is known, it is possible using the homogeneous model to follow the development of the CIV process in time by solving the coupled equations of energy, momentum, and particle balance. In the plasma rest frame, the energy equation is

$$\frac{d(n_e W_e)}{dt} = \eta \frac{m_n v^2}{2} (v_{\text{seed}} + \langle \sigma_i v_e \rangle n_n) - e U_i \langle \sigma_i v_e \rangle n_n + \text{other terms.} \quad (67)$$

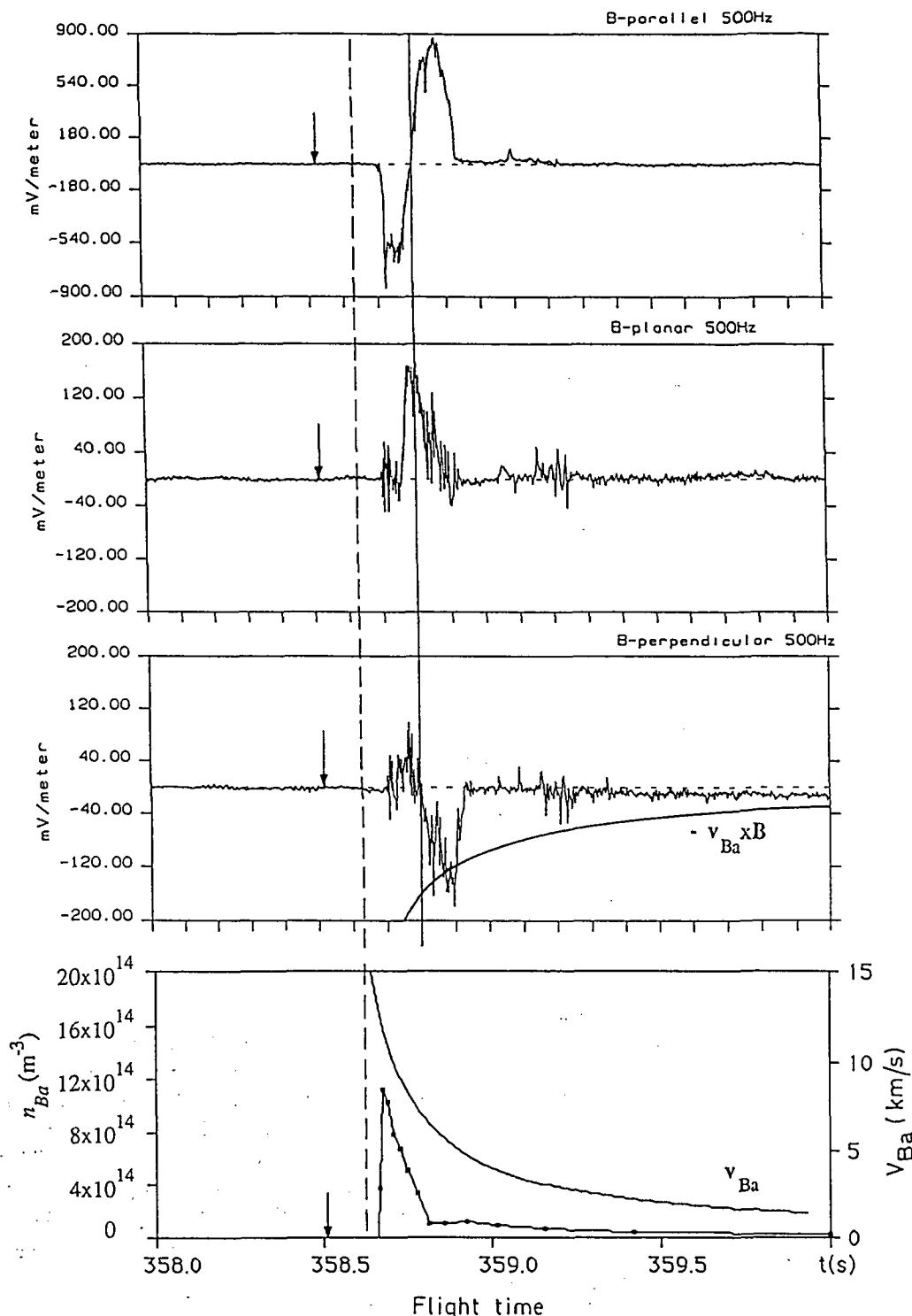


Fig. 4. The measured electric field at the main payload in burst 1: (top) the E_z field component along the direction of V_{Ba} , (second panel) the $-E_x$ component along $(V_{Ba} \times B) \times V_{Ba}$, and (third panel) the $-E_y$ component along $V_{Ba} \times B$. For reference, the expected "self-polarization field" $E_p = -V_{Ba} \times B$ is drawn in the third panel. (Bottom) The neutral stream density and velocity at the main payload. The arrows mark the time of the burst, and the dashed line marks the arrival time of the precursor.

Here, W_e is the average electron energy, and $V = (V_n - ExB/B^2)_{perp}$ is the velocity component across B of the neutrals relative to the plasma within the stream. The "other terms" are for example electron energy loss through line excitation and loss of energetic electrons along the magnetic field.

The velocity of the plasma within the stream is determined by the pickup of new ions and by the momentum coupling to the

ambient plasma; this coupling is, in the homogeneous model [Haerendel, 1982; Goertz and Machida, 1985; Torbert, unpublished manuscript, 1987] assumed to be through shear Alfvén waves as schematically shown in Figure 6. Inside the stream there is a partial self-polarization field, directed in the $E_p = -V_n \times B$ direction, which launches Alfvén waves in both directions along the magnetic field. The $j \times B$ force in the Alfvén

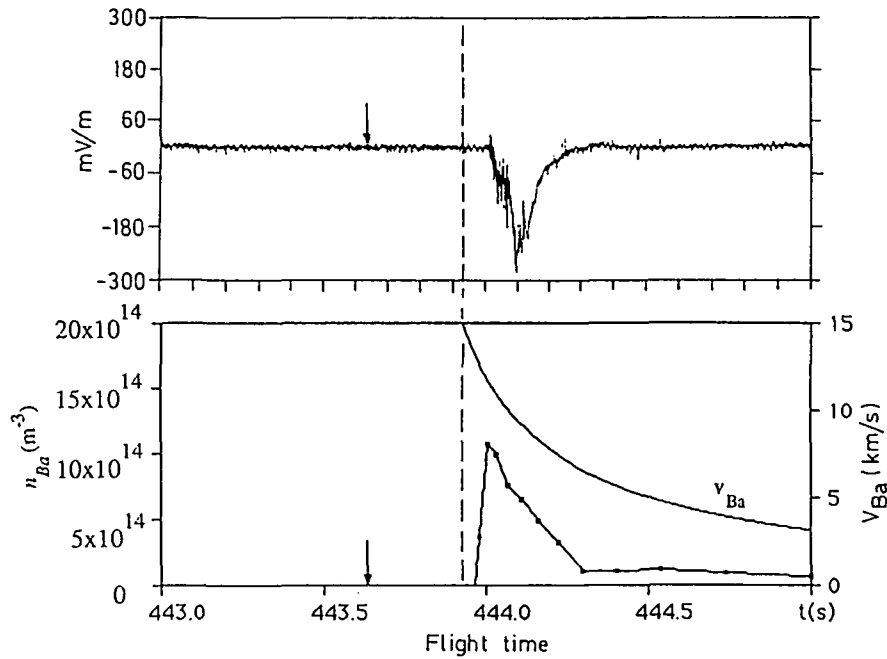


Fig. 5. The measured electric field component along the direction of V_{Ba} in burst 2, and the neutral stream density and velocity at the main payload. The arrows mark the time of the burst, and the dashed line marks the arrival time of the precursor.

wave front, where the magnetic-field-aligned currents close, accelerates the ambient plasma in the direction of the neutral jet, while the closure of the current inside the jet brakes the plasma there. In the homogeneous model the electric field takes such a value that momentum is conserved within the part of the flux tube

which extends out to the Alfvén wave front [Torbert, unpublished manuscript, 1987],

$$E_P = -v_{Ba} \times B \frac{\lambda_m}{1 + \lambda_m} \tag{3}$$

where λ_m is the mass-loading factor [Haerendel, 1982]

$$\lambda_m = \frac{dn_{Ba} + m_{Ba} \frac{L}{dt}}{4\rho_a V_A} \tag{4}$$

TABLE 1. Some Data for CRIT I.

Parameter	Value
Ambient Ionosphere	
Magnetic field	$B = 0.44 \times 10^{-4} \text{ T}$
Neutral density	$n_n = 4 \times 10^{13} \text{ m}^{-3}$
Plasma density (400 km)	$n_e = 6 \times 10^{10} \text{ m}^{-3}$
Plasma density (500 km)	$n_e = 2.2 \times 10^{10} \text{ m}^{-3}$
Alfvén velocity (400 km)	$V_A = 10^6 \text{ m/s}$
Lower hybrid frequency	$\omega_{LH}/2\pi = 6.3 \text{ kHz}$
Barium Stream	
Main payload - burst 1	$z_1 = 1.99 \text{ km}$
Main payload - burst 2	$z_2 = 4.34 \text{ km}$
Extent along B ($\Phi_{half} = 7^\circ$), burst 1	$L_{ } = 700 \text{ m}$
Extent along B ($\Phi_{half} = 7^\circ$), burst 2	$L_{ } = 1500 \text{ m}$
Barium mass	$m_{Ba} = 137.34 \text{ AU}$
Barium ionization energy	$U_i = 5.19 \text{ eV}$
Barium critical velocity	$V_c = 2.7 \times 10^3 \text{ m/s}$
Barium gyroradius ($7 \times 10^3 \text{ m/s}$)	$r_{gi} = 230 \text{ m}$
Barium energy ($7 \times 10^3 \text{ m/s}$)	$W_i = 35 \text{ eV}$
Cross Sections	
Charge exchange, $Ba + Ba^+$	$\sigma_{ch} = 2.6 \times 10^{-18} \text{ m}^2$
Stripping, $Ba + O \rightarrow Ba^+ + e + O$	$\sigma_{str} = 0.9 \times 10^{-22} \text{ m}^2$ ($V_{Ba} = 8.4 - 13 \text{ km/s}$)
Electron impact ionization, thermal electrons:	
$kT_e = 1 \text{ eV}$	$\langle \sigma_i V_e \rangle = 10^{-15} \text{ m}^3 \text{ s}^{-1}$
$kT_e = 2 \text{ eV}$	$\langle \sigma_i V_e \rangle = 1.7 \times 10^{-14} \text{ m}^3 \text{ s}^{-1}$
$kT_e = 3 \text{ eV}$	$\langle \sigma_i V_e \rangle = 5 \times 10^{-14} \text{ m}^3 \text{ s}^{-1}$
$kT_e = 5 \text{ eV}$	$\langle \sigma_i V_e \rangle = 1.2 \times 10^{-13} \text{ m}^3 \text{ s}^{-1}$
$kT_e = 10 \text{ eV}$	$\langle \sigma_i V_e \rangle = 2.5 \times 10^{-13} \text{ m}^3 \text{ s}^{-1}$

The ionizing front model was proposed by Piel *et al.* [1978] for CIV experiments in rotating plasma devices. Figure 7 shows the particle trajectories proposed by Piel *et al.* [1978], drawn in the plasma rest frame. The ionized neutrals overshoot from their electrons in the neutral flow direction and build up a space charge sheath with an electric field directed against the neutral stream. The thickness of the sheath is between the electron and ion gyroradii, and a lower limit to the potential Φ_0 across the sheath is given by the assumption that the ions are reflected by the electric field rather than by the Lorenz force, $e\Phi_0 \geq m_n V^2/2$. The electron Hall drift along the space charge sheath (across the neutral flow direction) drives the MTSI, which in turn heats the electrons.

The conservation of momentum along the neutral flow requires that a transverse current (the electron Hall current of the model) flows across the stream. In the laboratory experiments where this model was first proposed this current is driven by an external generator. In the present application the ionosphere has to replace the generator. The current has to close across the magnetic field somewhere in the ionosphere in order to transfer momentum between the two plasmas; the ionizing front model in its present form does not include this process.

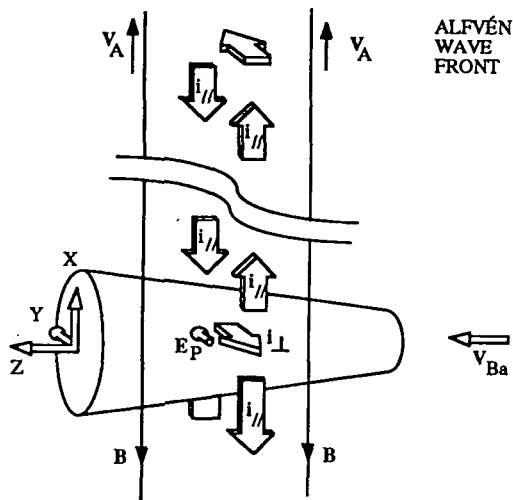


Fig. 6. The momentum coupling between the barium stream and the ambient ionosphere according to the homogeneous model.

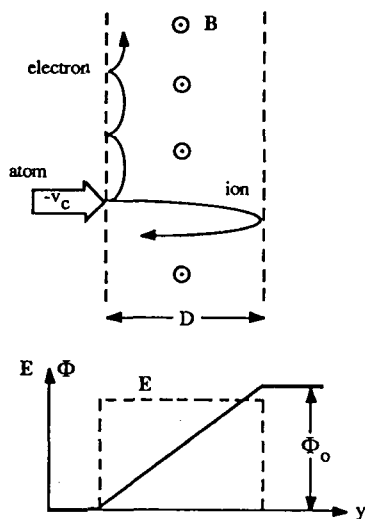


Fig. 7. The ionizing front model according to Piel et al., [1978].

The Precursors: "Homogeneous Model" CIV Interaction

Vertical dashed lines mark the arrival of the precursor waves at the main payload in Figures 4 and 5. In both bursts the precursor waves began about 0.05 s before the expected arrival of any barium atoms and continued until they were drowned in the strong broadband signal in the towards pulses. One possible explanation of the early start of the precursors is that the barium cloud would push before it a wave of neutral oxygen atoms that have collided elastically with the barium atoms. Due to the difference in mass between barium ($m = 137$ amu) and oxygen ($m = 16$ amu), the oxygen atoms would acquire velocities up to almost double the barium velocity. With a mean free path of several hundred kilometers in the ambient ionosphere, these atoms would not pile up into a shock front, but simply spread out ahead of the barium stream. The density of this neutral oxygen precursor can be estimated to be about 6% of the ambient neutral oxygen density in burst 1 and 1% in burst 2.

Resonant charge exchange of this neutral oxygen precursor against ambient O^+ ions would create fast O^+ ions ahead of the

barium stream. During a time about ω_{gi}^{-1} these ions would retain a beam character; the beam density would be about $5 \times 10^{-5} n_e$ in burst 1 and $10^{-5} n_e$ in burst 2. These densities are high enough to start driving the MTSI: the growth rate of the MTSI is $\gamma \approx \omega_{LH} (n_{stream}/n_e)^{1/3}$. Even such a low oxygen ion stream density as $10^{-5} n_e$ gives a MTSI growth time $\gamma^{-1} \approx 1$ ms. This is much shorter than the time duration of the precursor, and consequently the lower hybrid waves of the MTSI would have time to grow. However, the energy transfer from the O^+ precursors to the electrons cannot be very large: the O^+ ion would have at most a velocity about 20 km/s (which would result from a head-on collision with a barium atom). The energy per fast ion is therefore at most 33 eV. Even with a 100% efficient transfer to the electrons, the energy gain would be only 0.03 eV per electron in burst 1 and much less in burst 2.

A precursor with similar characteristics was seen in the earlier Star of Lima experiment [Kelley et al., 1986]. In contrast to CRIT I the precursor in Star of Lima occurred so long before the expected arrival of the neutral barium stream that it could not be driven by oxygen as discussed above. Wescott et al. [1986] suggest that the barium stream was preceded by material from 5 g of coating of vacuum grease on the surface of the barium cone. No such coating was used in the CRIT I experiment.

In both bursts the barium stream arrived at the main payload about 0.05 s after the onset of the precursor, and from this time, Ba^+ ions were added with a density that quickly exceeded that of the O^+ precursors discussed above. The ionospheric electron temperature was initially $kT_e = 0.1$ -0.3 eV. For such low temperatures, the dominating sources of Ba^+ ions are the "seeding" processes of charge exchange ($Ba + O^+ \rightarrow Ba^+ + O$) and stripping ($Ba + O \rightarrow Ba^+ + O + e^-$). In CRIT I, the combined seeding rate from these processes could be directly inferred from the optical observation [Stenbaek-Nielsen et al., 1990]:

$$\frac{dn_{Ba^+}}{dt} = n_{Ba} V_{Ba} (\sigma_{str} n_O + \sigma_{chex} n_{O^+}) = v_{seed} = \frac{n_{Ba}}{1800} \quad (5)$$

In CRIT I, equation (5) gives a higher Ba^+ production rate than electron impact ionization as long as the electron temperature is $kT_e \leq 1.7$ eV. This temperature can therefore be regarded as the ignition temperature for CIV interaction in this experiment. The electron heating according to the homogeneous model is given by (2). With V_{Ba} and n_{Ba} taken from Figures 4 and 5, $v_{seed} = n_{Ba}/1800$ according to (5), the "other terms" in (2) equal to zero, and $\eta = 0.5$, we can estimate the possible change in electron energy before the beginning of the towards pulses. In the precursor of burst 1 the result is $\Delta kT_e = 8$ eV. Thus the homogeneous model could well trigger CIV interaction during the precursor of this burst. In burst 2, the result is $\Delta kT_e = 1.5$ eV at the beginning of the towards pulse, which seems to be on the margin.

We conclude that the precursor oscillations agree well with the expected electron heating process of the homogeneous model: that the MTSI is driven first by a precursor of O^+ ions and then by a thin beam of barium ions. The observed weak quasi-dc electric field at the same time (an upper limit of 5 mV/m) also agrees with this interpretation; during the triggering phase, the momentum coupling of the homogeneous model (equations (3)

and (4), with (5) used for dn_{Ba}/dt gives an electric field below 5 mV/m in both bursts.

The Towards Pulses: "Ionizing Front Model" CIV Interaction

The towards pulses have many similarities to the ionizing front model by Piel et al. [1978]. The direction of the electric field was against the neutral flow, as in the model. Assuming that the observed electric field was caused by a steady structure which swept past the main payload with the velocity of the neutral stream, the potential across the towards pulse was about 400 V in burst 1, and about 200 V in burst 2. These values satisfy the condition $e\Phi_0 \geq m_n v^2/2$ for the ionizing front potential: the neutral barium velocities in the towards pulses lie in the range 7 - 12 km/s, corresponding to energies 35 - 100 eV.

Some calculated ion trajectories in the quasi-dc electric fields in burst 1 are shown in Figure 8. The towards and away pulses are for this calculation approximated by a one-period-long sinusoidal waveform in space which sweeps past the payload with the neutral barium velocity at the zero crossing between the towards and away pulses, 7 km/s. Inside the barium stream, the electric field is taken to be directed purely along the z direction. Outside the width of the fast part of the barium stream, $\pm 7^\circ$, the electric field is put equal to zero. The point of ionization is marked by an open circle; the ions in the figure are all added at 0.29 s after the burst, which is the time of the zero crossing between the towards and away pulses at the main payload. Each ion starts with a velocity determined by the time of flight from the burst point and is followed until its z coordinate becomes smaller than the z coordinate of the zero crossing between the towards and away pulses. The trajectories are terminated by two points, 5 ms apart, in order to give a measure of their velocity at that time. As far as individual ion motion is concerned, there is a good resemblance between these trajectories and those of the ionizing front model (Figure 7): the two important points are that the ions are inside the towards pulse long enough to turn around in the z direction but not long enough to pick up the $E \times B/B^2$ drift velocity in the +y direction. The same calculation for burst 2 (not shown here) shows that both these conclusions hold also in the towards pulse of that burst, with the difference that there is a stronger element of gyration in the orbits.

In the towards pulses of CRIT I the electrons Hall drift across the neutral flow. This is the drift which in the ionizing front model drives the MTSI in the y direction. According to Papadopoulos [1984], the MTSI produces a high-energy tail to the electron velocity distribution, where the velocity of the most energetic electrons is proportional to the drift velocity, here $V_D = (E \times B)/B^2$:

$$V_{max} = 2.5 \sqrt{\frac{m_i}{m_e}} V_D \tag{6}$$

For the CIV process to operate, at least these most energetic electrons must be able to ionize:

$$\frac{m_e V_{max}^2}{2} > eU_i \tag{7}$$

In CRIT I, this condition is satisfied if the electric field exceeds $E_z = 58$ mV/m. Such was the case in the towards pulses of both bursts.

There are also some discrepancies between the ionizing front model and the CRIT I observations. The space charge sheath in the ionizing front model is stationary in the plasma frame and moves through the neutral gas. The time shift between the appearance of the towards pulses in burst 1 and burst 2 indicates that in CRIT I, the sheath instead followed the neutral barium stream through the ambient plasma. The k vector of the wave field would according to the ionizing front model be expected to point predominantly in the direction of the relative drift, i.e., transverse to the neutral stream. The analysis of the wave data in the towards pulses [Kelley et al., this issue] shows that this is not the case: the waves are more or less isotropic for frequencies about the lower hybrid frequency. Also, there was no predominant peak at the lower hybrid frequency.

In this discussion of the precursors and the towards pulses we have concentrated on the MTSI for the reason that earlier theories on CIV centered on this instability. Our conclusion is that the MTSI probably was excited in the precursor phases of the two bursts, while its presence in the main interaction during the towards pulses still is an open question. The possible absence of the MTSI does not mean that the ionizing front model should be discarded as the main candidate for the towards pulses, since some other wave-particle interaction could take the place of the

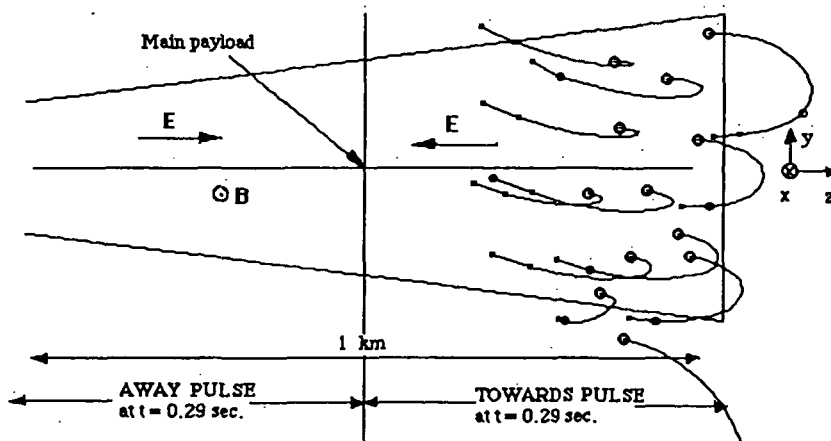


Fig. 8. Some ion trajectories inside the towards pulse of burst 1.

MTSI in the CIV process and transfer energy to the electrons. In CRIT I a wealth of plasma waves were excited, which are treated in the companion papers by Kelley et al. [this issue], Providakes et al. [submitted manuscript, 1990], and Pfaff et al. [submitted manuscript, 1991].

The Parallel Fields Model

There is a third possibility to energize electrons in CRIT I. The axial electric field in burst 1 (the top panel of Figure 4) indicates that a sequence of positive-negative-positive space charge swept past the main payload as shown in Figure 9. Consider the electrons that are drawn from the ambient plasma, along the magnetic field, to the positive space charges in the front of the towards pulse. A first estimate of the magnetic-field-aligned current density is obtained from the Alfvén conductivity [Mallinckrodt and Carlson, 1978]. We denote this value by $i_{\parallel A}$:

$$i_{\parallel A} = \frac{1}{\mu_0 V_A} \text{div } E_{\text{perp}} \quad (8)$$

At the rising flank of the towards pulse in burst 1, $i_{\parallel A}$ would exceed the ambient electron random current by a factor of 4. Such large current densities are not likely to be reached. Some process would probably limit the current to a lower value. Figure 9 shows schematically how the electric field could extend into the surrounding plasma if there is a strong limitation of the magnetic-field-aligned current to the positive space charges. At the negative space charge, about the zero crossing between the towards and the away pulses, we assume that the surplus of electrons can adjust rather easily along the magnetic field so that $E_{\parallel} \approx 0$. The electrons do not have to move out to infinity to achieve this: a displacement a few times the width of the barium stream is enough. Local magnetic-field-aligned potential drops would therefore arise predominantly at the positive space charges; in these regions, ambient electrons could gain energy directly from the electric field without involving any instability. With respect to the ambient ionosphere, the barium stream would act as a negatively grounded generator. This "negative ground

effect" of a polarized plasma stream is well known from laboratory experiments, [e.g., Lindberg, 1978]. The electric field pattern of Figure 9 would automatically cause a limitation of the parallel current below the value $i_{\parallel A}$ given by (8), since the mapped-out electric field E_{perp} in the distant ionosphere would be reduced.

In one important respect this electron acceleration along the magnetic field is different from the electron heating of the homogeneous model. In (2), the electron energy is calculated locally in each volume of plasma from the local ionization of the neutral stream, using an efficiency factor η . The limiting case $\eta = 1$ puts a strict upper limit on the electron temperature at any given time and place. The electron acceleration to the positive space charge in Figure 9 is not local in this sense: the electrons gain energy in a potential structure which is maintained collectively by the ionization in a larger volume of plasma. Such a mechanism could enable energy, which is released by electron impact throughout the volume, to be used for electron heating in the front of the neutral stream. In CRIT I, the evidence for this type of electron acceleration along the magnetic field is only indirect: the observed existence of strong magnetic-field-aligned components in the quasi-dc electric fields, and the early end of the precursor phase in burst 2, which indicates that some extra heating process operated at that time.

Even a rather small increase in the electron temperature T_{e0} at the front of the stream can have a large effect on the net ionization according to a computer model for ionospheric CIV experiments by Torbert [1990]. This is best illustrated by an example: let us assume that the magnetic-field-aligned current to the leading flank of the towards pulse is $i_{\parallel} = 0.06 \text{ mA/m}^2$. This is only a few percent of the current $i_{\parallel A}$ according to (8). The current flows from both directions along the magnetic field and delivers energy to the stream at a rate $2 i_{\parallel} U / L_{\parallel}$ ($\text{J m}^{-3} \text{ s}^{-1}$), where U is the potential drop along the magnetic field and L_{\parallel} is the extent of the stream along the magnetic field. At a value $U = 10 \text{ V}$ (which is only a small fraction of the total potential drop, 400 V, across the

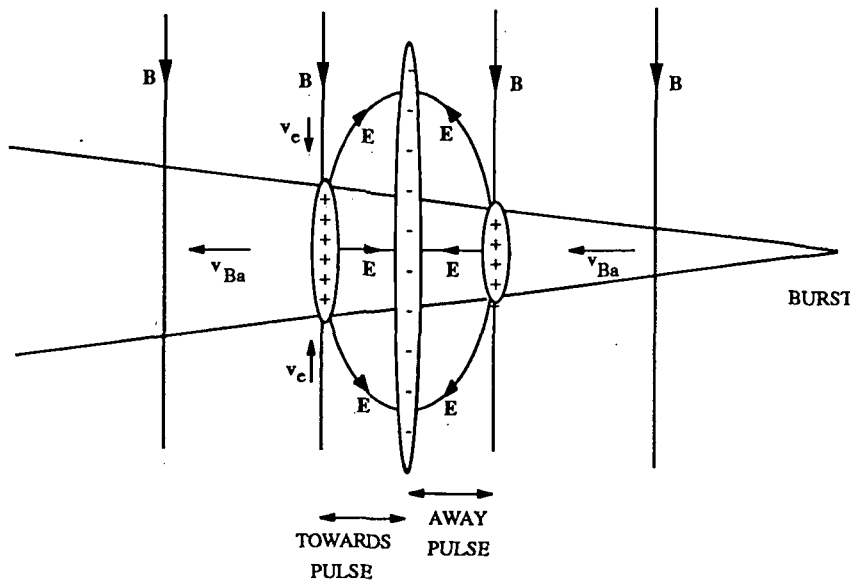


Fig. 9. The parallel fields model.

towards pulse) the energy would be enough to heat the electrons inside the stream to a temperature $kT_{e0} = 2\text{--}3$ eV. Although 2 eV is well below the ionization energy of barium (5.2 eV), the effect is dramatic because the interaction can be more rapidly triggered: the net ionization can increase by several orders of magnitude according to *Torbert's* [1990] computer model.

4. THE ELECTRODYNAMICAL PROBLEM

The electrodynamical problem of CRIT I concerns the coupling between the barium stream and the surrounding ionosphere. We here regard ionization in the barium stream as the starting point and concentrate on the internal characteristics of the barium stream MHD generator and on the coupling to the ionospheric load. We intend to show that the internal quasi-dc electric field in the barium stream is consistent with the assumption that the barium stream acts as an open-circuit generator in the sense that the magnetic-field-aligned currents have only a marginal influence on the internal electric field in the stream. The electric field must then adjust to such a structure that, to a first approximation,

$$\text{div } i_{\text{perp}} = 0 \quad (9)$$

This assumption has earlier proven fruitful in modeling the electric field both in high-altitude chemical releases [*Marklund et al.*, 1987] and in discrete auroral arcs [*Marklund*, 1984]. The main reason to use this assumption also in CRIT I is the presence of strong magnetic-field-aligned electric fields, which indicates that the plasma's classical high parallel conductivity is strongly reduced.

The Towards Pulses

The electrons can move in the direction of the jet by a combination of motion along and across the magnetic field. The velocity component across the magnetic field is given by the electric field in the $\mathbf{V}_{\text{Ba}} \times \mathbf{B}$ direction, which in both bursts was varying rapidly but always stayed below 80 mV/m during the towards pulses. With the 46° angle between the jet and the magnetic field taken into account, this puts the electron drift along the jet clearly below 3 km/s, while the barium ions start with 7–10 km/s in the towards pulse of burst 1 and with 7–12 km/s in burst 2. Under the assumption of (9), the electric field would have to establish such an electric structure inside the stream that the forward ion motion away from the electrons is stopped. The calculated ion orbits in Figure 8 show that the electric field was large enough to achieve this: the ions are rapidly turned around and even leave the towards pulse with a net velocity in the opposite direction.

This motion is such that the ions collectively contribute to uphold the towards pulse, but at the same time, individual ions are accelerated backwards on a time scale that is much shorter than the duration of the towards pulse. In order to keep up the electric field, a charge separation must be maintained with the ions slightly ahead of the electrons. This is essentially a problem of ion momentum in the z direction: fresh momentum must be fed into the ion population in order to keep it collectively ahead of the electrons. On the basis of the trajectories of Figure 8 we neglect the magnetic $\mathbf{V}_y \times \mathbf{B}$ force on the ions. The net force on the ion population in the z direction is then

$$\mathbf{F}_{i,z} = E_z \sigma_i + n_e n_{\text{Ba}} \langle \sigma_i V_e \rangle m_{\text{Ba}} V_{\text{Ba}} \quad (10)$$

The first term on the right-hand side is the electric force on the ion gas as a whole, and the second is the addition of momentum by new barium ions with the neutral velocity. The ion population as a whole can avoid being accelerated towards the explosion if the force is zero, which gives the electric field

$$E_z = - n_{\text{Ba}} V_{\text{Ba}} \langle \sigma_i V_e \rangle \frac{m_{\text{Ba}}}{e} \quad (11)$$

In CRIT I, the only unknown here is the ionization rate $\langle \sigma_i V_e \rangle$, which is determined by the electron temperature. Here we only want to illustrate that a crude match to the observed electric field can be obtained from (11) with a realistic electron temperature. For this purpose we have calculated the E_z field from (11) for both bursts, using n_{Ba} and V_{Ba} from Figures 4 and 5, and a time-constant electron temperature. In each burst we chose the temperature which gives most closely the correct amplitude of the towards pulse. We keep the temperature constant in time because we want to illustrate that the calculated towards pulse length is determined by the driving factor $n_{\text{Ba}} V_{\text{Ba}}$ in (11), and not by some arbitrarily chosen variation in temperature. In a realistic case, there should be a delay in the increase in temperature after the arrival of the barium stream. Also, the electron temperature would drop after the passage of the fast neutral stream, mainly due to radiative cooling and losses of energetic electrons along the magnetic field. In burst 1, the temperature $kT_e = 3$ eV gives the E_z field shown in the lower panel of Figure 10. The upper panel is the observed electric field. The detailed time variation is not important; what is of interest here is that the overall time duration and the magnitude of the towards pulse agree between model and observation. Figure 11 shows the result of the same calculation made for burst 2. Here the best fit to the observed field was achieved with $kT_e = 5$ eV.

The values $kT_e = 3$ eV and 5 eV were here chosen to give this match between (11) and the observed electric field. They are also realistic energies: the barium velocity in the middle of the towards pulse of burst 1 corresponds to a perpendicular energy of $(mV^2/2)\sin^2 46^\circ = 30$ eV. Both the ionization ($U_i = 5.2$ eV) and heating of the new electron to the thermal energy $3kT_e/2 = 4.5$ eV

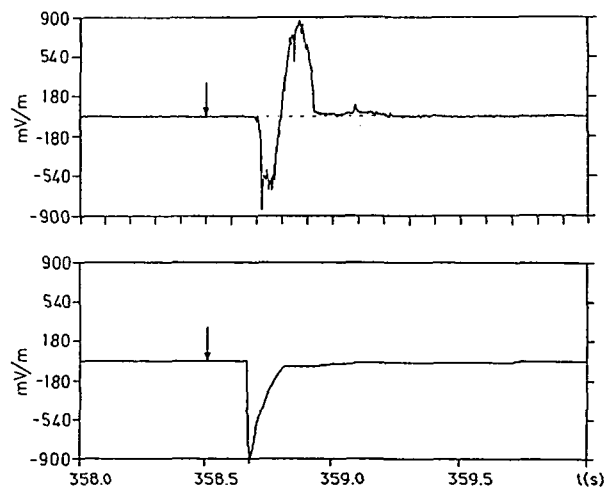


Fig. 10. (Upper panel) The measured axial component E_z of the electric field in burst 1. (Lower panel) The calculated field from equation (4), with the electron temperature chosen to give close to the observed amplitude, $kT_e = 3$ eV. The arrows mark the time of the burst.

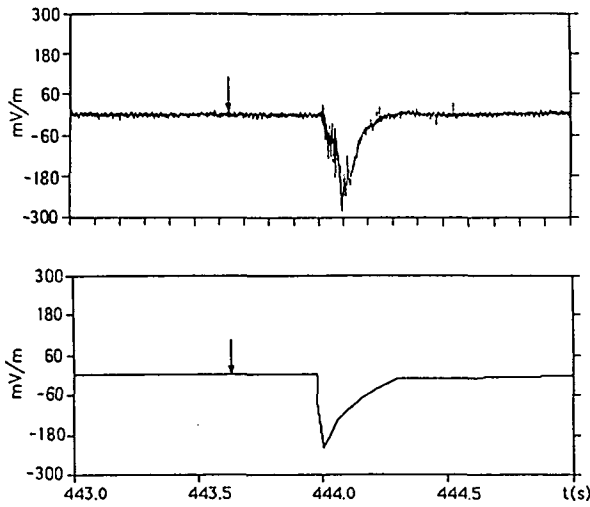


Fig. 11. (Upper panel) The measured axial component E_z of the electric field in burst 2. (Lower panel) The calculated field from equation (4), with the electron temperature chosen to give close to the observed amplitude, $kT_e = 5$ eV. The arrows mark the time of the burst.

can be achieved by an efficiency of energy transfer $\eta \approx 0.3$. In burst 2, the temperature $kT_e = 5$ eV can be achieved by a value $\eta \approx 0.4$. It is encouraging that approximately the same η value is obtained in both bursts, in spite of the fact that the neutral barium density was 10 times higher in burst 1 than in burst 2.

The conclusion of this section is that the electron temperature probably was 3 - 5 eV during the towards pulses, which in both bursts occurred in the fast part of the barium stream with velocities above 7 km/s. As mentioned in section 2, the ions which appeared above the solar UV terminator could be well explained by a "seeding" ionization time constant of 1800 s, with no observable enhancement along the field line of the burst. This is much below the values proposed here: a temperature of 3 eV would give an ionization time constant of about 330 s, and 5 eV would give 140 s. Thus the ionization inferred from the optical data seems to be a factor of 10 below the one proposed here.

The question arises why this large ionization does not show up on the TV picture. The answer probably is that the internal electric field in the stream would prevent the ions from reaching above the solar UV terminator fast enough. The optical system

saturated when the neutral jet appeared above the terminator, and the observed ionization therefore is based on a single frame which shows a time-integrated measurement of the ions that appear between 5 and 10 s after the burst. The fastest barium ions associated with the towards pulses start with a velocity about 12 km/s and have a magnetic-field-aligned velocity component about 8 km/s. If they did continue with this parallel velocity they would reach above the terminator after 6 s and appear on the TV picture. However, in the fast jet the magnetic-field-aligned component of the electric field (Figures 4 and 5) is directed downward. If the ions' parallel velocity is reduced below 5 km/s, they would get above the terminator later than 10 s after the burst and escape detection. The velocity change can be estimated as $\Delta V_{||} = E_{||}et/m_{Ba}$, where t is the time duration of the towards pulses, 0.1 s. A parallel velocity reduction from 8 to 5 km/s can be achieved by a value of $E_{||}$ as low as 40 mV/m, which is far below the observed fields which peaked at $E_{||} \approx 450$ mV/m in burst 1 and $E_{||} \approx 180$ mV/m in burst 2.

The Away Pulse

Because the barium stream density was typically 10 times higher in the towards pulses than later (Figures 4 and 5), it seems likely that ions produced in the towards pulses could dominate over the ions that were produced later in the streams. Figure 12 shows ion trajectories in burst 1 which are calculated using the same model as for Figure 8. The ions are here followed from the towards pulse into the away pulse, where they are marked with dots, 0.005 s apart, in order to give a time scale to their motion. At a time between 0.03 and 0.05 s after the ionization, these ions enter the away pulse with a velocity of typically $V_z = -10$ km/s. They are moving against the neutral stream as they enter the away pulse, and they stay inside the away pulse until they have lost all their velocity in the -z direction. These ions can therefore be the driving force which upholds the away pulse.

The electric field strength and the time duration of the away pulse support this interpretation: The measured electric field component in the $V_{Ba} \times B$ direction (third panel of Figure 4) gives the electrons inside the away pulse a drift about 3 km/s in the positive z direction. If magnetic-field-aligned currents cannot neutralize the space charges inside the stream (again the

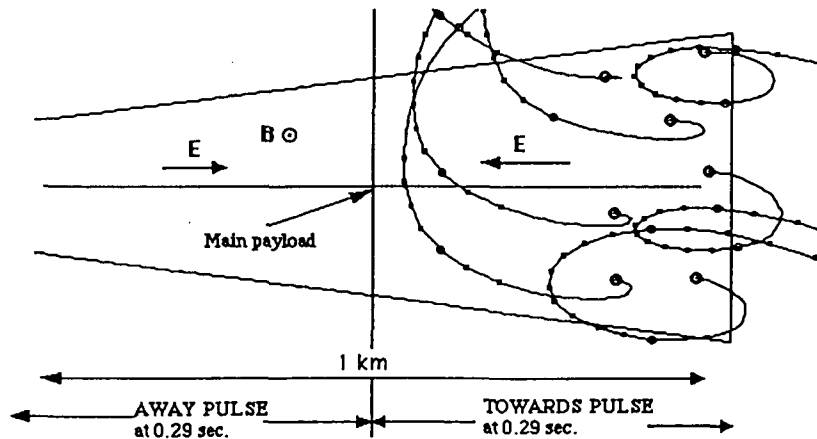


Fig. 12. Ion motion in burst 1. The trajectories are marked with dots while the ions are inside the away pulse.

assumption of (9)), the returning ions from the towards pulse would build up an electric field in the +z direction which stops them. A potential of 400 V across the towards pulse of burst 1 gives a velocity change of -24 km/s in the neutral stream frame. With an initial velocity $V_z = +10$ km/s, a typical neutral stream velocity at the leading edge of burst 1, the maximum velocity of the returning ions is $V_z = -14$ km/s in the payload frame. In the frame of the forward drifting electrons in the away pulse, their velocity is $V_z = -17$ km/s, which corresponds to an energy about 200 eV. This is of the same order as the potential across the away pulse, about 400 V, again assuming that the electric field derives from a structure which moves with the neutral stream velocity.

The absence of an away pulse in the second burst is probably due to a combination of several factors. The much weaker towards pulse in burst 2 would not produce such energetic returning ions. Ions which are produced in the leading edge would, if they could be accelerated over the full potential of the towards pulse, reach a backward velocity of only 5 km/s; a hypothetical away pulse which stops them would need a potential difference of only 18 V. Furthermore, there is a stronger element of gyration in the orbits. Calculations of the same type as those in Figures 8 and 12 indicate that these effects combine so that there is no strong population of returning ions from the towards pulse in burst 2.

The Current System

The currents in CRIT I were not measured directly, but have to be inferred from the electric field and other known data. The current systems were probably associated with the dense and fast parts of the beams, and changed with the distance from the explosions. The two shaped charges were designed to be identical. It is therefore probable that the differences between the two bursts which will be discussed below are mainly due to the different distances from the explosion. As in the rest of this paper, we assume that the observed electric field arises from a potential structure which sweeps past the payload and varies only slowly in the rest frame of the barium stream. That assumption gives, in burst 1, a topology of the electric field and current system which is schematically shown in Figure 13. There are five types of currents in that figure: Type 1 is magnetic-field-aligned currents $i_{//}$, which are drawn from the ionosphere in response to a divergence in the perpendicular electric field. If the concept of the Alfvén conductivity applies, the current is given by (8). In the Alfvén wave front, these currents close across the magnetic field in the form of plasma displacement currents i_{PD} . Type 2 is the internal axial current i_{Ba+} which sustains the space charges that draw $i_{//}$ and at the same time close the current loop $i_{//} - i_{PD} - i_{Ba+}$. Since this is a generator current, i_{Ba+} is directed against the electric field inside the barium stream. Type 3 is electron Hall currents i_H across the beam, driven by the electric field in the towards and away pulses. Type 4 is a hypothetical current i_{side} , which closes the current i_H on the sides of the barium stream. Type 5 is an axial-momentum-exchanging current in the ionosphere, which is required for the mass-loading process.

Let us first look at the magnetic-field-aligned currents $i_{//}$. A first estimate of their strength is the value $i_{//A}$ of (8). For a potential structure which moves with the neutral barium velocity,

(8) can be rewritten into

$$i_{//A} = \nabla \cdot \mathbf{v} E_{\text{perp}} \frac{1}{\mu_0 V_A} = \frac{dE_z}{dt} \frac{1}{V_{Ba}} \frac{1}{\mu_0 V_A} \quad (12)$$

For the steepest rising flank of the towards pulse in burst 1, $dE/dt = 100 \text{ V m}^{-1} \text{ s}^{-1}$ [Kelley *et al.*, this issue], which gives $i_{//A} = 8 \text{ mA/m}^2$. An average across the rising flank is $i_{//A} = 4 \text{ mA/m}^2$ in burst 1 and $i_{//A} = 0.2 \text{ mA/m}^2$ in burst 2. There are reasons to believe that the real magnetic-field-aligned currents were reduced below these $i_{//A}$ values: In both bursts, the quasi-dc electric field had magnetic-field-aligned components of the same time duration, strength, and amplitude as the perpendicular components. Any magnetic-field-aligned electric fields between the barium stream and the Alfvén wave front would reduce the mapped-out field E_{perp} , and thus reduce the current below the value $i_{//A}$ from (12). In burst 1, the current density $i_{//A}$ on the rising flank of the towards pulse exceeds the ambient random (thermal) electron current, which is $i_{th,e} = 2 \text{ mA/m}^2$. Such large currents are not likely to be reached; for example, both the Buneman instability [e.g., Lysak and Carlson, 1981] and double layer formation [Babic and Torvén, 1974; Raadu and Carlquist, 1981] could be excited and limit the current if $i_{//}$ approaches $i_{th,e}$. One more reason for current reduction below the value given by (12) is that the barium stream can deliver only a limited current i_{Ba+} in the axial direction. For an example we take burst 2: the ions lose their directed velocity on the gyrotime scale $\omega_{gi}^{-1} = 31$ ms. We take the barium stream density from Figure 5, and use the electron temperature $kT_e = 5$ eV derived from equation (11) above. This combination produces, by electron impact ionization during 31 ms, a density $n_{Ba+} \approx 2 \times 10^{10} \text{ m}^{-3}$. The highest current is obtained if the ions continue with the full neutral velocity, $i_{Ba+} = V_{Ba} e n_{Ba} = 10^4 \times 1.6 \times 10^{-19} \times 2 \times 10^{10} = 0.03 \text{ mA/m}^2$. The areas across which the currents i_{Ba+} and $i_{//}$ flow are of the same order. Therefore, current continuity requires that the magnetic-field-aligned current from the front, which is split up in two directions, in burst 2 was of the order $i_{Ba+}/2 = 0.015 \text{ mA/m}^2$. This is much below the value 0.2 mA/m^2 which (12) gives for burst 2.

A lower limit to the magnetic-field-aligned current density can be obtained from the observation in burst 1 of EIC waves 100 km above the release [Providakes *et al.*, submitted manuscript, 1990]. This indicates that the stream in burst 1, at an unknown distance from the explosion, drew an $i_{//}$ which exceeded the threshold for excitation of the EIC instability. This is 0.06 mA/m^2 at 500 km altitude (with the plasma density at 500 km taken from Table 1).

In the observed axial electric field, the Hall drift velocity across the beam $V_D = (E \times B)/B^2$ is of the order of 10 km/s in burst 1. According to Figure 8, the Ba^+ ions do not have time to follow in this drift; the electron E/B drift therefore gives Hall currents i_H as shown in Figure 13. If this current were not closed, space charges would rapidly build up at the sides of the beam and give rise to internal "self-polarization" electric fields across the beam. From the directions of the Hall currents in Figure 13 it is clear that such polarization fields would be directed in the +y direction in the towards pulse and in the -y direction in the away pulse. This polarization did not happen: the measured y component of the electric field is shown in the third panel of

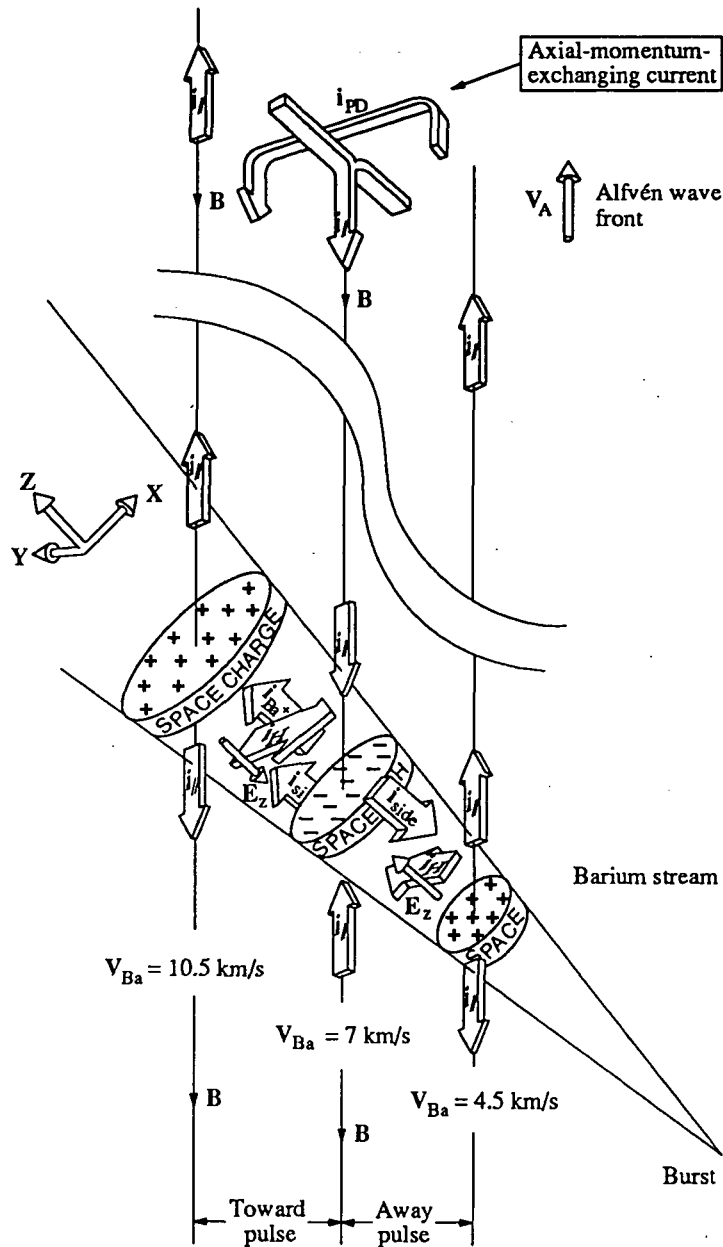


Fig. 13. A three-dimensional cartoon of the current system at a time 280 ms after burst 1, drawn under the assumption that the potential structure moves with the barium stream.

Figure 4; the sign is such that the positive y direction is downwards. The field was, both in the towards and the away pulses, rather weak and furthermore directed in the opposite direction compared to expected polarization field from an inhibition of i_H . The conclusion must be that the currents i_H close rather easily. One possibility is the currents i_{side} in Figure 13. The current loop consisting of i_H and i_{side} would be diamagnetic; it can be regarded as a weak diamagnetic cavity kept up by the dynamic ion pressure in the ion motion discussed earlier. The strength of the diamagnetic cavity could not be resolved in the magnetometer measurements where there was a strong fluctuation with higher frequencies [Kelley et al., this issue].

Regarding the closure of the Hall current, it is useful to distinguish between the background plasma consisting of ionospheric electrons and O^+ ions, and the additional plasma

Δn_e and n_{Ba^+} due to ionization in the stream. When the electron drift arises from a steady-state potential structure, the Hall drift of the homogeneous background is divergence-free; the current loop $i_H + i_{side}$ seems likely for this plasma component.

Current closure could be more problematic for the part of the Hall current that is associated with the density increase Δn over the ambient, which would tend to build up space charges wherever the current flows across a density gradient. There is the possibility that it could close in the axial-momentum-exchanging current on the top of Figure 13. This would also fit best into the ionizing front model for CIV interaction. There is, however, no observational support in CRIT I for the existence of this axial-momentum-exchanging current; it is included for the purely theoretical reasons that it has to flow for the mass-loading process. It would have to connect to the stream in magnetic-field-

aligned currents to the sides of the stream (not shown in Figure 13). In the homogeneous model (Figure 6), the partial self-polarization would quite naturally draw such magnetic-field-aligned currents; in the measured electric field of CRIT I, such a mechanism is lacking.

There is a seeming contradiction emerging from this discussion about the current system: on one hand, a high ionization makes the axial current system $i_{\parallel} - i_{PD} - i_{Ba^+}$ easier to understand: if there is a strong axial Ba^+ current inside the stream, it is more natural that the axial electric field cannot be short-circuited by magnetic-field-aligned currents. On the other hand, such a dense beam would be expected to self-polarize rather easily; the closure of the transverse electron Hall current becomes more problematic.

5. SUMMARY AND DISCUSSION

In order to get some perspective on the results from CRIT I, let us first consider what we should have expected to measure in the absence of electron impact ionization, i.e., without any CIV process. In this case, there are only two sources of Ba^+ ions, namely ions produced in collisions with the ambient O and O^+ and ions produced in the initial explosion. The Ba^+ ions from the initial explosion cannot be completely excluded at the payload position in burst 1; these ions could possibly be dragged with the stream, by resonant charge exchange collisions, out to 1.5 - 2 km: inside this distance the mean free path for these collisions is smaller than both the stream width and the Ba^+ gyroradius. At the payload position in burst 2, however, this possibility can probably be excluded. Due to the rapid decrease in neutral barium density (equation (1)), the Ba^+ ions would decouple from the neutral stream outside 2 km.

The ionizing collisions in the ambient ionosphere are charge exchange ($Ba + O^+ \rightarrow Ba^+ + O$) and stripping ($Ba + O \rightarrow Ba^+ + O + e^-$), which produce Ba^+ ions at a rate given by equation (5). From the optical observation [Stenbaek-Nielsen *et al.*, 1990] we have a good measured value of this seed Ba^+ production rate in the fast parts of the jets. According to the homogeneous model the ionosphere should have been able to handle this ionization rate by establishing rather weak electric fields, given by (3), (4), and (5): E_p would be only 2.4 mV/m in burst 1 and 0.4 mV/m in burst 2. Also, the alternative model of section 4 (equation (11)) gives electric fields an order of magnitude below the observed. We conclude that the mere existence of the strong quasi-dc electric fields, particularly in burst 2, indicates that there really was enhanced ionization in CRIT I.

The quasi-dc electric field, which is intimately linked to the mass loading mechanism in CIV theory, is at present only partly understood. Most notably there were large magnetic-field-aligned electric fields E_{\parallel} with long time duration. In burst 1 those could possibly be maintained because the stream demanded currents exceeding the ambient random electron current $i_{th,e}$. In burst 2, the E_{\parallel} fields existed at current densities which probably were more than one order of magnitude lower than $i_{th,e}$.

The perpendicular electric field in the stream was not the expected partial self-polarization of the homogeneous model, which would give a natural mass-loading process in CIV theory. The towards pulses could be explained in overall amplitude and time duration from the assumptions that the ionosphere cannot deliver magnetic-field-aligned currents large enough to neutralize

the space charges that appear in the axial ion-electron separation, and that the ions therefore have to build up such an electric field that their motion in the axial direction, on the average, is stopped. The presence and amplitude of the away pulse in burst 1 are shown to be a natural consequence of the ion motion in the towards pulse. This interpretation also agrees with the absence of an away pulse in burst 2.

However this understanding refers only to the relation between the quasi-dc electric fields and the internal ion motion in the beams. For an understanding of the coupling to the ambient ionosphere, i.e., the mass-loading process, more work is needed. A first step is made in a companion paper [Brenning *et al.*, this issue], where the motion of a cylindrical cloud of barium ions across the magnetic field is studied. A first finding is that the partial self-polarization in the $E_p = -V_{\parallel} \times B$ direction occurs only for very dense beams, far exceeding the values in CRIT I. For less dense beams, i.e., lower ionization rates, the electric field is close to antiparallel to the injection direction as it was in the CRIT I towards pulses. Apart from this observation, the applicability of the model to the strong quasi-dc electric field pulses in CRIT I is still limited, mainly because the model assumes infinite parallel conductivity.

Concerning mechanisms for electron heating, the ionizing front model seems to fit the observations in the region where the main interaction occurs, in the towards pulses. It has been proposed that the ionizing front model should apply when the ionization rate exceeds the ion gyrofrequency, $\nu_i/\omega_{gi} > 1$ [Haerendel, 1982; Brenning, 1986]. With the known neutral density at the position of the main payload, we can calculate the ionization rate at the temperatures proposed in section 4, namely $kT_e = 3$ eV in burst 1 and $kT_e = 5$ eV in burst 2. Using the peak values of the barium density, the result is fairly close to the required value for the ionizing front model: $\nu_i/\omega_{gi} = 2$ in burst 1 and $\nu_i/\omega_{gi} = 0.5$ in burst 2.

The homogeneous model fits the observations in the precursor at the front of the neutral stream, and in burst 1 it could probably heat the electrons above the ignition temperature which in CRIT I was $kT_e = 1.7$ eV. In burst 2, the homogeneous model would give a value about $kT_e = 1.5$ eV at the end of the precursor phase, which seems to be on the margin for ignition. The start of the towards pulse in burst 2 would therefore be easier to understand if there were some additional mechanism for electron heating operating at the onset of the towards pulse. One such possible mechanism is electron acceleration in magnetic-field-aligned electric fields at the leading edges of the towards pulses. Although this is still a hypothesis, it has some interesting consequences for the theory for ionospheric CIV experiments: according to a computer model which calculates the net ionization in ionospheric CIV experiments [Torbert, 1990] even a rather small increase in the initial temperature T_{e0} can increase the net ionization by orders of magnitude. Thus, although CRIT I was not a high-yield CIV experiment, we have some indications of a heating process which, in principle, could give a very high ionization yield.

We conclude that two, possibly three, different mechanisms for electron heating probably operated simultaneously in different parts of the streams of CRIT I. In the leading edge of the barium streams, the homogeneous model applies. There is also the

possibility of some extra electron heating by magnetic-field-aligned electric fields at the rising flank of the towards pulses. However, both these heating processes probably only act as triggering mechanisms to the ionizing front model which is associated with the main ionization.

Acknowledgments. This research was supported by the Swedish Board of Space Sciences, the Swedish Natural Science Research Council, the Max Planck Institute for Extraterrestrial Physics, and the U. S. National Association of Space Aeronautics. Support for the efforts by the Geophysical Institute, University of Alaska Fairbanks, was provided by NASA grants NAG6-1 and NAGW-269.

The Editor thanks P. T. Newell and P. Kintner for their assistance in evaluating this paper.

REFERENCES

- Babic, M., and S. Torvén, Current limiting space charge sheaths in a low pressure arc plasma, *Rep. TRITA-EPP-74-02*, R. Inst. of Technol., Stockholm, Sweden, 1974.
- Brenning, N., On the role of the ionization frequency to gyrofrequency ratio in critical ionization velocity interaction, *Rep. TRITA-EPP-86-10*, R. Inst. of Technol., Stockholm, Sweden, 1986.
- Brenning, N., M. Kelley, J. Providakes, H. C. Stenbaek-Nielsen, and C. Swenson, Barium swarm: An ionospheric alternating current generator in CRIT I. *J. Geophys. Res.*, this issue.
- Galeev, A. A., and R. Z. Sagdeev, Theory of a critical ionization rate, *Sov. J. Plasma Phys.*, Engl. Transl., 9 (1), 209-216, 1983.
- Goertz, C. K., and S. Machida, An asymptotic state of the critical ionization velocity phenomenon, *J. Geophys. Res.* 90, (A 12), 12,230, 1985.
- Haerendel, G., Alfvén's critical velocity effect tested in space, *Z. Naturforsch. A*, 37, 728, 1982.
- Kelley, M. C., R. F. Pfaff, and G. Haerendel, Electric field measurements during the Condor critical velocity experiment, *J. Geophys. Res.* 91, (A9), 9939, 1986.
- Kelley, M. C., C. Swenson, N. Brenning, K. Baker, and R. Pfaff, Electric and magnetic field measurements inside a high velocity beam undergoing ionization, *J. Geophys. Res.*, this issue.
- Lindberg, L., Plasma flow in a curved magnetic field, *Plasma Phys.* 13, 303, 1978.
- Lysak, R. L., and C. W. Carlson, The effect of microscopic turbulence on magnetospheric-ionospheric coupling, *Geophys. Res. Lett.* 8, (3), 269, 1981.
- Mallinckrodt, A. J., and C. W. Carlson, Relation between transverse electric fields and field-aligned currents, *J. Geophys. Res.*, 83, 1426, 1978.
- Marklund, G., Auroral arc classification scheme based on the observed arc-associated electric field pattern, *Planet. Space Sci.*, 32, 193-211, 1984.
- Marklund, G., N. Brenning, G. Holmgren, and G. Haerendel, On transient electric fields associated with chemical release experiments by rockets, *J. Geophys. Res.*, 92, 4590 - 4600, 1987.
- McBride, J. B., E. Ou, J. P. Boris, and J. H. Orens, Theory and simulation of turbulent heating by the modified two-stream instability, *Phys. Fluids*, 15, (12), 2367, 1972.
- Newell, P. T., Review of the critical ionization velocity effect in space, *Rev. Geophys.*, 23, 93 - 104, 1985.
- Papadopoulos, K., On the shuttle glow (the plasma alternative), *Radio Sci.*, 19, 571, 1984.
- Piel, A., E. Möbius, and G. Himmel, The origin of turbulent heating in a critical velocity rotating plasma, *Res. Rep. 78-M2-037*, Inst. für Experimentalphys. II der Ruhr-Univ. Bochum, Bochum, Germany, 1978.
- Piel, A., E. Möbius, and G. Himmel, The influence of the plasma inhomogeneity on the critical velocity phenomenon, *Astrophys. Space Sci.*, 72, 211-221, 1980.
- Providakes, J., W. E. Swartz, M. C. Kelley, F. T. Djuth, S. Noble, and R. J. Jost, Radar observations of ion cyclotron waves associated with two barium shaped charge releases, *J. Geophys. Res.*, 95, 21,050-21,067, 1990.
- Raadu, M. A., The role of electrostatic instabilities in the critical ionization velocity mechanism, *Astrophys. Space Sci.*, 55, 125-138, 1978.
- Raadu, M. A., and Carlquist, P., Electrostatic double layers and a plasma evacuation process, *Astrophys. Space Sci.*, 74, 189, 1981.
- Sherman, J. C., Some theoretical aspects of the interaction between a plasma and a neutral gas in a magnetic field., *Rep. TRITA-EPP-69-29*, R. Inst. of Technol., Stockholm, Sweden, 1969.
- Stenbaek-Nielsen, H. C., E. M. Wescott, D. Rees, A. Valenzuela, and N. Brenning, Non-solar UV produced ions observed optically from the "CRIT I" critical velocity ionization experiment, *J. Geophys. Res.*, 95, (A6), 7749-7757, 1990.
- Torbert, R., Review of ionospheric CIV experiments, Proceedings of the XXVII COSPAR Meeting in Espoo, Finland, 1988, *Adv. Space Res.*, 10, (7), 47, 1990.
- Torbert, R., and P. T. Newell, A magnetospheric critical velocity experiment: Particle results, *J. Geophys. Res.*, 91, (A9), 9947-9955, 1986.
- Vainshtein, L. A., V. I. Ochkur, V. I. Rakhovskii, and A. M. Stepanov, Absolute values of electron impact ionization cross sections for magnesium, calcium, strontium and barium, *Sov. Phys. JETP*, Engl. Trans., 34, 271-275, 1972.
- Wescott, E. M., H. C. Stenbaek-Nielsen, T. Hallinan, H. Föppl, and A. Valenzuela, Star of Lima: Overview and optical diagnostics of a barium Alfvén critical velocity experiment, *J. Geophys. Res.* 91, (A9), 9923, 1986.
- Wescott, E. M., H. C. Stenbaek-Nielsen, D. W. Swift, A. Valenzuela, and D. Rees, SR90, A strontium shaped-charge critical ionization velocity experiment, *J. Geophys. Res.*, 95, (A12), 21,069-21,075, 1990.
- N. Brenning, C.-G. Fälthammar and G. Marklund, Royal Institute of Technology, Department of Plasma Physics, S-10044 Stockholm, Sweden.
- G. Haerendel, Max-Planck-Institut für extraterrestrische Physik, 8046 Garching, Germany.
- M. C. Kelley and C. Swenson, School of Electrical Engineering, Cornell University, Ithaca, NY 14853.
- R. Pfaff, NASA Goddard Space Flight Center, Code 696, Greenbelt, MD 20771.
- J. Providakes, MITRE Corporation, Burlington Road, Bedford, MA 01730.
- H. C. Stenbaek-Nielsen and E. M. Wescott, Geophysical Institute, University of Alaska, Fairbanks, AK 99775.
- R. Torbert, Space Science Center - IEOS, Univ. of New Hampshire, Durham, NH 03824.

(Received January 2, 1990;
revised February 26, 1990;
accepted March 19, 1990.)

Rapid Ray Motions in Barium Plasma Clouds and Auroras

E. M. WESCOTT, T. J. HALLINAN, H. C. STENBAEK-NIELSEN, D. W. SWIFT, AND D. D. WALLIS¹

Geophysical Institute, University of Alaska, Fairbanks

Barium plasma clouds released at high latitudes characteristically become striated with many field-aligned rays. The rays which often resemble auroral features usually drift as a whole with the $\mathbf{E} \times \mathbf{B}/B^2$ drift of the cloud and alter position only slowly (order of tens of seconds). On two evenings in 1968, in released from Andøya, Norway, anomalous field-aligned brightenings or emission enhancements of up to 3X were observed to move rapidly (10–20 km/s) through three different Ba^+ clouds. Similar effects were observed in Ba^+ clouds released from rockets launched from Poker Flat, Alaska: On March 21, 1973, in two Ba thermite releases and on March 22, 1980, in the Ba-shaped charge experiment "Miss Peggy." On these occasions, auroras on or near the Ba^+ L shell, also exhibited active rapid ray motions. This leads us to the assumption that the two phenomena are related and the expectation that an explanation of the rapid ray motions in the Ba^+ clouds would lead to a better understanding of the physics of auroral ray motions and the auroral ionosphere. Seven possible mechanisms to produce the observed moving emission enhancements are discussed. Direct excitation by energetic electron bombardment is ruled out on the basis of energy fluxes required for realistic cross sections. Direct motion of an isolated Ba^+ ray past the other rays by $\mathbf{E} \times \mathbf{B}/B^2$ motion seems very unlikely due to the observed variations in the enhancements and the large \mathbf{E} field required (>500 mV/m). Compressional waves do not seem to be of sufficient amplitude or velocity. Formation of folds or curls in a sheet beam instability require moving radial fields of 500 mV/m but would explain the auroral features as well as the Ba^+ by the same mechanism. Qualitatively, the redistribution of Ba ions as a flux tube encounters a higher electron density in the ionosphere may result in enhancements. Absorption or radiation of Doppler shifted Ba^+ emissions by ions gyrating or moving at a few kilometers per second seems to be the most promising mechanism for producing the enhancements. The observations provide compelling evidence for the existence of transient electric fields of order 100 mV/m at altitudes as low as 200 km during active aurora with rapid ray motions. The affected regions have dimensions of order a few kilometers across B and move eastward at 10–20 km/s.

INTRODUCTION

Since early in the history of barium release experiments, the development of field-aligned striations in the ion clouds has been a subject of great interest [Haerendel *et al.*, 1967]. In particular, at high latitudes, striated clouds, often quite extended laterally, bear a superficial resemblance to rayed auroras [Davis *et al.*, 1974]. In fact, from black and white still photography, it is often difficult to distinguish between them; however, the Ba^+ striations are more stable than auroral features. In both phenomena the striations or rays are field-aligned and can have the same range of ray spacings. This has led some investigators to seek clues to the behavior of auroral features in the evolution and subsequent motion of plasma cloud structures. The barium plasma clouds are usually much higher in altitude than the auroras, and the height-luminosity profiles are dissimilar due to the entirely different mechanism of light emission processes. The light emitted from auroras is due primarily to electron bombardment, while that from barium ions is due to solar resonance fluorescence. Usually, while the source providing the auroral electrons may move and change rapidly, the barium ion striations tend to drift as a whole with the $\mathbf{E} \times \mathbf{B}/B^2$ motion, while the individual features change position or evolve only slowly (tens of seconds). However, the evidence presented in this paper suggests to us that in small barium thermite (3 kg of thermite mixture) and shaped

charge releases, the configuration and motion of barium striations in high latitude releases are due to naturally existing nonhomogeneities in the ambient ionospheric plasma density or electric fields. It is our thought that certain features in auroral forms may have a common cause with analogous barium ion structures or motions.

The barium release program of the NASA Goddard Space Flight Center (GSFC), initiated in 1966, was planned to emplace barium clouds near or hopefully within magnetic shells on which auroras were occurring to study auroral and electrojet electric fields. As one of the goals, it was planned to determine whether rapid motions occurring in auroral forms were accompanied by corresponding effects in the barium clouds, i.e., to determine the involvement of transient electric fields.

To observe real time rapid motions in both auroras and plasma clouds, image orthicon unfiltered TV systems were operated at several sites during a series of NASA GSFC barium release rocket flights from Andøya, Norway, in fall 1967 [Wescott *et al.*, 1969]; however, the auroras did not exhibit rapidly moving rayed forms and neither did any of the barium clouds. For a second series of GSFC Andøya releases in 1968, the University of Alaska participated by operating both an unfiltered and a 4554-Å (Ba^+ line) filtered TV system and an eight-filter scanning photometer at an additional site. On two evenings, September 20 and 21, 1968, rapid ray motions or rapidly moving emission enhancements were observed in several different barium clouds contemporaneously with rapid ray motions in auroras on or near the same L shell. In rocket experiments from Poker Flat, Alaska, two ionospheric Ba^+ clouds released March 21, 1973, and one on March 22, 1980, have also exhibited similar rapid ray motions during active auroral activity. There have

¹Now at Herzberg Institute of Astrophysics, National Research Council Canada, Ottawa.

been probably over 100 auroral zone Ba release experiments over the years, but to our knowledge only these exhibited ray motions, and only when similar rapid ray motions were occurring in nearby auroras. Not all of the releases were covered by low light level televisions, which is required to record rapid changes, but we think it is a tenable assumption that rapid ray motions in barium clouds occur only when similar motions are evident in auroras on or near the same magnetic shell.

This paper deals with the circumstances and validity of the observations and discusses possible mechanisms.

EQUIPMENT AND CALIBRATIONS

For the 1968 Norway barium release series, unfiltered image orthicon (IO) television systems were operated at three field sites: At the Andøya (Andenes) launch site, at Tromsø 120 km to the east, and at Bodø 200 km to the south. An additional IO TV system at Bodø was fitted with a 25-Å-wide filter centered on the 4554-Å line of ionized barium. No auroral contamination could be discerned when this system was pointed at the brightest auroras. The systems at Bodø and Tromsø were video recorded at 60 fields per second to provide excellent real-time coverage of any motions in either auroral or barium forms. The system at Andøya recorded on film from the monitor at 10 frames/s.

A scanning photometer was mounted on the Bodø TV mount so that the central portion of its scan was directly along a line centered in the TV field of view. The photometer employed a filter wheel carrying 8 filters (BaI, 5535 Å; BaII, 4934 Å, 6142 Å, 5843 Å; BaO, 5350 Å; and auroral wavelengths 6300 Å, 4278 Å, 5577 Å; all of F.W.H.M. 15-35 Å). The photometer scanned through each filter sequentially and was operated so that scans in all wavelengths were made in about 2.5 s. The field of view was 0.5°.

At all field sites, including Gravdal 167 km south west of Andenes, 35-mm all-sky cameras with 160° fields of view were operated at 12 frames/min in order to provide data on auroral morphology. The positions of barium ion clouds were calculated by triangulation from pairs of 4.5 × 4.5 inch K-46 camera photographs using star backgrounds. For detailed position information on both barium and auroral locations during rapid ray motion events, TV data were also used in triangulation calculations. Location accuracy of the barium clouds is of the order of 1 km; however, the exact dimensions and alignments of the forms are often somewhat uncertain due to the angles involved, obscuring clouds, or confusion with auroral positions. The barium cloud positions and auroral features were translated down the magnetic field lines to a 100-km datum altitude.

The positions and details of auroral forms are the most uncertain, depending upon the amount of overlapping coverage and distance from the camera sites. Every effort was made to locate the lower border of arcs and other features as accurately as possible, using a technique of plotting overlapping data at various assumed heights until coalescence was obtained. Star backgrounds from TV or all-sky cameras were used to determine angular information.

Postflight calibration of the television/recorder combination demonstrated that up to the point where "blooming" appeared on the screen, the video signal above background was linearly dependent on the scene brightness. However, due to the modulation transfer function of the system, the

signal between two closely spaced barium striations is somewhat higher than the actual brightness. To determine the brightness enhancement of the moving rays, the video amplitude above the background level of various portions of the striated clouds was measured prior to the ray and then at the same position that the ray passed through. The ratio of enhanced video amplitude to the normal value then gives the minimum enhancement factor. "Minimum" because both the nonlinearity near blooming and the higher between-lines background would tend to make the actual enhancement higher.

The TV system at Bodø (the basis of our quantitative analyses) was operated so that scan lines were vertical looking in the direction of the magnetic meridian and thus were parallel to the field-aligned striations. In determining the width of ray features a thin, sharp-edged feature could appear to be one to two lines wider than it really was because of the signal spread on the TV target and the finite sweep width.

OBSERVATIONS

Rapid intensity fluctuations or ray motions were observed in one cloud on September 20 and in two clouds on September 21, 1968, during four main intervals. These range from solitonlike single separate ray motions to fluttering. Numerous separate events occurred ranging from very pronounced and obvious to barely discernable. We have analyzed the main events in detail as described below.

The first event occurred on September 20, 1968, from 1934:19 to 1934:30 UT in the first ion cloud (I1), 59–70 s after release at a cloud center altitude of 203 km. The main auroral arc was located 25 to 30 km in L shell separation from the barium cloud, I1, at this time as shown in Figure 1. No auroral forms were detected closer to the L shell containing the cloud I1 or I2 which had just been released. The cloud I1 had already become striated and elongated nearly parallel to the auroral arcs. A series of bright rays appeared to move rapidly eastward through more or less stationary Ba^+ striations with a tenuous trail of ions connecting the main ion cloud to the neutral cloud, IR (Figure 1). Rapid ray motions were also observed moving eastward along the auroral form at this time.

The second event, occurred about 80 s later at 1935:40–45 in the same ion cloud, I1, and at similar altitude, before the release of cloud I3. During the time between events the auroral arc had moved poleward, while the ion cloud had been drifting equatorward. Figure 2 shows the triangulated auroral position to be on the same L shell as the barium cloud I1 at the time of the phenomenon. Several wavelike brightenings were observed to move eastward along the striated ion cloud at different velocities. Measurements from the TV frames indicate apparent velocities between four identifiable ray positions of 17.5, 26.3, and 21.9 km/s in the direction of horizontal elongation of the ion cloud. Very similar appearing motions (in direction and velocity) were occurring in the auroral arc at the same time. Due to the difference in height between the aurora and ion clouds and thus the viewing angle at any station, the portion of the arc coincident with the ion cloud is out of view of the TV frame. Thus it is not possible to make a one-to-one comparison of a moving feature in the ion cloud with one in the auroral form. At subsequent times the auroral arc moved farther pole-

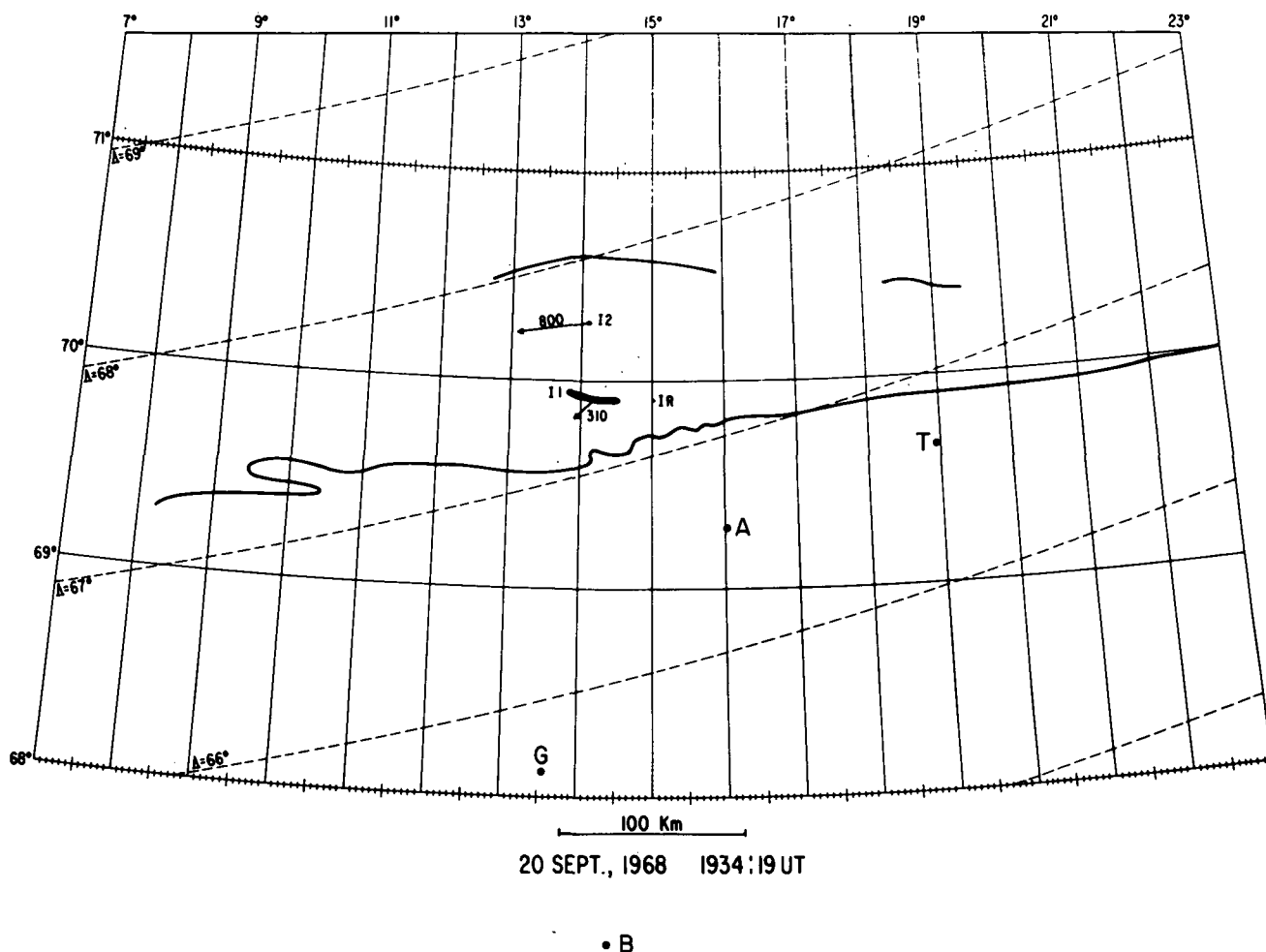


Fig. 1. Auroral features and Ba^+ clouds, 1934:19 UT, September 20, 1968, projected down magnetic field lines to 100 km altitude. Rapid eastward ray motions were observed in ion cloud I1 and also in the nearest aurora 25–30 km away. IR is the release point and the location of the neutral cloud. The arrows and numbers show the average ion cloud velocity in meters per second at this time. Optical observing sites shown are A (Andenes), T (Tromsø), G (Gravdal), and B (Bodø).

wards and passed across the L shells containing the second and third ion clouds, I2 and I3, but no more rapid ray motions were observed.

The nearest magnetometer (at Andenes, 100 km SE of the cloud) during the events described registered +30 nT in H and a magnetic westward component of 20 nT.

A third event occurred on the next evening, September 21, 1968, after about 20 min of observation of the motions of four Ba^+ ion clouds. For about 15 min after the barium releases there was aurora south of all the barium clouds with a $-\Delta H$ of about 20 nT at Andenes. At 1951:00 a steep decrease in H began with poleward motion of the aurora and auroral brightening. A series of ray motions occurred in the second ion cloud, I2 (center altitude 222 km) around 1957:33 UT when the aurora was very close to being on the same L shell. The Andenes magnetometer registered -108 nT in H and 30 nT westward magnetic component. Prominent rays of enhanced Ba^+ emissions were observed to move eastward along the ion cloud in a similar manner to contemporaneous auroral motions as shown in Figure 3. In one prominent event, apparent ray velocities eastward along the barium cloud (which was much elongated east-west) were measured at 6.34 and 9.55 km/s.

The fourth event occurred in ion cloud I3 with center altitude 240 km at 2003:03 UT, September 21, 1968. The ion cloud had a brightness of 4 kR in 4934 Å. This corresponds to 7 kR in 4554 Å and indicates an optically thin cloud. This is the most prominent event of all and has been studied in the greatest detail. At Andenes the H component had decreased to -210 nT with zero disturbance in the east-west component. The auroral breakup had occurred to the east over Tromsø, Norway, but the aurora was locally very active. As shown in Figure 4, the aurora, as best can be determined, was nearly in the same L shell as the ion cloud. In Figure 4, eastward auroral ray motions of 75, 42, and 60 km/s are shown. These velocities are consistent with the velocity distribution of small auroral features measured by *Davis and Hicks* [1964] but are near the upper limit of velocities. They exceed by a factor of 3 the most rapid ray velocities reported by *Hallinan and Davis* [1970]. During this period, a bright ray was observed in the 4554-Å emission to travel west to east through the barium cloud at a speed of 10.7 km/s. The ion cloud was striated. As the enhancement progressed through the striations, several of the brightest rays appeared to move a kilometer or two eastward at the closest approach of the enhancement, then return westward after the passage.

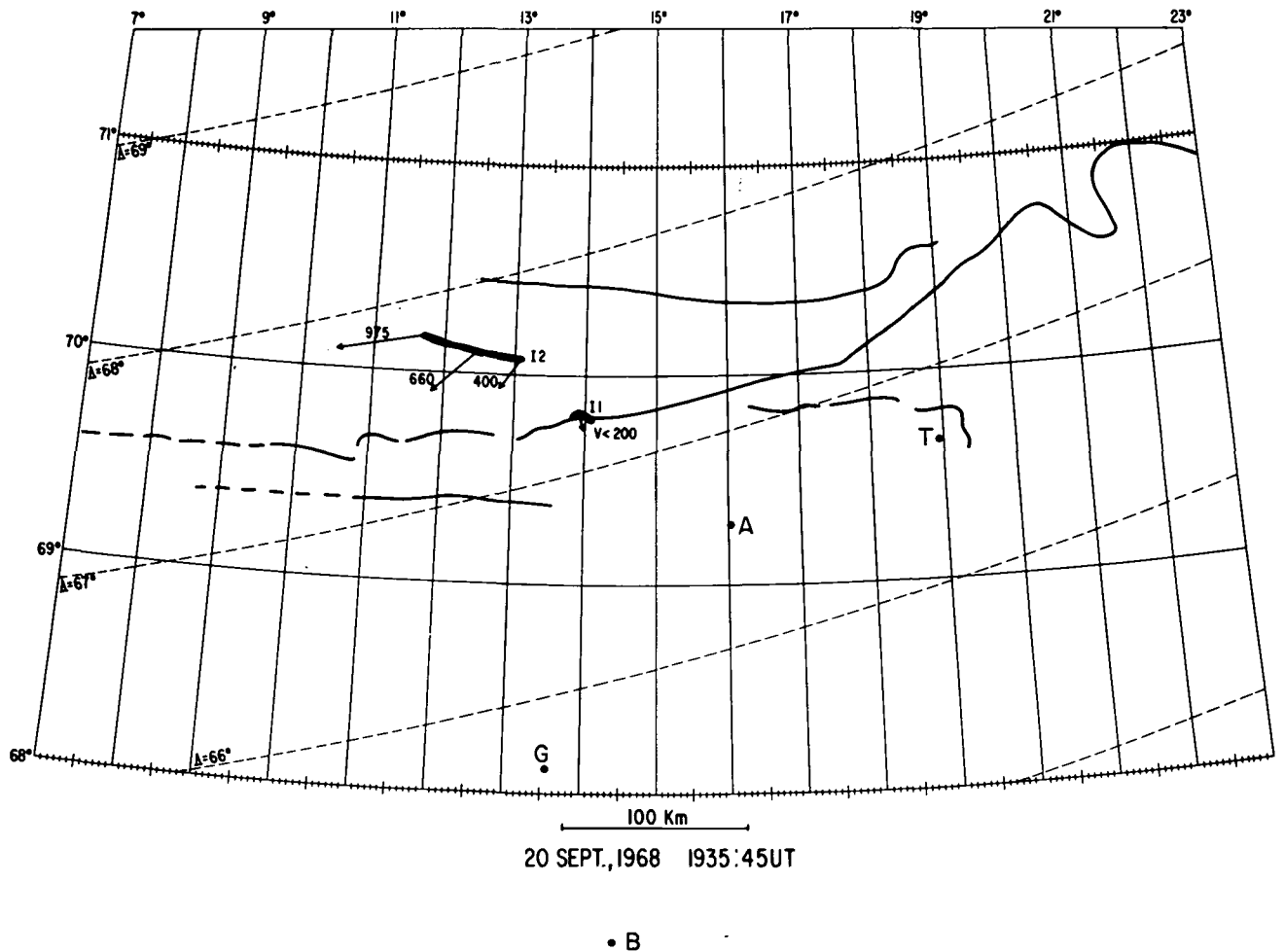


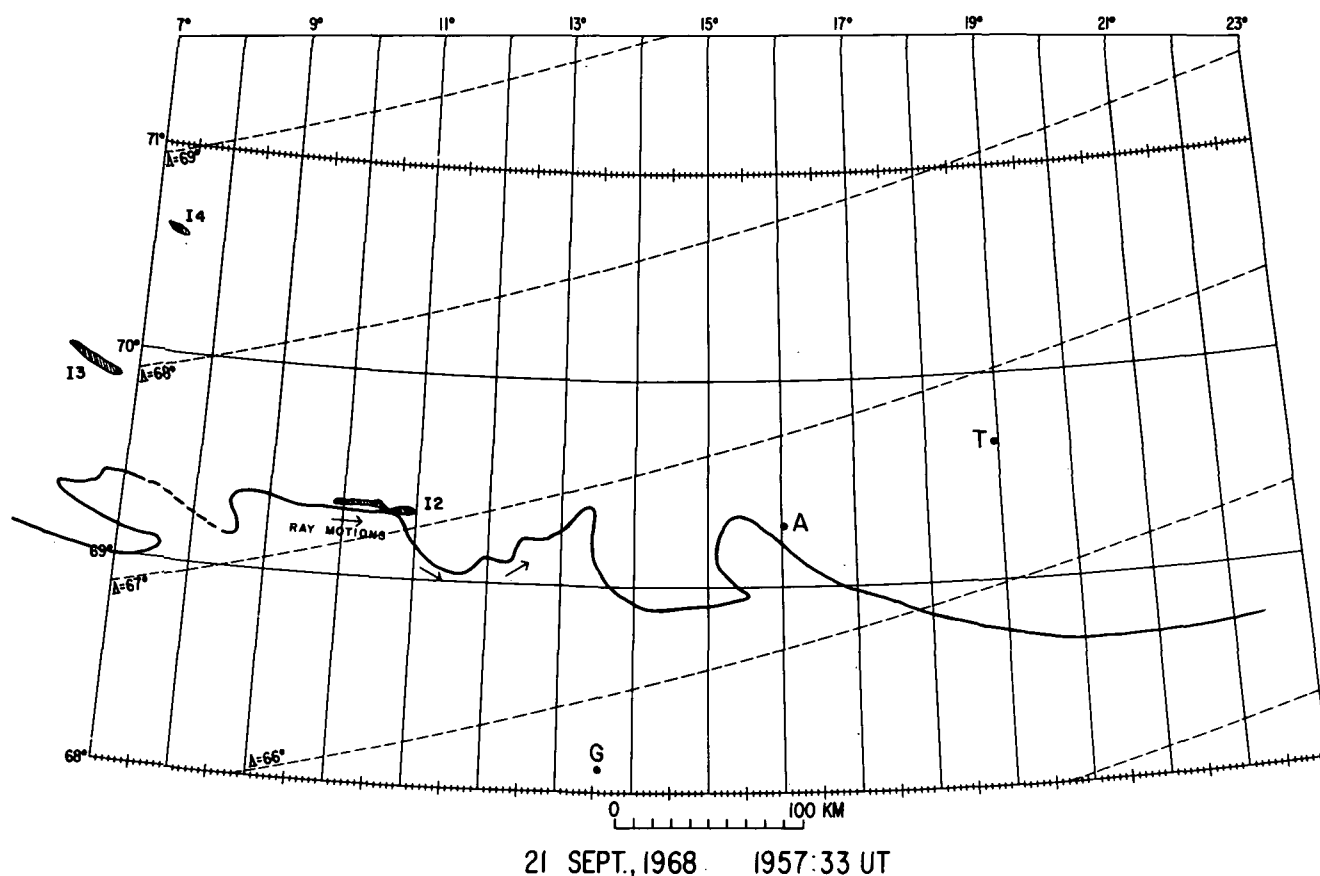
Fig. 2. Auroral features and Ba^+ clouds, 1935:45 UT, September 20, 1968, projected down magnetic field lines to 100 km altitude. A series of rapid ray or enhancements were observed moving eastward in ion cloud I1 at around 20 km/s, while it was in the same L shell as the aurora exhibiting similar ray motions. The arrows and numbers show the ion cloud velocities in meters per second at this time. Clouds I3 and I4 have not yet been released.

This effect was also noticed in the March 7, 1972, Ba -shaped charge experiment "Oosik" surge event [Wescott *et al.*, 1975]. The Ba^+ striations appeared to be the same before and after the event.

Figure 5 shows an 8-s sequence of TV pictures from the 4554- \AA (ionized Ba line) filtered system looking northwest from Bodø. These frames illustrate some important features of the moving enhancement and its brightness relative to the essentially motionless existing barium striations. The top pictures, 1 s apart, were taken at 1/4 s exposure thus integrated over 15 TV fields and somewhat smeared the ray due to its motion. The bottom sequences are single TV frames (1/60 s exposure) at 1/6 s apart on an expanded time scale between 2003:03 and 2003:04. The position of the enhancement is shown by the upper arrows. When the enhancement reached the bright barium ray (see 2003:02.5), the added signal intensity caused the image orthicon tube to "bloom" as evidenced by the elliptical bright region. As discussed earlier, the video signal amplitude from the tape playback was determined to be a linear function of light input up to the point of blooming. Video signal levels at a number of portions of the cloud were measured every 10 TV fields as the enhancement moved through the cloud. This provides a

measure of the percent increase over cloud background throughout the passage. Only cloud background levels significantly above the noise were considered. The enhancement tends to be proportional to the background level and is definitely not a constant incremental addition. The percent enhancement was not a constant, varying from 50% to greater than 300%, but the average was around 250%. Note particularly the brightness of the moving enhancement between 03:03 and 03:04 (Figure 5, lower section expanded time frames) as it passes in the region between the two bright rays (indicated by the lower arrows in frame 2003:01.5). Intensity measurements from the video tape signal level indicate an enhancement of at least a factor of 3 over the undisturbed level.

Note the close similarity of the ion cloud striations before and after the enhancement passage by comparing 2002:59.5 with 2003:06.50. Another important feature of this event is that a few kilometers separates the most eastward barium ray from the main portion of the cloud. The enhancement is just barely discernable near the eastern edge of the main cloud in frame 2003:0605. After that frame the enhancement disappeared, but after the appropriate time lapse for a wave moving at about 11 km/s, an enhancement appeared in the



• B

Fig. 3. Auroral features and Ba^+ clouds, 1957:33 UT, September 21, 1968, projected down magnetic field lines to 100 km altitude. Similar eastward rapid ray motions around 10 km/s, occurred in ion cloud I2 when the aurora was partially in the same L shell. The motions in the barium were noticeable in the eastern half of the cloud coinciding with a loop in the aurora.

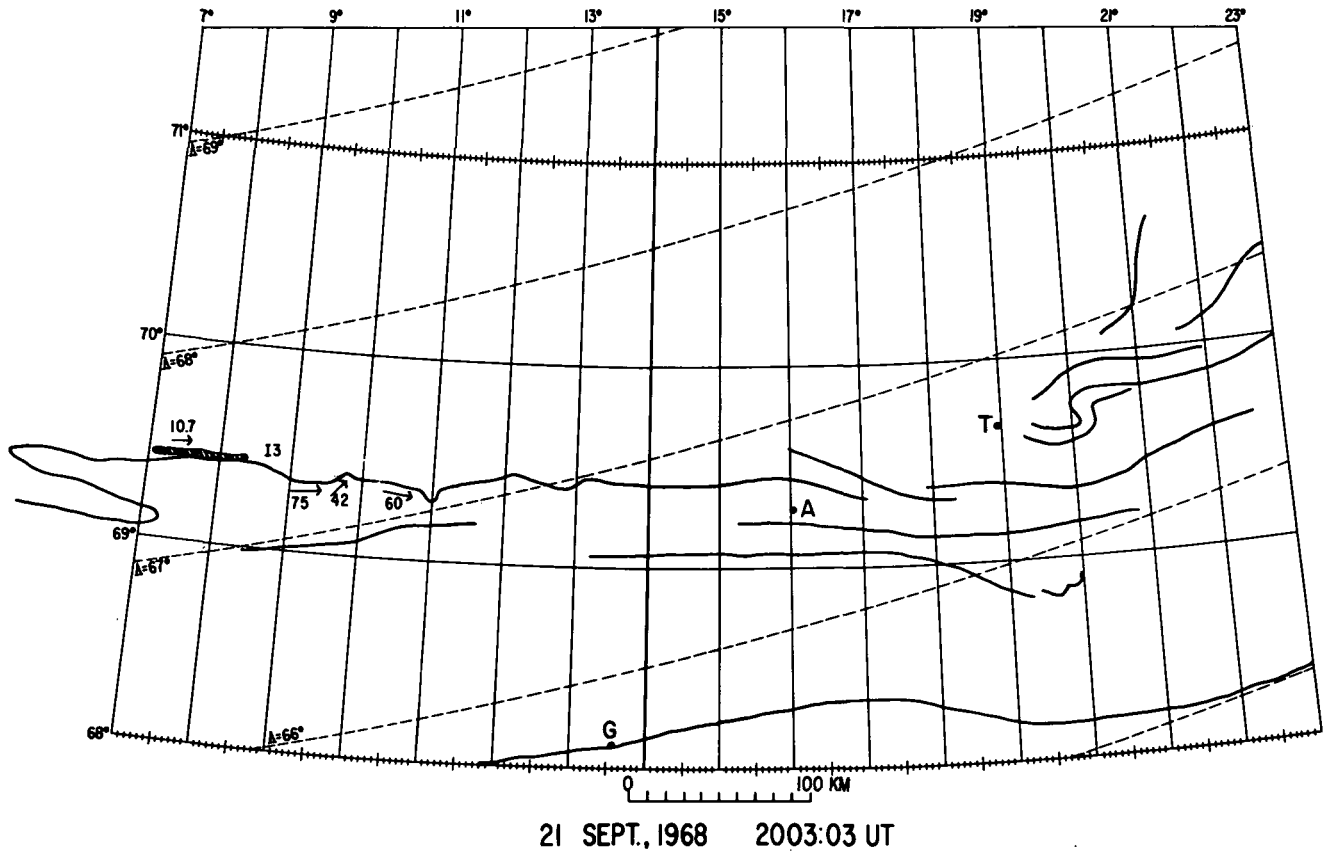
isolated ray near the right or eastern edge of the pictures and then disappeared. This strongly suggests that the phenomenon is an enhancement of the local barium ion emissions rather than the physical motion of some portion of the barium ion cloud with that velocity.

Another significant fact derived from the sequence of single TV frames (Figure 5) is that the enhancement between the bright rays 2003:03.00–2003:04.00 was moving a distance equal to its width in about $1/6$ s. The $1/6$ s rise and fall time is very close to the local Ba^+ gyro frequency, or close to resonance.

Another series of rapid ray motions and brightenings occurred on March 21, 1973, after the release of two Ba thermite clouds at 262 and 274 km altitude from NASA GSFC rocket 18.144 GE, launched from Poker Flat, Alaska, at 0600 UT. The releases were tracked from the University of Alaska observatory on Ester Dome with a multi-IO color TV system. The blue camera, which is sensitive to the 4554-Å line, during four intervals (0604:37 to 0604:52 UT in cloud I1; 0605:31 to 0608:15 UT, 0612:58 to 0613:45 UT, and 0615:00 to 0615:32 UT in cloud I2) recorded rapid flutterings and narrow brightenings moving west to east through nearly stationary striated clouds which were very similar to the September 1968 Norwegian events. Figure 6 shows the blue

TV signal intensity traces vs. time from 0605:35 to 0606:00 UT, at nine locations spaced 1.63 km apart west to east (top to bottom) in the second ion cloud, which was drifting westward at about 750 m/s. In the moving narrow brightness waves the enhancement was not as great as the September 21, 1968, 2003 UT ray. But the velocity, proportional brightening, and nonpermanent disturbance of the striated Ba^+ form were similar. There are several waves moving through at around 10 km/s. From about 0605:46 to 0605:50 a complicated brightening with a sharp peaked ray which had a brightness increase over the barium cloud background of 25–30%, moved from the west edge to the east edge with an apparent velocity of 13 km/s. The amplitude decayed to zero at the east edge. The rise and fall time of the brightest ray is about 1 s compared to the $1/6$ s of the Andøya ray of Figure 5. The moving ray enhancements were not seen in the green camera, which is not sensitive to Ba II lines but is sensitive to auroral emissions.

The last example of the phenomena occurred during a NASA sponsored University of Alaska shaped charge experiment "Miss Peggy" launched from Poker Flat, Alaska, March 22, 1980, with detonation at 617 km altitude at 1143:04 UT. The detonation occurred very near the magnetic zenith at Fort Yukon, Alaska, where we observed with an IO



• B

Fig. 4. Auroral features and Ba^+ clouds, 2003:03 UT, September 21, 1968, projected along magnetic field lines to 100 km altitude. A very bright ray ($\geq 3X$ undisturbed value) moved eastward along cloud 13 with average velocity of 10.7 km/s. Other arrows and numbers indicate the location of measurable auroral ray motions in kilometers per second.

system identical to the one used for the Bodø experiments. By 45 s after the injection, the field-aligned upward streaming plasma was well within a band of active aurora essentially in the magnetic zenith. For about 2 min there were rapid auroral ray motions with typical velocities of a few kilometers per second. During this period the barium striated along field lines and sheared horizontally, and various portions of flux tubes exhibited rapid fluctuating horizontal motions. Some were similar to a flag waving in the wind. The typical fluctuation had a period of about 2 s and an apparent velocity of about 2 km/s. By the end of the fluctuating phenomena the tip of the plasma jet would have been near 2000 km altitude. Figure 7 shows a pair of Fort Yukon TV frames in white light taken 3 s apart at 1144:30 which shows the rapid flag waving distortion. The TV recordings also showed higher-frequency fluttering of the Ba^+ , indicating the presence of higher-frequency waves.

It is a curious fact that in all cases of single moving raylike enhancements the motion was from west to east, while rapid ray motions in auroral arcs are often observed both eastward and westward.

DISCUSSION OF MECHANISMS

There is a range of phenomena which have been observed, which may involve several mechanisms. We will use the

September 21, 2003:03 event as a classic example of the solitonlike single rays to examine various physical processes.

The first point to be considered discussing various mechanisms for the enhancement phenomenon is the physical situation of the undisturbed Ba^+ cloud. At the time of observation the cloud was fully ionized; that is, there was no reservoir of Ba neutrals in the region to be ionized by some process to increase the ion density and hence the ion line emissions. The light observed in the 4554-Å line from the normal cloud is due almost entirely to solar resonance fluorescence. Nonoptically thick clouds illuminated by sunlight produce, on the average, 0.38 photons/ion/s at 4554 Å [Stenbaek-Nielsen, 1989]. In order to have an enhancement of emissions in an optically thin cloud there must either be an increase in the number of excited Ba^+ ions in the optical path length or an increase of the emission rate. The first could occur by a local compression or a redistribution, with the total number of excited ions remaining constant. Alternatively, there could be an increase in the number of excited ions produced by energetic particle excitation or by collisional excitation with energetic atmospheric constituents. Finally, an increase in the emission rate is possible by an increase in the solar flux at Ba^+ wavelengths by Doppler shifting of the resonance lines.

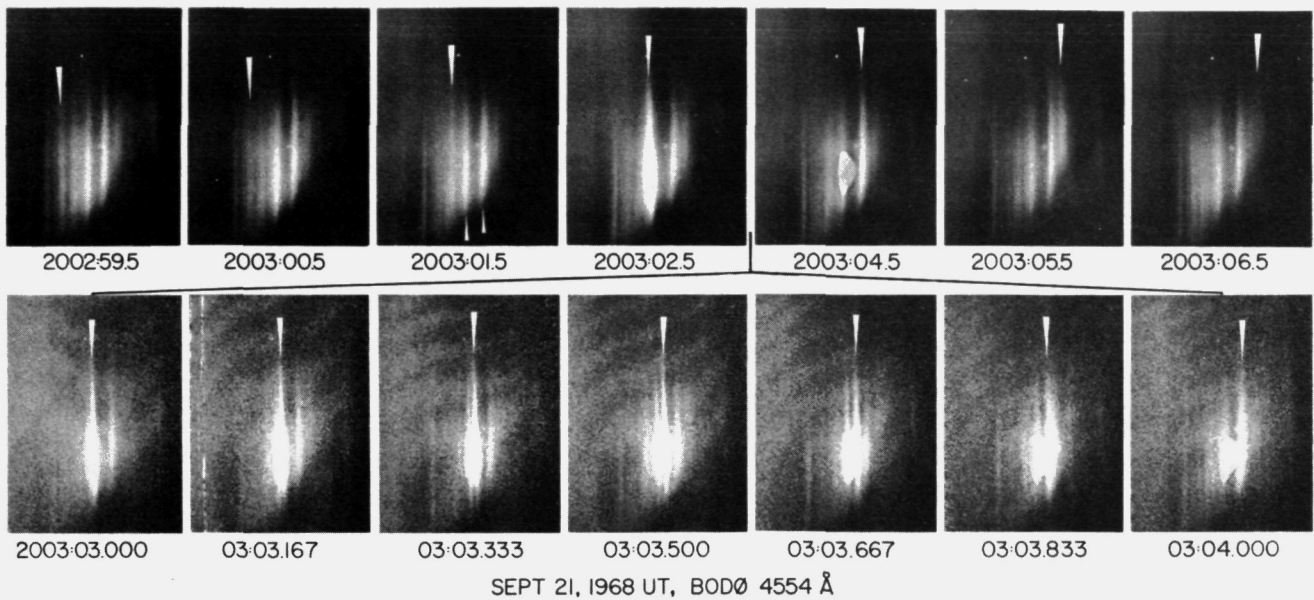


Fig. 5. TV pictures filtered for the 4554-Å Ba^+ emission taken looking NNW from Bodø, Norway, of the 2003:03 UT, September 21 event shown in Figure 4. The top pictures are 1 s apart at 1/4 s exposure (integrating over 15 TV fields). The bottom pictures are single TV fields (1/60 s) taken 1/6 s apart between 03 and 04 s of 2003 UT. The rapidly moving enhancement is indicated by the upper arrows. Note the relative brightness of the ray as it passes between the marked two bright stationary rays. Also note the similarity of the striated Ba^+ cloud in the first and last photographs, indicating the phenomenon did not permanently affect the cloud.

The observed enhancements were seen in a situation where the overall Ba^+ cloud was already fully solar illuminated. We will use a factor of 2 increase as the basis of discussion of mechanisms even though a factor of at least 3 was observed in some events.

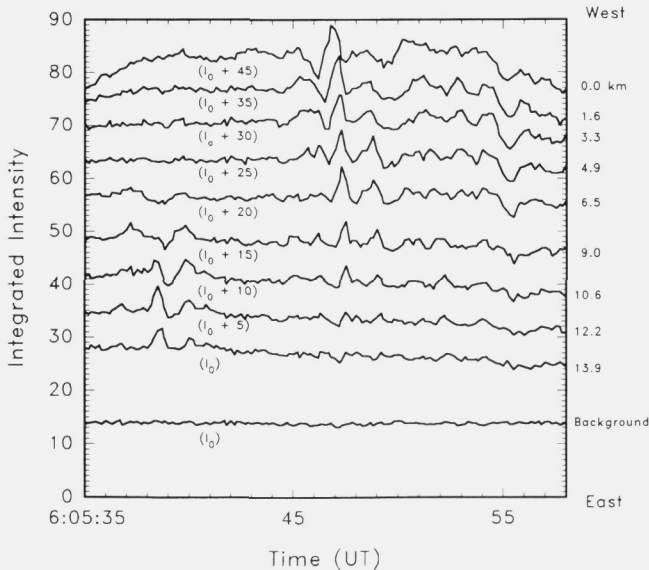


Fig. 6. Several of the March 23, 1973, brightenings illustrated by the relative intensity of the blue camera as a function of time at nine locations spaced 1.63 km apart along ion cloud I2 in a west to east direction. The traces are offset successively by 5 units of intensity. The bottom trace shows the background, including any auroral contamination, just outside the cloud. The traces show intensity fluctuations with periods from 1 s to 10 s. The bright sharp peak near 0605:47 represents an approximate 25–30% enhancement above the quiescent level and propagates eastward at an apparent velocity of 13 km/s.

POSSIBLE MECHANISMS

Energetic Particle Excitation

The most straightforward explanation for the enhancements and moving rays would be to assume that the same streams of electrons that are responsible for the auroral rays also excite the barium ions. If we must produce an enhancement equal to the solar resonance fluorescence, then $\sigma N_e = 0.38$ photons/ion/s, where σ is the excitation cross section and N_e is the energetic particle flux. Bacon and Hooper [1969] and Davis and Morin [1970] have measured the Ba ion excitation cross section in the laboratory at electron energies less than 100 eV. A typical value for 4554 Å is $\sigma = 10^{-15}$ cm² at 30 eV. Substituting this in the above equation, we find $N_e = 3.8 \times 10^{14}$ electron/cm²/s, with energies of 30 eV or a net energy flux of 1.7×10^4 ergs/cm²/s. This energy flux is 2 orders of magnitude greater than an IBC IV aurora. The brightest aurora seen on September 21 was approximately IBC III. Conversely, using a realistic flux requires a cross section 3–4 orders of magnitude larger than measured, so there is little likelihood that direct excitation by energetic particles could produce the observed enhancements. Such a large flux would produce detectable 5577-Å auroral emission even at the altitude of the cloud. In the March 21, 1973, event, the barium cloud was observed with an additional camera filtered at 5577 Å. No auroral emissions were observed.

Bulk Motion of Ba^+ Under $E \times B/B^2$ Drift

Another possible mechanism is a strong local E field directed southward which moves a portion of the barium cloud rapidly past the rest of the cloud as shown in Figure 8a. The very localized E field would have to be about 535 mV/m to produce the average rapid ray velocity, as compared to the field of about 10 mV/m deduced from the general

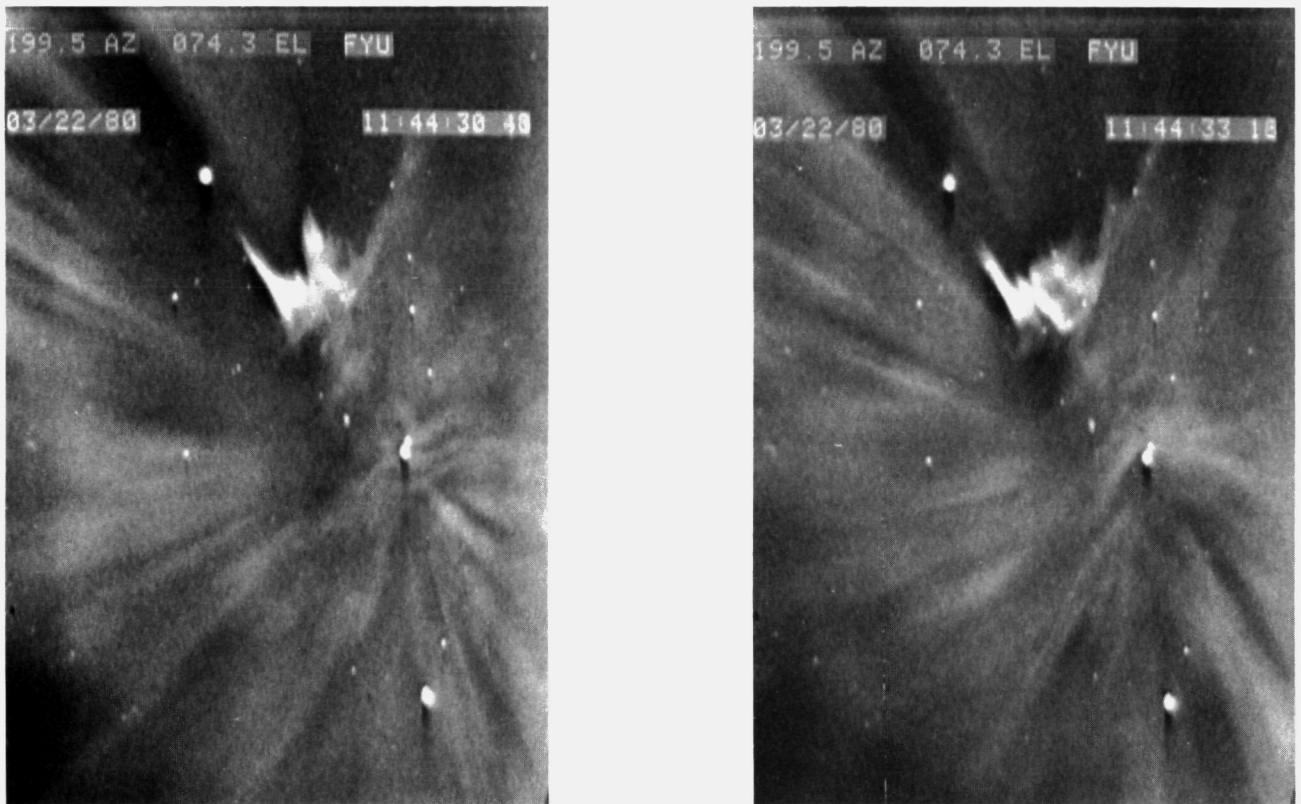


Fig. 7. A pair of TV frames from March 22, 1980, "Miss Peggy" experiment, 3 s apart (86 and 89 s after injection). The rapid fluctuating (like a waving flag) distortion of the barium can be seen (bright jagged form left center). Rapidly moving coronal auroral rays are also visible with similar motions. From Wescott [1981].

cloud drift in the region at the time. But this mechanism would not fit the observation that the moving ray disappeared between the main cloud and the last eastern ray. Furthermore, the enhancement tends to be proportional to the existing intensities rather than a constant incremental addition.

Consequences of Irregular Plasma Density on Ba^+ Cloud Motions

Heppner *et al.* [1971] have shown in a qualitative manner how the shape of a Ba^+ cloud (drifting with $\mathbf{E} \times \mathbf{B}/B^2$) is altered as it passes over ionospheric density irregularities.

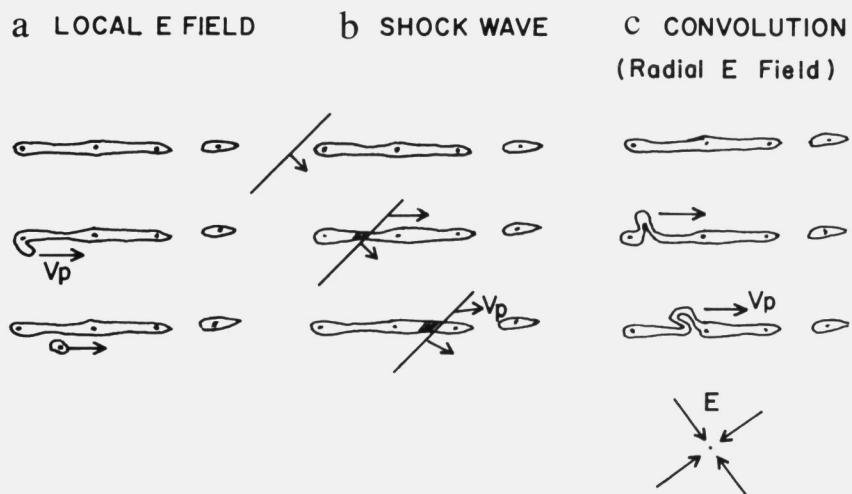


Fig. 8. Schematic diagram of three of the mechanisms investigated for the September 21, 2003:03 event. (a) Bulk motion of Ba^+ under $\mathbf{E} \times \mathbf{B}/B^2$ drift. (b) Solitonlike wave, either compressional or electrostatic. (c) Kelvin-Helmholtz instability.

To conserve Hall current continuity and to have no excess charge as a flux tube moves from a region of low electron density to one of high density, the velocity must decrease or field-aligned current must flow out of the ionosphere, and vice versa in going from a high to a lower density region the velocity increases or current flows into the ionosphere. Imagine a thin, not necessarily uniform, barium sheet, moving with $\mathbf{v} = \mathbf{E} \times \mathbf{B}/B^2$ parallel to the plane of the sheet, intersecting a stationary sheet of plasma density. As \mathbf{v} would decrease in the area of intersection, Ba ions would pile up, increasing the density and thus causing a local emission enhancement. The enhancement would appear to move through the Ba⁺ cloud in the opposite direction as the $\mathbf{E} \times \mathbf{B}/B^2$ drift. In the case of the 2003:03 event, however, the drift motion of the cloud was eastward in the same direction as the motion of the enhancement. In this case, or where the high density irregularity (the auroral shell) moves in the same direction as the $\mathbf{E} \times \mathbf{B}/B^2$ drift, it is easy to demonstrate that a rarefaction rather than a compression of Ba⁺ ions would be formed solely on the basis of velocity decrease.

The second effect of maintaining Hall current continuity suggested by *Heppner et al.* [1971] is field-aligned current into the ionosphere as the foot of the Ba⁺ tube of force encounters a higher electron density in the lower ionosphere, if one does not allow excess ions in the tube. Accompanying such a redistribution of charge, there might be a flow of Ba ions in the vicinity of the lines of force encountering the higher electron density. However, it is not clear that such a redistribution could produce a sufficient increase of Ba⁺ in the line of sight column to increase the intensity sufficiently.

Kelvin-Helmholtz Instability

Hallinan and Davis [1970] have presented evidence from auroral TV pictures and laboratory photographs of electron sheet beam instabilities that small-scale spatially periodic distortions of auroral forms are a result of this instability. Earlier theoretical work had suggested the creation of auroral folds by radial electric fields in $\mathbf{E} \times \mathbf{B}/B^2$ drift [*Alfvén*, 1950]. *Webster* [1957] suggested the possible connection between the "sheet beam instability" and auroral rays and pointed out that the rotational sense of the folds indicates the sign of the charge carrier in the beam. *Hallinan and Davis* [1970] have shown from TV data that small-scale rays (with velocities similar to those being considered here) occur as quasi-periodic vortices or tight curls. "The curls (94 examples) generally have a near circular symmetry, a wavelength of less than 10 km, a lifetime of less than 2 s and apparent horizontal velocities of between zero and 20 km/s" [*Hallinan and Davis*, 1970, p. 1738]. All 94 examples in the northern hemisphere were curled counterclockwise viewed from the ground. Motions both eastward and westward were observed but when seen in the zenith motions were often in the northernmost or southernmost elements of a multiple arc and then motions were without exception counterclockwise with respect to the center of the arc.

The time scale for the formation and decay of a curl is short, and *Hallinan and Davis* [1970] require an E field of 500 mV/m across the arc and reversing sign on the other side. The instability in such a field configuration arises naturally with small perturbations and develops quickly. At the time

scale of the fast barium ray enhancements, this would feed the cyclotron motion and would not produce any bulk velocity. But at a slower ray speed, the barium could by $\mathbf{E} \times \mathbf{B}/B^2$ motion follow the auroral ray. Figure 8c illustrates this convolution of the cloud.

This theory of auroral ray motions would appear to be applicable to at least one type of event seen in the barium clouds. This would seem most applicable to the March 1980 "Miss Peggy" events where the Ba⁺ was observed to fold and curl like a waving flag. If radial fields develop in the arcs and are present in the barium cloud, the fold to curl development and motion would produce the observed results. Large fields of near 250 mV/m and reversals across arcs have been observed from the DE 2 satellite at around 950 km altitude with scale sizes of 10 km or less [*Heelis and Vickerey*, 1991]. Auroral zone fields at 200 km altitude of greater than 100 mV/m are exceptional, most being near 50 mV/m or less. The existence of larger fields is suggested by Ba⁺ ion cloud data, but they are probably of short duration and not common.

Compressional Wave

It might be possible to produce the enhancement by increasing the line-of-sight number density locally without increasing the rate of excitation by means of a wave front moving horizontally with a compressional phase. To produce the enhancement, the local barium ions would have to be compressed at the expense of a rarefaction elsewhere in the cloud. There are no suitable waves known to us which travel at approximately 10 km/s in the ionosphere and with compressions of up to a factor of 3. Such a wave, however, need not travel at the observed phase velocity. For instance, as shown in Figure 8b, a plane wave front traveling at 2 km/s impinging on the cloud at an angle of 11.5° off perpendicular would have an apparent phase velocity along the cloud of 10 km/s. For smaller angles, less velocity is required, so one might think in terms of acoustic waves, generated in the auroral process propagating away from the aurora. *Farley* [1963] discussed a two-stream ion wave instability resulting in field-aligned irregularities in the ionosphere. Perhaps under some auroral conditions where the rapid motions arise, the strong velocity shears near the edges of arcs produce moving instabilities applicable to this phenomenon. This mechanism does not require a large E field but does require a strong compressional (3X) wave. If one considers the Ba ions to be tightly bound to the magnetic field lines, this suggests the same compression in the magnetic field, which does not seem possible on an energy basis and on the near incompressibility of the field at these altitudes.

The velocity of a field line as a magnetoacoustic wave passes by is independent of the wavelength and independent on the ΔB and phase velocity. It is given by

$$v_{\parallel} = [B_0/(B_0 + \Delta B) - 1]v_{\text{ph}}$$

For $v_{\text{ph}} = 10.7$ km/s, $\Delta B = 0.1B_0 = 4700$ nT, $v_{\parallel} = 0.98$ km/s. But clearly 4700 nT is an unreasonably large number.

Differential Motion Producing Doppler Broadening in an Optically Thick Cloud

In an optically thick Ba⁺ cloud the solar continuum emissions at Ba⁺ wavelengths are absorbed and scattered as

TABLE 1. Thermal Doppler Broadening

T , K	FWHM, Å	ξ , m/s
1000	0.0088	578
2000	0.0124	817
3000	0.0159	1001

they pass through the cloud to such an extent that for $\tau = 1$ the intensity of direct radiation on the side opposite the sun is down by a factor of $1/e = 0.368$. Consequently, some Ba^+ ions will not be radiating at the average 0.38 photons/s and the cloud will not be as bright as the number density in a line-of-sight path predicts. If by some acceleration process the ions "shaded" from the solar light at 4554 Å were Doppler shifted away from the line, they could absorb and radiate as if that part of the cloud were optically thin, thus increasing the observed intensity. This mechanism requires differential motion within the cloud.

The change in wavelength $\Delta\lambda$ of a line emission of wavelength λ due to motion of the emitting atoms with velocity component ξ along the line to the Sun is given by $\Delta\lambda/\lambda \cong \xi/c$. From this relationship one may calculate the shape of the emitted line due to the Doppler effect resulting from thermal motions, assuming that resonance broadening is negligible. Table 1 gives the full width at half maximum (FWHM) from a formula given by Breene [1964] for the $BaII$ line at 4554 Å and the corresponding velocity components ξ as derived from the above equation to give a Doppler shift equal in magnitude to the line width.

An atom moving along a line away from a source of light will absorb a Doppler-shifted photon. The same atom could emit an unshifted photon in the plane perpendicular to its motion, or a Doppler-shifted one in any other direction, with the maximum shift along the line of motion. This fact can enable Ba^+ ions inside an optically thick cloud to appear brighter as a result of motion. Let us consider two limiting cases where a localized group of ions move with sufficient velocity such that either the absorbed or radiated photons are Doppler-shifted away from the optically thick line.

Case I. The Ba^+ motion is along the Sun-cloud line. The moving ions absorb Doppler shifted photons from the full unreduced solar flux. An observer in a plane perpendicular to the motion would see an enhancement in the unshifted emission with some absorption by any non-moving Ba^+ ions in the cloud observer path. An observer on the line of motion would also observe an enhancement with a Doppler shift and no absorption by stationary Ba^+ in the path. The Doppler shift is much smaller than the passband of the filter used.

Case II. The ion motion is perpendicular to the Sun-cloud line. Only unshifted (optically thick) photons would be absorbed, but emissions along the line of motion would be Doppler-shifted. There would be some enhancement due to the lack of absorption by stationary ions.

This mechanism seemingly could apply to the September 20, 1934:19 event. Photometric measurements with atmospheric extinction taken into account [Guttman, 1968] indicate that for the September 20, 1934:19 event the main cloud was 83 kR in 4554 Å and may have been optically thick [Horak and Whittaker, 1982]. However, the ray enhancements were seen in the diffuse portion of the cloud between

the main cloud and the neutral cloud, and this portion of the cloud was almost certainly optically thin.

Doppler Shifting of Resonance Lines Relative to Fraunhofer Line

An important effect which can appreciably increase the emission rate of Ba ions moving with a velocity component parallel to the Sun-cloud line arises from the shape of the solar spectrum near each of the five prominent visible lines. Each of the $BaII$ lines (4554.033 Å, 4934.088 Å, 5853.675 Å, 6141.718 Å, and 6496.896 Å) are the minima of sharp, deep Fraunhofer absorption lines [Beckers et al., 1976]. The flux at 4554.03 Å is approximately 8% of the solar continuum level.

The presence of these deep, narrow Fraunhofer lines will make the barium ion emission rates highly velocity dependent. If Ba^+ ions move toward or away from the Sun, then the solar radiation they absorb will be Doppler-shifted away from the absorption lines. The consequence of this is that the effective solar flux absorbed and thus the volume emission rate could increase significantly. This could occur and create an enhancement even though the cloud was optically thin. The Doppler brightening from accelerated Ba^+ was invoked by Wescott et al. [1976] to explain the brightening of the high-altitude Skylab Ba^+ streak reacting to the E field of a double layer.

A general discussion of the Doppler effect on the barium ion emission rates has been given by Stenbaek-Nielsen [1989]. While the 4554-Å emission rate at zero Doppler velocity is 0.38 photons/ion/s, at a Doppler velocity of 3 km/s the rate increases to 1.0 photons/ion/s and at 6 km/s the rate is 2.0 photons/ion/s. Emission rates were also calculated including the effects of ion gyromotion showing a similar, but not as drastic, increase with velocity. The emission rates were calculated for radiative equilibrium which cannot be assumed to be maintained during the 1/6 s rise time for the events considered here. For this condition the change in brightness would initially be closer to the change in solar illumination, followed by a slower change toward radiative equilibrium. For the 4554-Å emission a rapid change in velocity should initially increase the emission rate somewhat more than given by Stenbaek-Nielsen [1989].

To assess the effect more quantitatively, the computer codes used by Stenbaek-Nielsen [1989] were adapted to reflect the conditions for the events reported here. At the time of the releases the angle between B and the direction toward the Sun was approximately 75°. The ion cloud drifted toward the west at 200 m/s, essentially canceling the eastward velocity due to the rotation of Earth. Thus the cloud itself had zero Doppler velocity. Because of the near perpendicularity between B and the direction to the Sun, the Doppler brightening is most sensitive to changes in the gyromotion of the barium ions. (For motion along B velocities of 10–30 km/s would be required, which we find unrealistic.) The temperature at the events, as given by MSIS86 [Hedin, 1987], was 1050 K, corresponding to a barium ion gyrovelocity of 0.357 km/s. In radiative equilibrium this results in a 4554-Å emission rate of 0.39 photons/ion/s compared with 0.38 for zero Doppler velocity. A rapid increase in the gyrovelocity to 3.5 km/s will double the emission rate, and it will triple at a gyrovelocity of 4.7 km/s.

A computer code to calculate the motions of an ensemble

of barium ions was used to assess the response of barium ions to a transient electric field. Since the $1/6$ s time constant of the electric field transient is comparable to the 0.2-s Ba^+ gyroperiod, it is necessary to integrate the full equation of motion

$$dv/dt = q(\mathbf{E} + \mathbf{v} \times \mathbf{B})$$

The model electric field is taken to be a moving electrostatic disturbance of the form

$$\mathbf{E} = \mathbf{1}_x 2.33 E_0 \alpha \exp(-\alpha^2)$$

where $\alpha = (x/u - t)/t_0$, where u is the propagation velocity of the disturbance and t_0 is the disturbance time constant. For the model calculations, we take the electric field amplitude E_0 to be 100 mV/m and the magnetic field intensity to be 0.5G in the z direction.

Figure 9 shows scatter plots of an ensemble of 5000 ions distributed over a horizontal distance of 20 km. The top frame shows a $v_y - x$ scatter plot, while the bottom frame shows the $v_x - x$ scatter plot. The solid curve is the $\mathbf{E} \times \mathbf{B}/B^2$ drift, which shows also the electric field profile. Since the wave propagates to the right, the ions to the right are undisturbed. The thermal velocity is 357 m/s, corresponding to a temperature of 1050 K. The full scale velocity is 6.25 km/s, and the $\mathbf{E} \times \mathbf{B}/B^2$ drift velocity maximum is 2 km/s. In this particular example, the time constant $t_0 = 1/6$ s, and the wave velocity $u = 10.8$ km/s. The scatter plot shows that the wave accelerates the ions momentarily to a speed of somewhat more than 3 km/s and leaves the ions gyrating with a speed of 1.5 km/s after the passage of the wave.

Figure 10 shows scatter plots similar to those in Figure 9, except that the time constant is $t_0 = 1/15$ s, less than that of

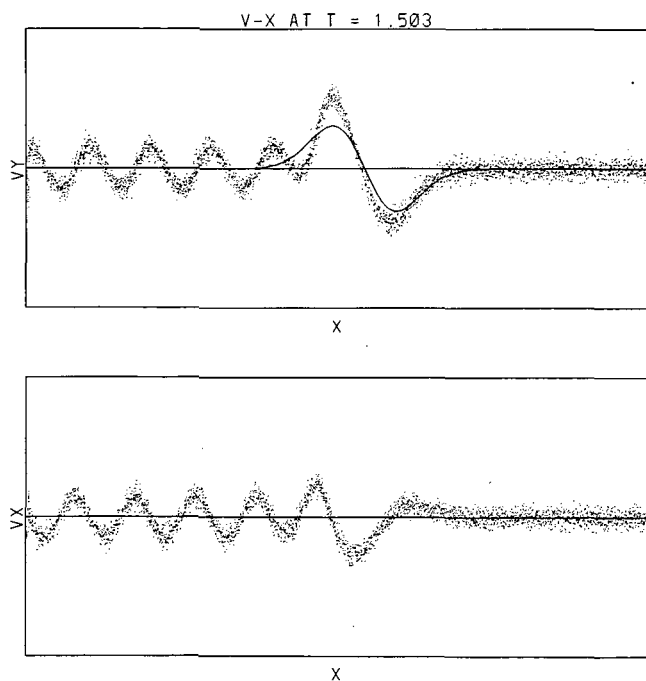


Fig. 9. Scatter plots of 5000 Ba^+ ions in $x - v_y$ space (top) and $x - v_x$ (bottom), at $T = 1.503$ s. The horizontal scale is 20 km, and full scale velocity is 6.25 km/s. The solid curve in the top frame is the $\mathbf{E} \times \mathbf{B}/B^2$ drift velocity. The electrostatic wave propagates from left to right.

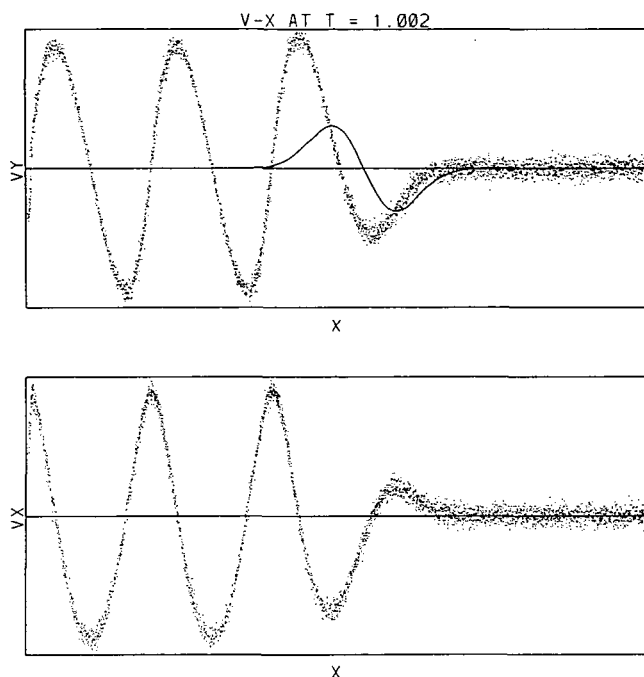


Fig. 10. Same as Figure 9, at $T = 1.002$ s, except the wave has a smaller time constant and double the wave propagation speed.

the previous example, and the wave speed is double at 20.16 km/s. The wave couples more efficiently to the ions so the gyrotational speed of the ions is about 6 km/s. Moreover, the ions retain most of the gyrotational motion after the passage of the wave.

The example shown in Figure 9 indicates a velocity sufficient to nearly double the emission rate, while the examples in Figure 10 shows a sufficient velocity to more than triple the rate. However, the simple trajectory calculations also indicate the high gyrotational velocities will persist after the passage of the wave. This would imply that the brightening should persist for some time after the wave had passed. Since the brightening is promptly extinguished with the passage of the wave, there must be mechanism to rapidly damp the barium gyromotion within a gyroperiod. Collisions with atmospheric atoms and molecules are too few to explain the energy loss. The collision frequency assuming a collision cross section of 3×10^{-15} cm² for the gyrovelocities under consideration here is no more than 5/s which, given the large mass ratio between barium and the atmospheric constituents, leads to a too large time scale for collisional thermalization of the ions. A more likely explanation for damping is that energy could be lost to radiation of waves from one or more plasma instabilities, such as the modified two-stream instability, quickly damping the gyro motion after the transient \mathbf{E} field has passed. We discuss this possibility in the next section.

The combination of the effects appears capable of producing the observed enhancement with reasonable E fields.

ANALYSIS OF DAMPING OF ENHANCED GYROMOTION

Figure 10 indicates that the effect of the electrostatic disturbance is to generate an ion beam with a velocity considerably in excess of both its thermal velocity and the thermal velocity of the ambient O^+ ions. Such a velocity

distribution is highly unstable to both the modified two-stream instability with the electrons and a two stream instability with the ambient ions. The major question is whether the instability will grow fast enough to quickly damp the ion gyromotion and whether the wave lengths are short enough to fit within the spatial volume of the barium and the disturbed region.

To investigate these questions, we analyzed the following dispersion relation for electrostatic waves generated by a beam of barium ions moving in the x direction with velocity U :

$$k_{\parallel}^2 + (1 + \Pi_e^2/\Omega_e^2)k_{\perp}^2 = \Pi_b^2 Z'(\zeta_b)/v_{thb}^2 + \Pi_o^2 Z'(\zeta_o)/v_{tho}^2 + \Pi_e^2 Z'(\zeta_e)/v_{the}^2$$

where Z' is the derivative of the plasma dispersion function, and the subscripts b , o , and e refer to the barium, ambient oxygen, and electrons, respectively. The components of the wavenumber parallel and perpendicular to the magnetic field are denoted by the parallel and perpendicular symbols, respectively. Π is the plasma frequency, Ω_e is the electron gyrofrequency, and v_{th} denotes the thermal speed. The arguments of the dispersion function in the barium, oxygen, and electron terms are $\zeta_b = (\omega - \mathbf{k} \cdot \mathbf{U})/kv_{thb}$, $\zeta_o = \omega/kv_{tho}$, and $\zeta_e = \omega/k_{\parallel}v_{the}$, respectively.

This dispersion relation approximates both the barium and ambient oxygen ions as being unmagnetized, and the electrons as being strongly magnetized. The assumptions are that the wavelengths are short in comparison to the ion gyroradii and the wave frequencies and growth rates are large in comparison to the ion gyrofrequencies. The strongly magnetized electron approximation assumes the electron gyroradius is small in comparison to the wavelength and the electron gyrofrequency is much larger than the wave frequency. These assumptions will be verified a posteriori. As a specific example, we take both the barium and ambient oxygen ion density to be 10^5 cm^{-3} and both species to have a temperature of 1050 K. The electron density is then $2 \times 10^5 \text{ cm}^{-3}$, and the electron temperature is also taken to be 1050 K. With these values, the electron Debye length is 0.7 cm, and the electron gyroradius is 2.0 cm.

Taking the barium ion velocity to be 6.2 km/s, as indicated by the example of Figure 10, we find solutions to the dispersion relation for growing waves at a perpendicular wavenumber of 0.15 cm^{-1} for wave normal angles of 90° and 89° but no growing solutions at 88° . At 90° the frequency and growth rate are $8.3 \times 10^4 \text{ s}^{-1}$ and 3116 s^{-1} , respectively, and the frequencies and growth rates are about the same at 89° . At 90° the instability is a two-stream interaction between the barium and ambient O^+ ions, while at 89° the interaction is more of a modified two-stream instability between the barium and electrons. At smaller wave normal angles, the electrons absorb too much energy through parallel Landau damping to permit wave growth.

The effect of the wave is to slow down the gyrational motion of the barium ions. We therefore checked the dispersion relation at a beam velocity of 3.1 km/s. Keeping the same wavenumber but decreasing the beam velocity by a factor of 2 decreases the resonant wave velocity and the frequency by a factor of 2. The frequency and growth rate at a wave normal angle of 90° are $3.52 \times 10^4 \text{ s}^{-1}$ and 7791 s^{-1} , respectively. There are no growing waves at a wave normal

angle of 89° due to strong electron Landau damping, but there are modified two-stream instability waves at a wave normal angle of 89.5° with a frequency of $4.4 \times 10^4 \text{ s}^{-1}$ and a growth rate of 2493 s^{-1} .

The examples were for an arbitrarily chosen wavenumber, so the growth rates are not necessarily the maximum possible growth rates. However, it is clear that the frequencies and growth rates are far in excess of the ion gyrofrequencies but considerably less than the electron gyrofrequency. The perpendicular wavenumber used in the examples also justifies the assumptions of considering the ions to be unmagnetized, but the electrons to be strongly magnetized. The rapid growth rates calculated also suggest that the waves should reach an amplitude sufficient to significantly modify the barium beam within a fraction of an ion gyroperiod. Moreover, the perpendicular and parallel wavelengths for a wave normal angle of 89.5° are 0.4 m and 48 m, respectively. These are far smaller than the dimensions of the barium cloud, implying that geometrical considerations should not be a significant factor in the interpretation of the analysis.

The growth rates for the beam-generated electrostatic waves are so large that it should not be at all surprising that the beam is quickly stopped. The large wave growth rates indicated by the analysis, in fact, raise the question of how the barium ions could even be accelerated to velocities approaching 3 km/s. Referring to Figures 9 and 10 and inspection of the leading edge of the wave suggests the answer. Initially, the differences between the barium ion velocity and $\mathbf{E} \times \mathbf{B}/B^2$ drift velocity are small. This means that since the electrons and O^+ ions are moving at approximately the same speed, the wave growth rates will be small. The big velocity differences between the barium and ambient species show up after the center of the wave has passed, leaving the barium ions with a relatively large velocity difference with respect to the ambient species.

CONCLUSIONS

The observed rapid motions of emission enhancements in 4554 \AA through several Ba^+ clouds while nearby (but lower altitude) auroras were undergoing rapid ray motions suggest a close connection between the two phenomena. Apparent velocities along the extended and striated Ba^+ clouds of 2–20 km/s were measured. Enhancements of the order of 2 km width of at least 3X in one case were measured. Furthermore, the moving ray disappeared in the space devoid of Ba^+ between two parts of a cloud but reappeared with the proper time delay for a wave moving eastward at around 10.7 km/s. Several suggested mechanisms to explain the phenomena have been discussed. We consider the following:

1. Incremental increases of the Ba^+ excitation rate by energetic electrons is ruled out on energy flux and cross section considerations.
2. $\mathbf{E} \times \mathbf{B}/B^2$ motion under a field of $>500 \text{ mV/m}$ is unlikely.
3. A redistribution of Ba^+ ions as a high electron density irregularity passes through the field lines containing the cloud seems possible, but the magnitude of the effect cannot be estimated on the present qualitative theory.
4. Another mechanism based on sheet beam instabilities is aesthetically pleasing in that it would produce the moving rays in the Ba^+ cloud by the same mechanism as in the

auroras, but it requires an E field of 500 mV/m and field direction reversal across the arc. Such large fields have not been observed near 200 km altitude on the basis of many satellite passes and rocket flights over the auroral zones.

5. Local density increases by compressional waves (perhaps an acoustic wave with local propagation velocity impinging at a small angle to the cloud) seem to be unable to produce the factor of three brightness observed and no other waves with velocities near 10–20 km/s are known to us.

6. The Doppler broadening due to differential velocities within an optically thick cloud could produce noticeable brightening. This is an unlikely mechanism for any of the events described here since all of the brightenings appear to have occurred in optically thin clouds. In any case, the velocities required for this mechanism are similar to those required for mechanism 7, so the distinction is not crucial.

7. Localized velocity toward or away from the Sun can increase the brightness of the barium by Doppler shifting the resonance line away from the deep Fraunhofer minimum in the solar spectrum. This effect is substantial and is regularly observed in barium experiments. For example, inclusion of this effect is necessary to model the brightness distribution with altitude in barium shape charge experiments [Stenbaek-Nielsen *et al.*, 1984; Hoch and Hallinan, 1993]. The same effect was cited to explain a brightening by a factor of three in the Skylab barium jet [Wescott *et al.*, 1976]. The brightenings observed here are of the same magnitude and could easily be produced by the same mechanism. However, they are more complicated as they also involve rays moving through the cloud.

At a fixed point, as a ray appears to move through the cloud, the ions must first increase in brightness and then return to their original brightness. If we are to invoke the Doppler mechanism, we conclude that the ions speed up and then slow down as the ray moves through. This localized ion velocity is distinct from the ray velocity which must be regarded as the phase velocity for some disturbance propagating through the cloud. Moreover, since the time scale, at least for the more dramatic examples, is similar to the Ba⁺ gyrofrequency, the ion velocity is not $\mathbf{E} \times \mathbf{B}/B^2$. Because of the near-resonance condition, a transient field with a peak amplitude near 100 mV/m could be sufficient to produce the observed brightening.

To account for both the brightening and its apparent motion through the cloud, it is necessary to assume a localized electric field that propagates through the cloud. The disturbance might occur within and also at some distance from an auroral arc but in all cases seems to be associated generally with fast auroral ray motions. This suggests several possibilities. One is a traveling potential minimum, such as due to a field-aligned negative charge concentration associated with an auroral ray. Another is an electrostatic wave generated in the auroral vicinity with properties similar to a soliton traveling through the cloud. Model calculations for the 2003:03 Bodø situation show that either of these two moving electric fields are near resonance with the Ba⁺ gyrofrequency and can produce the brightening with a fluctuation of about 100 mV/m. Other single ray brightenings at higher and lower velocities would be further away from resonance and presumably would have less brightening. This is qualitatively in agreement with the observations as the 2003:03 event had the most intense brightening.

The chief difficulty with the proposed mechanism for the brightenings by increasing the gyrovelocity and Doppler shifting out of the Fraunhofer lines is that a mechanism other than collisions with ambient atmosphere is required to decelerate the ions to near their original thermal velocity within a gyroperiod. Our analysis of the dispersion relation for the Ba⁺ ion beam with an ambient O⁺ and electron background indicates rapid growth rates of a two-stream interaction between the barium and O⁺ ions and a modified two-stream instability between the barium and the electrons after the center of the wave has passed. The rapid growth rates indicate that the waves should reach an amplitude to sufficiently damp the gyromotion within a fraction of the gyroperiod.

In conclusion, we have documented several cases of severe disturbances propagating through barium ion clouds. The disturbances were associated with auroral arcs that were on or near the same L shell as the barium and that indicated rapid ray motion. The most plausible interpretation of the observations is that there are localized solitonlike electric field pulses with peak amplitudes of about 100 mV/m generated in the active aurora. The disturbances are observed in barium clouds near 200 km altitude. They have spatial dimensions of the order of 1 km and phase velocities of 5–20 km/s. At a fixed point, this produces a pulse duration of 0.1–0.2 s.

Acknowledgments. We particularly thank M. Miller for her efforts in programming and reducing some of the barium photographs in the analysis. Russell Beach provided excellent assistance in making TV observations and photographs. We especially acknowledge the contributions and discussions of J. Romick, J. P. Heppner, and John Stolarik. We thank E. Hoch for his analysis of the March 21, 1973, events. This work was supported in part by NASA grants NAG6-1, NSR 02-001-025, and NSR 02-001-035 and by NASA GSFC contract NAS 5-21220.

The Editor thanks J. H. Doolittle and another referee for their assistance in evaluating this paper.

REFERENCES

- Alfvén, H., *Cosmical Electrodynamics*, p. 206, Oxford University Press, New York, 1950.
- Bacon, F. M., and J. W. Hooper, Relative experimental cross sections for excitation of Ba ions by electron impact (8.0–98 eV), *Phys. Rev.*, **178**, 182, 1969.
- Beckers, J. M., C. A. Bridges, and L. B. Gilliam, A high resolution spectral atlas of the solar irradiance from 380 to 700 nanometers, *Rep. AFGL-TR-0126*, Air Force Geophys. Lab., Bedford, Mass., 1976.
- Breene, T. G., Line width, in *Handbuch der Physik*, vol. XXVII, edited by S. Flugge, p. 2–3, Springer-Verlag, New York, 1964.
- Davis, J., and S. Morin, Excitation of singly-ionized barium ions by electron impact, *Can. J. Phys.*, **48**(3), 275, 1970.
- Davis, T. N., and G. T. Hicks, Television cinematography of auroras and preliminary measurements of auroral velocities, *J. Geophys. Res.*, **69**, 1931, 1964.
- Davis, T. N., G. J. Romick, E. M. Wescott, R. A. Jeffries, D. M. Kerr, and H. M. Peek, Observations of the development of striations in large barium ion clouds, *Planet. Space Sci.*, **22**, 67–78, 1974.
- Farley, D. T., Jr., A plasma instability resulting in field-aligned irregularities in the ionosphere, *J. Geophys. Res.*, **68**, 6083, 1963.
- Guttman, A., Excitation coefficient measurements on clear atmospheres and thin cirrus clouds, *Appl. Opt.*, **7**(12), 2377, 1968.
- Haerendel, G., R. Lüst, and E. Reiger, Motion of artificial ion clouds in the upper atmosphere, *Planet. Space Sci.*, **15**, 1, 1967.
- Hallinan, T. J., and T. N. Davis, Small-scale auroral arc distortions, *Planet. Space Sci.*, **18**, 1735, 1970.

- Hedin, A. E., MSIS-86 thermospheric model, *J. Geophys. Res.*, **92**, 4649, 1987.
- Heelis, R. A., and J. F. Vickery, Energy dissipation in structured electrodynamic environments, *J. Geophys. Res.*, **96**, 14,189, 1991.
- Heppner, J. P., J. D. Stolarik, and E. M. Wescott, Field-aligned continuity of Hall current electrojets and other consequences of density gradients in the auroral ionosphere, in *The Radiating Atmosphere*, edited by B. M. McCormac, p. 407, D. Reidel, Norwell, Mass., 1971.
- Hoch, E. L., and T. J. Hallinan, Time series measurements of the time constant for steady ionization in shaped charge barium releases, *J. Geophys. Res.*, in press, 1993.
- Horack, H. G., and R. W. Whittaker, Resonance-fluorescence in barium ion clouds, *Planet. Space Sci.*, **30**, 897, 1982.
- Stenbaek-Nielsen, H. C., Calculated emission rates for barium releases in space, *Planet. Space Sci.*, **37**, 1441, 1989.
- Stenbaek-Nielsen, H. C., T. J. Hallinan, and E. M. Wescott, Acceleration of barium ions near 8000 km above an aurora, *J. Geophys. Res.*, **89**, 10,788, 1984.
- Webster, H. F., Structure in magnetically confined electron beams, *J. Appl. Phys.*, **28**, 1395, 1957.
- Wescott, E. M., The electric field structures of auroral arcs as determined from barium plasma injection experiments, in *Physics of Auroral Arc Formation*, *Geophys. Monogr. Ser.*, vol. 25, edited by S.-I. Akasofu and J. R. Kan, p. 175, AGU, Washington, D. C., 1981.
- Wescott, E. M., J. P. Heppner, and J. D. Stolarik, Electric fields in the vicinity of auroral forms from the motions of barium vapor releases, *J. Geophys. Res.*, **74**, 3469, 1969.
- Wescott, E. M., H. C. Stenbaek-Nielsen, T. N. Davis, W. B. Murcray, H. M. Peek, and P. J. Bottoms, The $L = 6.6$ Oosik barium plasma injection experiment and magnetic storm of March 7, 1972, *J. Geophys. Res.*, **80**, 951, 1975.
- Wescott, E. M., H. C. Stenbaek-Nielsen, T. J. Hallinan, T. N. Davis, and H. M. Peek, The Skylab barium plasma injection experiments, 2, Evidence for a double layer, *J. Geophys. Res.*, **81**, 4495, 1976.
-
- T. J. Hallinan, H. C. Stenbaek-Nielsen, D. W. Swift, and E. M. Wescott, Geophysical Institute, University of Alaska, C. T. Elvey Bldg., Fairbanks, AK 99775-0800.
- D. D. Wallis, Herzberg Institute of Astrophysics, National Research Council Canada, 100 Sussex Dr., Ottawa, Canada K1A 0R6.

(Received June 4, 1992;
revised October 16, 1992;
accepted October 16, 1992.)

Convection and Electrodynamic Signatures in the Vicinity of a Sun-aligned Arc: Results from the Polar Acceleration Regions and Convection Study (Polar ARCS)

L. A. WEISS,¹ E. J. WEBER,² P. H. REIFF,¹ J. R. SHARBER,³ J. D. WINNINGHAM,³
F. PRIMDAHL,⁴ I. S. MIKKELSEN,⁵ C. SEIFRING,⁶ AND E. M. WESCOTT⁷

An experimental campaign designed to study high-latitude auroral arcs was conducted in Sondre Stromfjord, Greenland, on February 26, 1987. The Polar Acceleration Regions and Convection Study (Polar ARCS) consisted of a coordinated set of ground-based, airborne, and sounding rocket measurements of a weak, sun-aligned arc system within the duskside polar cap. A rocket-borne barium release experiment, two DMSP satellite overflights, all-sky photography, and incoherent scatter radar measurements provided information on the large-scale plasma convection over the polar cap region while a second rocket instrumented with a DC magnetometer, Langmuir and electric field probes, and an electron spectrometer provided measurements of small-scale electrodynamic. The large-scale data indicate that small, sun-aligned precipitation events formed within a region of antisunward convection between the duskside auroral oval and a large sun-aligned arc further poleward. This convection signature, used to assess the relationship of the sun-aligned arc to the large-scale magnetospheric configuration, is found to be consistent with either a model in which the arc formed on open field lines on the dusk side of a bifurcated polar cap or on closed field lines threading an expanded low-latitude boundary layer, but not a model in which the polar cap arc field lines map to an expanded plasma sheet. The antisunward convection signature may also be explained by a model in which the polar cap arc formed on long field lines recently reconnected through a highly skewed plasma sheet. The small-scale measurements indicate the rocket passed through three narrow (≤ 20 km) regions of low-energy (≤ 100 eV) electron precipitation in which the electric and magnetic field perturbations were well correlated. These precipitation events are shown to be associated with regions of downward Poynting flux and small-scale upward and downward field-aligned currents of $1-2 \mu\text{A}/\text{m}^2$. The paired field-aligned currents are associated with velocity shears (higher and lower speed streams) embedded in the region of anti-sunward flow.

1. INTRODUCTION

The "polar cap boundary," the boundary between the bright, approximately circular, oval of auroral emission and the darker, interior polar region, has been variously defined on the basis of magnetospheric topology (the mapping of an assumed open/closed field line boundary) [Birn et al., 1991; Elphinstone et al., 1991], the locus of the electric field (convection) reversal [Heelis et al., 1980; Torbert et al., 1981], and the poleward extent of plasma sheet particle

precipitation [Winningham and Heikkila, 1974; Meng, 1981; Makita et al., 1988; Rich et al., 1990]. Although these boundaries may be located near one another, they often do not coincide and become especially difficult to interpret during times of northward Interplanetary Magnetic Field (IMF $B_z > 0$) when sun-aligned arcs, additional field-aligned current systems, and highly structured electric fields can extend over the entire high-latitude region [Burke et al., 1979, 1982; Iijima et al., 1984; Hardy, 1984; Zanetti et al., 1990].

Polar cap aurorae are observed in the polar cap during quiet magnetospheric times when the auroral oval is least active, (i.e., when the IMF B_z component is northward), and are predominantly aligned along the earth-sun line [e.g., Lassen and Danielsen, 1978; 1989]. A common type of polar cap aurora is created by precipitating electrons with average energies between 50 and 300 eV, resulting in weak (usually subvisual) multiple, F-layer arcs [Weber and Buchau, 1981; Hardy, 1984]. A less common type of polar cap aurora is one which stretches across the entire polar cap from noon to midnight, forming what appears from high altitude spacecraft as a 'theta' aurora [Frank et al., 1986; Nielsen et al., 1990]. Bright sun-aligned arcs are also often observed at the poleward

¹Department of Space Physics and Astronomy, Rice University, Houston, TX

²Phillips Laboratory, Hanscom AFB, Bedford, MA

³Southwest Research Institute, San Antonio, TX

⁴Danish Space Research Institute, Lyngby, Denmark

⁵Danish Meteorological Institute, Copenhagen, Denmark

⁶Naval Research Laboratory, Washington, DC

⁷Geophysical Institute, University of Alaska, Fairbanks, AK

boundary of a region of soft electron precipitation extending poleward from one or both edges of the auroral oval, resulting in a 'D' or 'teardrop' shaped polar cap, respectively [Murphree and Cogger, 1981; Elphinstone et al., 1990; Hones et al., 1989]. Recent attempts at mapping the open/closed field line boundary to the ionosphere as a function of IMF have had moderate success in reproducing the observed changes in polar cap shapes [Birn et al., 1991; Elphinstone et al., 1991; Toffoletto and Hill, 1990; 1992].

Like arcs in the auroral oval, polar cap aurorae are believed to be the optical signature of upward field-aligned currents where $\nabla \cdot \Sigma E < 0$ [Reiff et al., 1978; Lyons, 1980; Burke et al., 1982; Chiu and Gorney, 1983; Chiu, 1989; Valladares and Carlson, 1991]. On the dayside, the electrons carrying the majority of this upward current have either been interpreted as precipitating on closed field lines threading the LLBL [Lassen and Danielsen, 1989; Lundin et al., 1990] or on open field lines threading the plasma mantle [Newell et al., 1991]. At other local times, it has been suggested that weak, polar cap arcs result from the precipitation of accelerated polar rain electrons on open field lines [Hardy et al., 1982; Burke et al., 1982; Gussenhoven and Mullen, 1989], or from plasma sheet or low latitude boundary layer electrons on closed field lines [Meng, 1981; Murphree et al., 1982; Lundin and Evans, 1985; Lundin et al., 1990].

The Polar Acceleration Regions and Convection Study (Polar ARCS) was designed to provide the simultaneous convection and electrodynamic information needed to investigate the magnetospheric topology and generation mechanisms of high-latitude polar cap arcs. This paper summarizes the primary measurements and results of this study, which can be divided into two categories: large-scale phenomena, which lead to the examination of different models of polar cap morphology; and smaller-scale phenomena, which allow the investigation of the electrodynamic structure of the arcs. More detailed descriptions of the instruments, measurements, and results of Polar ARCS can be found in Weiss [1991].

2. EXPERIMENT DESCRIPTION

Polar ARCS consisted of a coordinated set of ground-based, airborne, and in situ measurements of high-latitude sun-aligned arcs over Sondrestrom, Greenland, on February 26, 1987. Three charges of barium were injected into the F-region ionosphere immediately prior to the launch of a Black Brant IX instrumented with a DC magnetometer, Langmuir and electric field probes, and an electron spectrometer. Simultaneous electron density and line-of-sight velocity measurements were made by the Sondrestrom Incoherent Scatter Radar, and all-sky images of auroral activity were recorded using the All-Sky Imaging Photometer (ASIP) aboard the Airborne Ionospheric Observatory (AIO).

Figure 1 (a) summarizes, in geographical coordinates, the relative orientations of a large, sun-aligned arc observed by the ASIP, the ground trajectories of two DMSP satellite passes occurring within 30 minutes of launch, and the position of the auroral oval (as inferred from the DMSP electron measurements

and ground-based all-sky images from Dye 2). The fields-of-view of the ASIP and the radar are denoted by the circular and semi-circular regions, respectively. The rocket's ground trajectory is shown as a straight line stretching from Sondrestrom to the northeast, and the three ionized barium tracks (resulting from rocket-borne releases just prior to launch of the instrumented rocket) are shown as irregular lines at the end of the rocket trajectory. The sun-aligned arc is oriented along a line 50° west of north, between the magnetic meridian (39° west of north) and the sun-aligned direction ($\sim 60^\circ$ west of north).

The 6300 Å ASIP images indicated the presence of diffuse, sun-aligned precipitation throughout the region over Sondrestrom between the sun-aligned arc and the auroral oval. The dawn - dusk F6 number flux spectrograms [Weiss, 1991] show a clearly defined region of enhanced electron and ion precipitation over the middle of the polar cap, indicative of the presence of a transpolar (theta) aurora [Frank et al., 1986] at the time of the pass; the theta aurora would appear just off the scale of Figure 1 (a), to the upper right. The theta aurora, auroral oval, and sun-aligned arc are shown in MLT/IL coordinates in Figure 1 (b).

The instrumented rocket was launched at 2349:10 UT (~ 22 MLT) to the northeast, reaching an apogee of 380 km and covering a ground range of 166 km. Shortly after launch, the nosecone portion of the rocket separated from the main payload in order to provide a magnetically clean environment for the DC science magnetometer aboard this separated section. Data were obtained from both payloads for nearly 600 seconds after launch. Electron precipitation measurements indicate that the rocket passed through three narrow (≤ 20 km) regions of low-energy (≤ 100 eV) electron precipitation. These events are interpreted as small-scale structures that lie within the region of weak, sun-aligned precipitation in the region between the auroral oval and the large sun-aligned arc in the all-sky images. Shortly after the decision to launch was made, the large arc began to fade from a pre-launch brightness of about 300 R (subvisual) to less than 100 R by 2358 UT. This type of weak, F-region sun-aligned arc is typical of those identified by Weber and Buchau [1981] as resulting from the structured precipitation of electrons with average energies of only a few hundred eV.

Although IMP-8 was in the magnetosheath at the time of the experiment (and thus no IMF measurements are available), the presence of sun-aligned arcs, the precipitation over the center of the polar cap, and the contracted state of the auroral oval (Figure 1 (b)) argue that the IMF B_z component was northward during this period. Moreover, the geomagnetic three-hourly average K_p index was 1 for the six hours prior to and three hours after the flight, confirming that the magnetosphere was in a very quiet state.

3. OBSERVATIONS

3.1. Large-scale measurements

The large-scale Polar ARCS measurements consist of the all-sky images, incoherent scatter radar measurements, DMSP

Polar ARCS

February 26, 1987

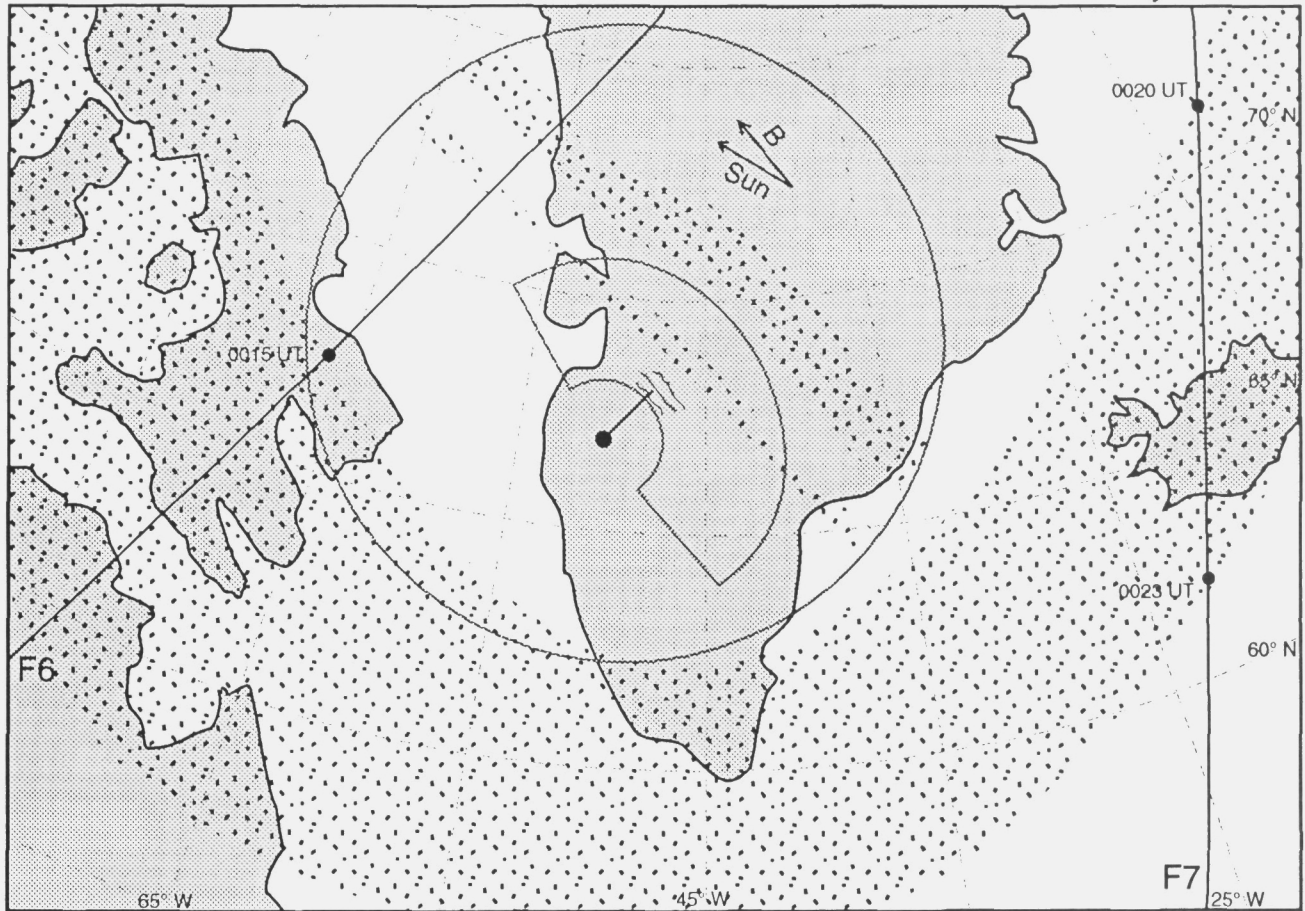


Fig. 1(a). A geographic diagram showing the location and orientation of the sun-aligned arc and auroral oval, and the spatial relationship between the different measurement regions. The large circle represents the ASIP field-of-view and the smaller partial circle is the radar field-of-view. The instrumented rocket track is denoted by the line stretching from Sondrestrom to the northeast. The motion of the three barium tracks are shown as irregular lines at the end of the rocket trajectory.

particle measurements, barium convection data, and DC convection electric field measurements. The all-sky images and DMSP overflight data are used to establish the scale and relative orientation of the sun-aligned arc and auroral oval, as shown in Figures 1 (a) and (b). The ionospheric convection signature in the region between the sun-aligned arc and the dusk-side auroral oval is inferred from the remaining independent measurements: the motion of the three barium jets, the radar l.o.s. velocities, and the rocket electric field data.

A detailed description of the barium release experiment is given by Mikkelsen [1987]. The horizontal motion of the three barium jets (projected along the field line to 100 km altitude) is shown in geographic coordinates in Figure 2. The rocket's ground trajectory, the three observation sites, and the rocket range east of the radar have also been noted. The horizontal drift speed and direction was determined by plotting the position of the three ionized jets (labeled with time

markers in minutes after 2300 UT) in planes perpendicular and parallel to the local magnetic meridian plane; the result was found to be an average plasma drift speed of 440 m/s in a direction 50° east of south (i.e., the antisunward direction).

The plasma convection between the precipitation events and the large sun-aligned arc is corroborated by the radar l.o.s. velocity measurements. Prior to and during the instrumented rocket flight, the Sondrestrom radar operated in a mode combining both azimuth and elevation scans, directly measuring the electron number density, line-of-sight (l.o.s.) plasma velocity, and ion and electron temperatures in the region northwest of the rocket trajectory (see Figure 1(a)). Figure 3 shows l.o.s. velocity measurements for two combined azimuth scans from 2333:07 - 2340:45 UT. The l.o.s. vectors indicate antisunward flow at approximately 500 m/s in a direction slightly east of the magnetic meridian, or about 50° east of south. Figures 4 (a) and (b) show electron number densities and l.o.s. velocities from an elevation scan from 2346:17 -

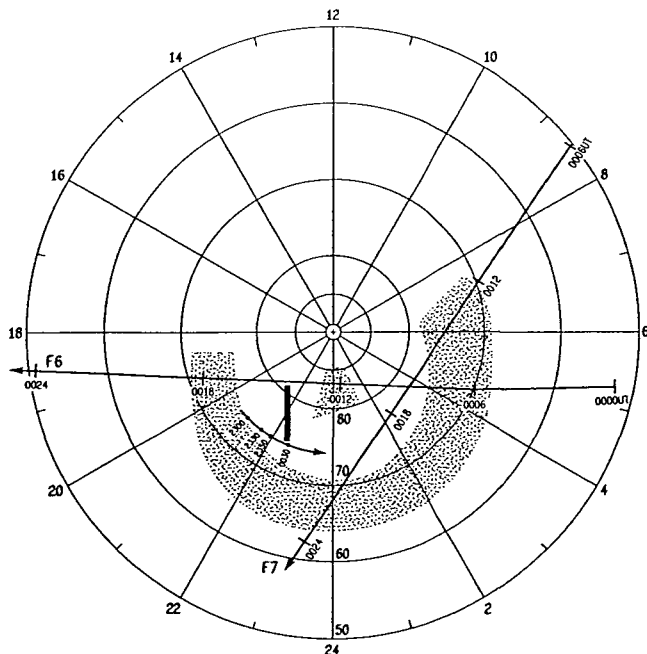


Fig. 1(b). The location of the sun-aligned arc (dark gray bar) and the tracks of the Sondrestrom ground station (from 2300 - 0030 UT) and DMSP F-6 and F-7 satellites in Magnetic Local Time / Invariant Latitude (MLT / IL) format. The observed portion of the transpolar arc and the auroral oval (as inferred from the DMSP spectrograms) are shown in light gray.

2349:11 UT in a plane perpendicular to the magnetic meridian. The region of enhanced density at a range of 600 km is associated with the large, sun-aligned arc seen in the ASIP images. Negligible l.o.s. velocity measurements indicate that the convection is either negligible or is nearly perpendicular to this plane, i.e. along the magnetic meridian. If the latter interpretation is true, the measurements agree with and extend the region of anti-sunward convection determined by the motion of the barium jets.

Finally, the rocket-borne electric field measurements indicate that the large-scale (convection) electric field in the region traversed by the rocket had an average westward component of 10 mV/m and average southward component of 12 mV/m, corresponding to plasma convection in a direction $\sim 50^\circ$ east of south at an average velocity of 300 m/s. Superposed on these large-scale components (not shown) are deviations occurring on time scales of 40 - 60 seconds associated with the precipitation events and small scale current structures traversed by the rocket (see Figures 5 and 6).

3.2. Smaller-scale measurements

The smaller scale data consist of measurements made by the electron spectrometer, electric field detector, magnetometer, and Langmuir probe during the instrumented rocket flight. Three electron precipitation events were detected during the flight by a tophat electrostatic analyzer [Sharber et al., 1988]. The events have the appearance of high latitude arcs but are

very narrow in extent, the widest being about 20 km. The precipitating energy flux profiles in the energy range 1.0 eV - 1.0 keV integrated over the downcoming hemisphere for the first two precipitation events are shown in the top panel of Figures 5 and 6. The events are very weak, with an average electron energy ≤ 100 eV and a maximum energy flux of 0.12 erg / cm² s. Since the third precipitation event was weaker yet, the electrodynamics study will be restricted to the first two events. The horizontal scale of Figures 5 and 6 corresponds to 22 km and 27 km, respectively.

During the course of the flight, measurements of the ambient electric and magnetic fields were made by a double-probe electric field detector and a three-axis fluxgate magnetometer

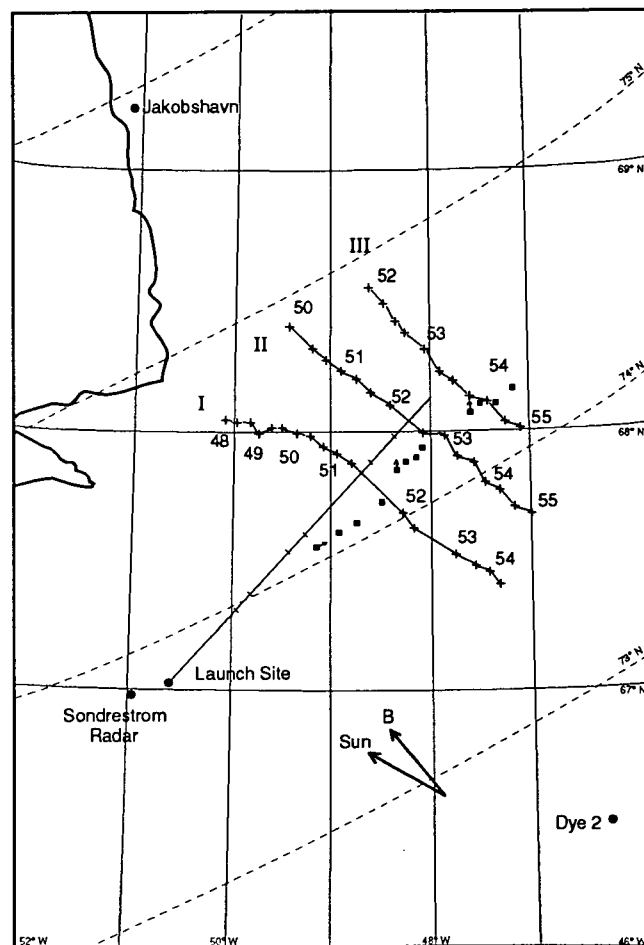


Fig. 2. The horizontal motion of the three barium jets plotted in geographic coordinates at a reference altitude of 100 km. Time markers along each trajectory are in minutes after 2300 UT. The tracks of the neutral barium / strontium clouds are indicated by squares and the firing directions of the three shaped charges are indicated by arrows. Note that the direction of magnetic north (azimuth of the line perpendicular to invariant latitude, -27°) differs from that of the magnetic meridian plane (azimuth of the plane passing through the local magnetic field line and local zenith, -39°)

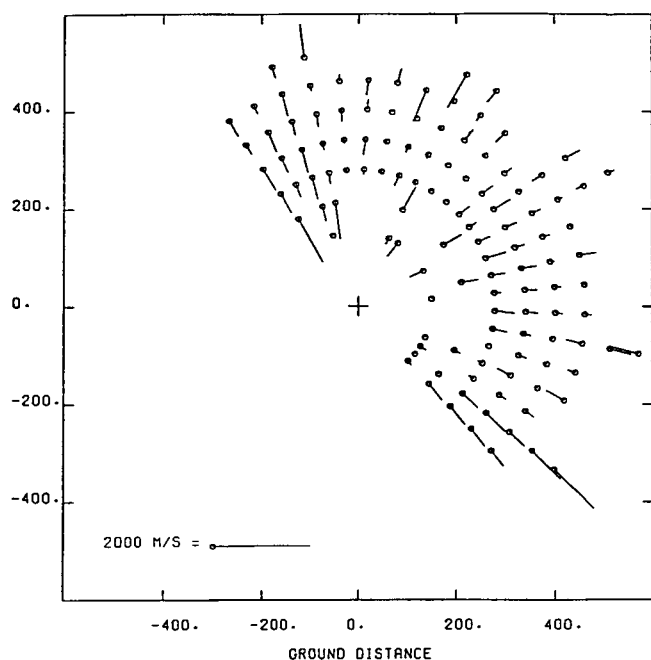


Fig. 3. Line-of-sight velocity measurements from two combined azimuth scans (at 35° elevation angle) from 2333:07 - 2340:45 UT. The sunward direction is $\sim 60^\circ$ west of north, which is at the top of the figure. Ground distances are in km.

[Primdahl, 1979]. After the appropriate data reduction, the perturbation electric and magnetic field components were rotated into a coordinate system in which x is perpendicular to the arc (positive eastwards), y is parallel to the arc (positive northward), and z is directed upward antiparallel to the magnetic field. The cross-arc electric field perturbation (δE_x) and arc-aligned magnetic field perturbation (δB_y) are shown in the second panel of Figures 5 and 6. Both sets of data have been smoothed to remove the spin period oscillation, and the average convection electric field (-15 mV/m) was subtracted from E_x for the purpose of highlighting the anticorrelation between E_x and δB_y (discussed in Section 4.2). The electric field data are consistent with arc-aligned ionospheric shear flows embedded in a region of anti-sunward convection. No significant cross-arc component of the flow (i.e., arc-aligned electric field) remained after the rotation.

The Langmuir probe measured the thermal electron density and temperature throughout the flight. No significant enhancement in electron density was detected in association with the precipitation events, a result consistent with the softness of the precipitation [e.g., Roble and Rees, 1977]. In contrast, significant increases in the electron temperature were observed in the precipitation regions due to the short time constant for heating the electron gas at F-layer altitudes. The average background Pedersen conductivity in the region traversed by the rocket was found to be 0.6 mho using the measured electron number density profile.

4. DISCUSSION

4.1. Morphology of the Polar Cap

The large-scale measurements presented in Section 3.1 are used in this section to explore the feasibility of four different models of polar cap morphology that have been used to explain the presence of weak sun-aligned arcs. These models are here called the 'open' [Hardy et al., 1982; Burke et al., 1982; Chiu, 1989; Gussenhoven and Mullen, 1989], 'bifurcated tail' [Frank et al., 1982; Kan and Burke, 1985; Frank and Craven, 1988; Toffoletto and Hill, 1990], 'expanded plasma sheet' [Meng, 1981; 1988; Murphree et al., 1982; Makita et al., 1991], and 'expanded low-latitude boundary layer (LLBL)' [Lundin and Evans, 1985; Lundin et al., 1990] models. A fifth model, which relies on the rotation of the tail x -line, is also introduced and discussed briefly [Reiff et al. 1992].

Figure 7 schematically summarizes these five different models. The left side of the figure shows distant ($x \geq 10 R_E$) cross-sections of the northern magnetotail lobe (y - z plane, looking from the distant tail sunward), while the right-hand column displays the corresponding topology of the high-latitude ionosphere, including the predicted ionospheric plasma flow (dotted lines). Regions of antisunward plasma

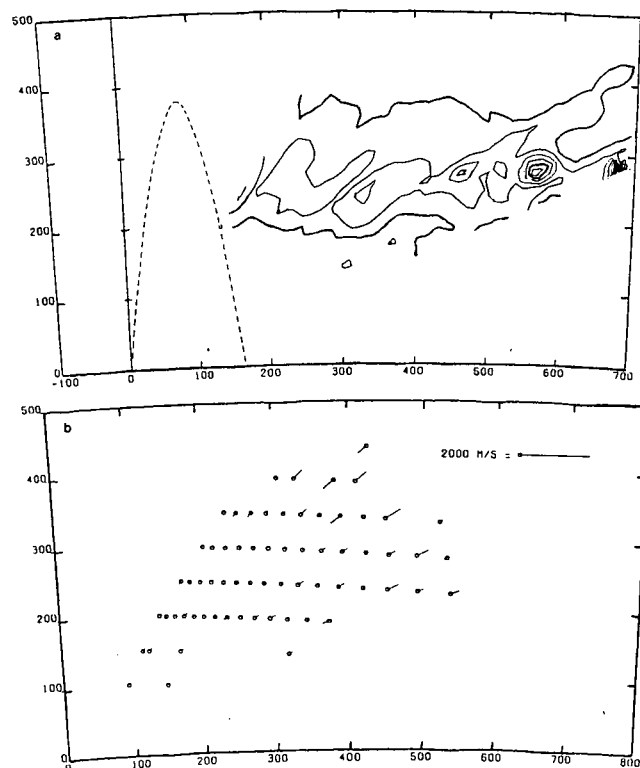


Fig. 4. (a) Electron number density and (b) line-of-sight velocity measurements from an elevation scan from 2346:17 - 2349:11 UT in a plane perpendicular to the magnetic meridian. The rocket's trajectory is shown in the top panel. The density contours are plotted in increments of 0.5×10^5 , reaching a peak density of 3.0×10^5 cm^{-3} .

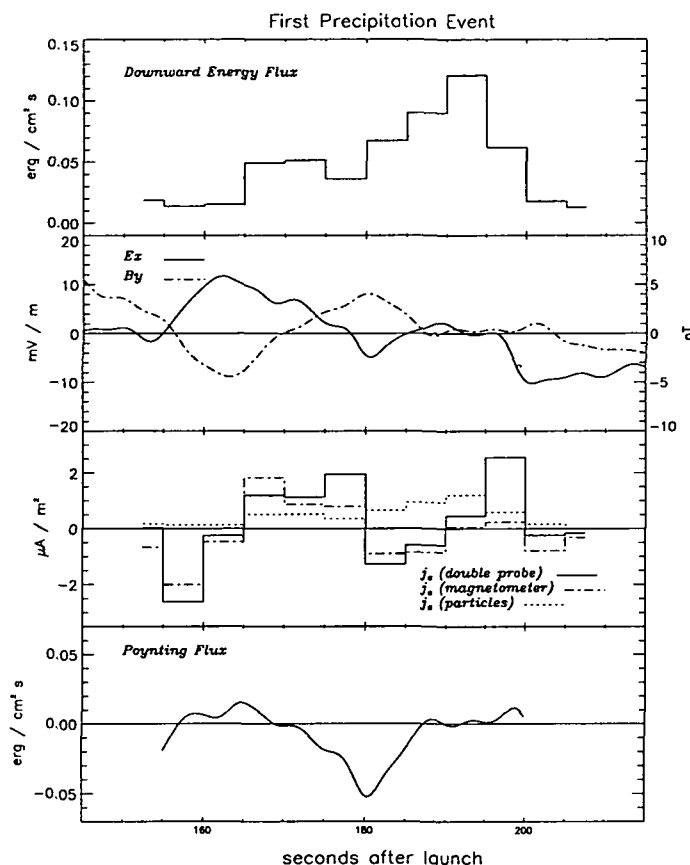


Fig. 5. Relationship between (a) particle precipitation, (b) cross-arc and parallel electric and magnetic field perturbations, δE_x and δB_y , (c) field-aligned current density, and (d) Poynting flux for the first precipitation event.

convection in the tail (LLBL and lobe) are labeled with circled dots, while regions of sunward convection (PSBL and plasma sheet) are denoted by circled crosses. In both the magnetotail and ionosphere, closed field line regions are shown in light gray (LLBL), medium gray (plasma sheet), or dark gray (PSBL), while open field line regions are shown in white. We have denoted the ionospheric projection of the PSBL as the boundary region separating open and closed field lines. Counter-streaming particle distributions and velocity dispersed ions, on the other hand, would only be observed in that portion of the PSBL in which there is a merging outflow. The (observed) sun-aligned arc is designated by the short solid line at ~ 22 MLT and the (inferred) theta aurora is shown as a solid line extending from noon to midnight across the polar cap.

Polar cap arcs have been argued to occur on open field lines on the basis of two types of observations: the measurement of electron spectra within polar cap arcs with the appearance of an accelerated polar rain (magnetosheath) distribution [Hardy et al., 1982; Burke et al., 1982] and, secondly, observations of sun-aligned arcs imbedded in regions containing simultaneous solar flare (> 100 keV) and polar rain electron precipi-

tation [Gussenhoven and Mullen, 1989]. If the Polar ARCS data are interpreted in terms of an open model, shown in Figure 7 (a), the weak, sun-aligned arc would map along open field lines to a position in the tail lobe denoted by the black dot. Antisunward convection of plasma along these open field lines maps directly to the polar ionosphere, where the arc is shown imbedded in a region of antisunward convection. Although the ionospheric convection in Figure 7 (a) has been depicted as a four-cell pattern with an extended region of sunward flow over the center of the polar cap (i.e., $B_y \approx 0$), alternate versions of the open model for northward IMF with a strong B_y component consist of three-cell convection patterns [Reiff and Burch, 1985; Chiu, 1985]. The (inferred) theta aurora is depicted at the central convection reversal of the dawn NBZ Birkeland current region [Reiff and Burch, 1985; Lyons, 1985; Zanetti et al., 1990].

In a bifurcated tail interpretation, Figure 7 (b), the sun-aligned arc also maps to the open tail lobe, but the transpolar aurora instead maps to a region of closed field lines extending upward from the central plasma sheet. The bifurcated tail model was originally developed to explain observations of

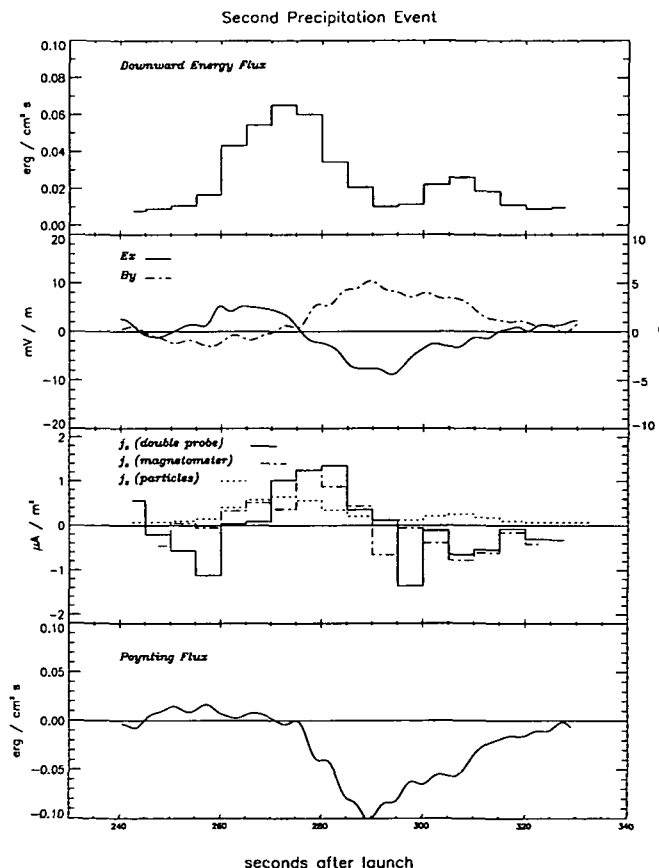


Fig. 6. Relationship between (a) particle precipitation, (b) cross-arc and parallel electric and magnetic field perturbations, δE_x and δB_y , (c) field-aligned current density, and (d) Poynting flux for the second precipitation event.

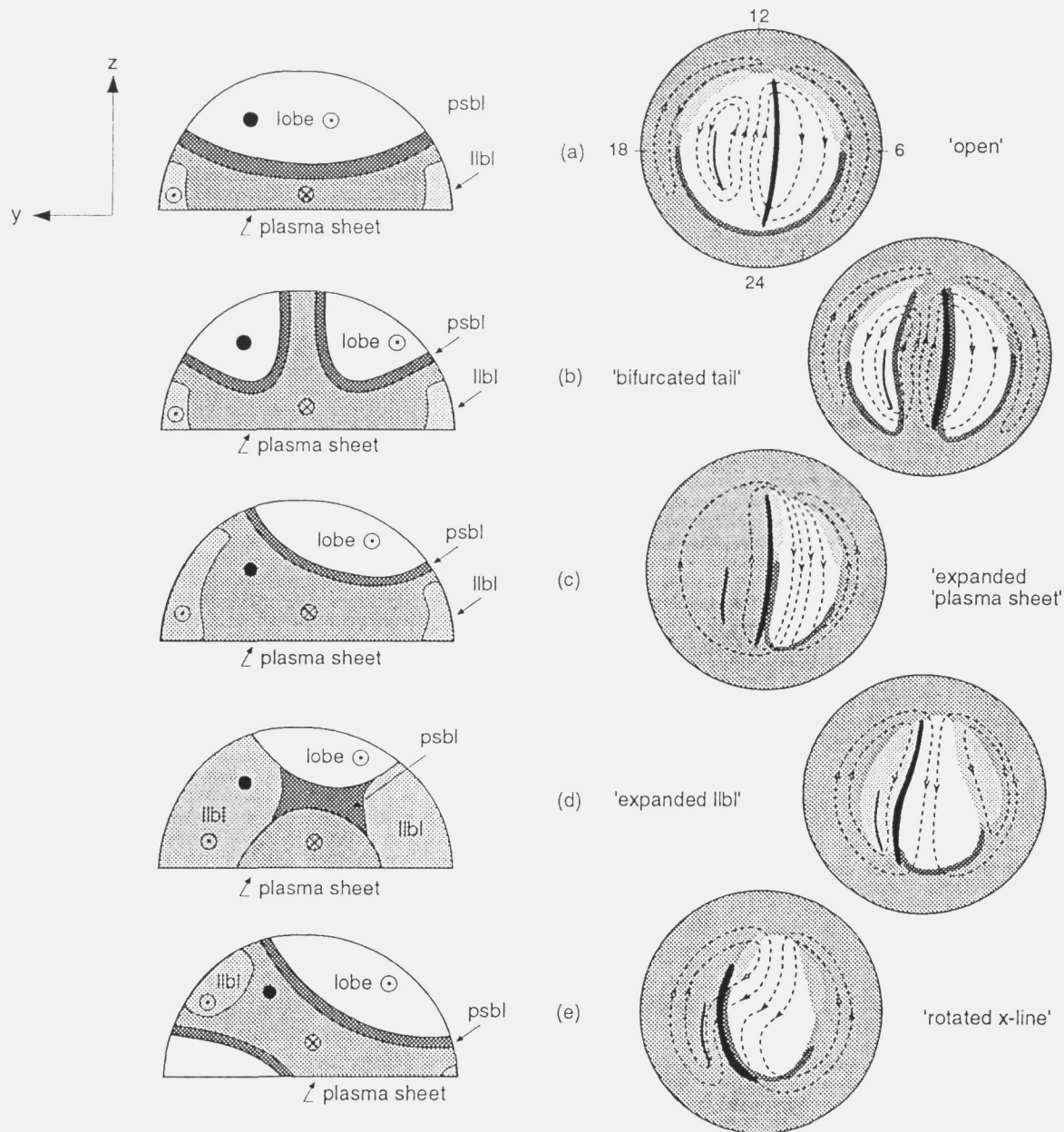


Fig. 7. Schematic diagram of the mapping of the high-latitude ionosphere to the distant magnetotail for the (a) 'open', (b) 'bifurcated tail', (c) 'expanded plasma sheet', (d) 'expanded LLBL', and (e) 'rotated x-line' models of polar cap morphology. A cross-section of the northern magnetotail lobe (y - z plane, looking from the tail sunward) is shown on the left, and the corresponding ionospheric convection pattern (dotted lines) and location of the sun-aligned and theta arc (solid lines), is shown on the right. Closed field line regions are shown in light gray (LLBL), medium gray (plasma sheet), and dark gray (PSBL), while open field line regions are shown in white. The solid dot in each figure on the left represents a field line threading the weak, sun-aligned arc at 22 MLT.

\sim keV ion precipitation and sunward plasma convection within arcs which appeared to be flanked by open field lines [e.g., Kan and Burke, 1985; Frank et al., 1988; Frank and Craven, 1988]. This model has been supported by magnetotail observations of plasma sheet protrusions into the lobe [Huang et al., 1987, 1989], and antiparallel merging models

suggesting a split dayside merging line [Crooker, 1979; Toffoletto and Hill, 1990]. In a bifurcated tail scenario, weak, sun-aligned arcs observed on either side of a theta aurora occur on open field lines.

Both the expanded plasma sheet model and the expanded LLBL model (Figures 7 (c) and (d), respectively) propose that

sun-aligned arcs occur on closed field lines threading a widened auroral oval. A closed field line source region of polar cap arcs has been supported by observations of trapped-particle signatures and the 'filled-in' nature of optical, electron, and ion measurements in the region between the average auroral oval and the polewardmost bright arc [Peterson and Shelley, 1984; Eliasson et al., 1987; Makita et al., 1991; Hones et al., 1989]. The difference between the expanded plasma sheet and LLBL models is really an issue of basic magnetospheric configuration; i.e., where the field lines in the widened auroral oval map to in the magnetosphere. In an expanded plasma sheet model, Figure 7 (c), the sun-aligned arc maps on closed field lines to an asymmetrically expanded plasma sheet in the tail. In the ionosphere, the region of open field lines is much smaller and shifted toward dawn to accommodate the expansion of the duskside oval; the theta aurora occurs at the poleward boundary of the expanded auroral oval, and the sun-aligned arc maps to the (sunward convecting) plasma sheet. This model was originally based on the continuous nature of simultaneous optical and electron precipitation measurements across the polar cap during quiet geomagnetic conditions [Meng, 1981, 1988; Murphree and Cogger, 1981; Murphree et al., 1982] and has been supported by observations of the poleward expansion of the soft (< 500 eV) electron precipitation region during northward IMF conditions [Makita et al., 1988; Rich et al., 1990].

In the expanded LLBL model, Figure 7 (d), the low-latitude boundary layer is significantly larger in the tail cross-section with the result that the sun-aligned arc field line maps to the antisunward convection region within the LLBL. The theta aurora, which maps to the boundary between open and closed field lines, is connected to the LLBL on the dayside and the plasma sheet boundary layer (PSBL) on the nightside [Lundin et al., 1990]. This model relies on an alternate view of solar wind - magnetosphere interaction in which the transfer of solar wind energy to the magnetosphere is primarily accomplished not through magnetic merging but through viscous interactions and actual mass transfer in the LLBL [Axford and Hines, 1961; Eastman et al., 1976; Sonnerup, 1980; Zhu and Kivelson, 1988; Stasiewicz, 1989]. Specifically, sun-aligned arcs map to polarization features resulting from finger-like injections of plasma into the LLBL [Lundin and Evans, 1985], which has been shown to widen during quiet times [Williams et al., 1985; Mitchell et al., 1987]. Vasyliunas [1979] argued that the LLBL should map to the ionosphere as a crescent shaped region near local noon; this projection would seem to be confirmed by studies of auroral oval-magnetosphere mapping using low-altitude particle measurements [e.g., Newell and Meng, 1992]. Studies using the Tsyganeko '87 and '89 magnetic field models have shown, however, that the ionospheric footprint of the LLBL (closed field lines near the dawn and dusk flanks of the magnetotail) may be significantly larger during quiet times, filling the region between a teardrop shaped polar cap and the auroral oval [Elphinstone et al., 1991; Birn et al., 1991].

The weak, sun-aligned arc system of February 27, 1987 can be examined in light of these models of polar cap arc forma-

tion using the convection information presented in Section 3.1. Though arguably limited in spatial extent, the barium motion, radar l.o.s. velocities, and rocket electric field measurements indicate an extended region (~400 - 500 km) of antisunward convection in the region between the large sun-aligned arc and the duskside auroral oval. Furthermore, the DMSP F-6 electron spectrogram shows an extended region of soft, sporadic electron precipitation poleward of the duskside auroral oval up to a magnetic latitude of ~82°, where strong electron and ion precipitation signatures have been identified as a theta aurora over the center of the polar cap. The sun-aligned arc identified by ASIP and the soft precipitation events encountered by the rocket lie within this precipitation zone (though further into the nightside than the DMSP pass). These observations may be accounted for by sun-aligned arc formation on closed field lines threading an expanded (antisunward convecting) LLBL, but are also consistent with a model in which they formed on open field lines on the dusk side of a bifurcated tail lobe (Figure 7 (b)). A model in which the polar cap is entirely open (Figure 7 (a)) appears to be ruled out, since it is inconsistent with the strong ion precipitation observed over the center of the polar cap (unless you invoke the Gussenhoven and Mullen [1989] scenario of an earthward-streaming lobe ion component). The antisunward convection signature appears least consistent with a model in which the polar cap arc field lines map to an expanded plasma sheet (Figure 7 (c)), since one would expect sunward convection in this region.

Although it would seem clear (from both modeling and magnetotail measurements) that the ionospheric footprint of the LLBL should expand during quiet times, it is still questionable whether arcs deep within the nightside polar cap can be magnetically connected to this source. We are beginning to explore a different model of polar cap arc formation, shown in Figure 7 (e), which accounts for sun-aligned arcs (as well as their IMF B_y dependence) at the poleward boundary of a closed field line region [Reiff et al., 1992]. In this model, a transpolar arc occurs as the result of the conductivity gradient across the ionospheric projection of the tail x-line, which is both sun-aligned and separated from the auroral oval for near-northward IMF B_z [Toffoletto and Hill, 1992]. In this skewed plasma sheet geometry, the region between the sun-aligned arc (open-closed boundary) and the auroral oval (convection reversal boundary) maps to very long, plasma sheet field lines recently reconnected through the rotated x-line. In this sense the model is topologically an 'expanded plasma sheet' model, with the significant difference that the region between the x-line and the auroral oval is still convecting antisunward in the polar cap. Flow irregularities of plasma sheet or ionospheric origin could account for the presence of weak sun-aligned arcs in this closed region.

4.2. Electrodynamic Structure

Figures 5 and 6 summarize the relationship between particle precipitation, cross-arc and parallel electric and magnetic field perturbations (δE_x and δB_y), field-aligned current density, and Poynting flux for the first and second precipitation events,

respectively. Note the high degree of anti-correlation between δB_y and δE_x in Figures 5 and 6. Smiddy et al. [1980] and Sugiura et al. [1982] have shown that anti-correlation between the perturbation magnetic field parallel to an infinite field-aligned current sheet and the cross-sheet component of the electric field results from a combination of current continuity, Ohm's law, and Ampere's law such that $\Delta E_x / \Delta \delta B_y = -(\mu_0 \Sigma_p)^{-1}$, where Σ_p , the height-integrated Pedersen conductivity, is assumed to be uniform over the interval Δx . This relationship has been demonstrated with electric and magnetic field data acquired by the DE, HILAT and VIKING satellites [Sugiura et al., 1982; Sugiura, 1984; Vickrey et al., 1986; Bythrow et al., 1984] and several rocket experiments [Primdahl and Marklund, 1986; Primdahl et al., 1987]. The Polar ARCS measurements extend those results, showing that the relationship holds for δB perturbations of magnitude ≤ 10 nT. Using the measured values of δB_y and E_x , the calculated height-integrated Pedersen conductivities in the two events fall between 0.4 - 0.5 mho. As one would expect for such weak events, these values of Σ_p are comparable (within experimental uncertainty) to the average background Pedersen conductivity (0.6 mho) calculated from the Langmuir probe number density profile.

The current density in each event, shown in the third panel of Figures 5 and 6, respectively, was calculated using three different measurements: (1) magnetic field perturbations in the arc coordinate system ($j_z = \partial B_y / \mu_0 \partial x$); (2) spatial variations in the cross-arc electric field and/or conductivity ($-j_z = \Sigma_p \partial E_x / \partial x + E_x \partial \Sigma_p / \partial x$); and (3) precipitating electron fluxes ($j_z = env_d$, where nv_d is the electron flux over the downcoming hemisphere). The first two calculations yield well-correlated, paired, upward and downward field-aligned currents of densities between 1-2 $\mu A / m^2$, with the upward currents associated with regions of $\nabla \cdot \mathbf{E} < 0$. The currents computed using the number flux measurements are upward throughout both events due to the fact that a significant portion of the downward current is carried by thermal electrons with energies less than 10 eV [Burch et al., 1983]; with the addition of an onboard noise source, low-energy upflowing electrons and thus downward current regions were undetectable [Weiss, 1991]. Magnetosphere-ionosphere coupling models have shown that locally-closed, paired, upward and downward field-aligned currents in polar cap arcs can result from either mesoscale velocity shear structures in the ionosphere [Chiu, 1989], or from multiply-bouncing Alfvén waves originating at mesoscale velocity shear structures in the magnetosphere [Zhu et al., 1993]. The latter model predicts a paired current structure scale size of tens of kilometers, with a spacing between arcs on the order of 50 km.

The energy flux into the ionosphere due to particle precipitation is plotted in the top panels of Figures 5 and 6 to show the relationship between particle precipitation and the field-aligned current density. One would normally expect the maximum particle energy flux to be coincident with an upward field-aligned current. In both events, however, the maximum energy flux is displaced by ~ 5 s from the region of peak upward current, a situation not observationally uncommon in auroral arcs [Lu et al., 1991]. This displacement may be explained by

either an asymmetric parallel potential drop or by mapping to a nonuniform density structure in the magnetosphere. A second form of energy input into the high-latitude ionosphere is through the Joule dissipation of electromagnetic energy. Kelley et al. [1991] have shown that a reliable measure of electromagnetic energy flux into the ionosphere is the vertical component of the Poynting flux, in this case, $P_z = E_x \delta B_y / \mu_0$, plotted in the bottom panels of Figures 5 and 6 in units of $erg / cm^2 \cdot s$. In both events the Poynting flux is downward, indicating a transfer of energy from the magnetosphere to the ionosphere. The maximum electromagnetic energy input is comparable to the kinetic input due to particle precipitation (but both are significantly smaller than the 1-10 $erg / cm^2 \cdot s$ typically observed in auroral oval arcs). Note also that the Poynting flux maximizes in the region between upward and downward currents (where the product of the quantities E_x and δB_y have their largest values), while the maximum energy flux due to electron precipitation is displaced toward the upward current region, a situation expected in a paired current sheet geometry.

5. SUMMARY AND CONCLUSIONS

Radar, optical, and in situ (rocket and satellite) data from the Polar ARCS campaign have been presented and used to analyze the electrodynamic structure of a weak, sun-aligned arc within the duskside polar cap as well as its relationship to large-scale magnetospheric boundaries. Electron precipitation measurements indicate that the rocket passed through three narrow (≤ 20 km) regions of low-energy (≤ 100 eV) electron precipitation. These events are interpreted as small-scale structures that lie within a region of weak, sun-aligned precipitation in the region between the auroral oval and the brightest sun-aligned arc in the all-sky images. DMSP F-6 measurements of enhanced ion and electron precipitation over the center of the polar cap further suggests the presence of a transpolar ('theta') aurora at this time.

The relationship between the high latitude ionosphere and the magnetosphere, especially the question of whether field lines on which polar cap arcs occur are open or closed, has been widely debated and remains one of the outstanding topics of magnetospheric physics today. In this paper we have used one aspect of the Polar ARCS measurements, namely the anti-sunward convection signature in the region between the sun-aligned arc and the dusk-side auroral oval, as a means of evaluating different models of polar cap arc formation. The observed convection (as determined by the radar l.o.s. velocity measurements, barium convection data, and electric field double probe measurements) is least consistent with a model in which the auroral field lines map to an expanded plasma sheet [Meng, 1981; Murphree et al., 1982], since one would expect sunward convection on these reconnected field lines. An exception to the expected sunward convection signature on plasma sheet field lines might arise if the polar cap arc maps to field lines recently reconnected through a highly skewed x-line [Reiff et al., 1992]; in this case, the ionospheric end of the field line may still be convecting antisunward even though it

is moving earthward in the plasma sheet. The antisunward convection signature is also consistent with a model in which the weak, sun-aligned arc system formed on open field lines on the dusk side of a bifurcated tail lobe [e.g., Kan and Burke, 1985; Frank and Craven, 1988; Toffoletto and Hill, 1990] or a model in which it formed on closed field lines threading the low-latitude boundary layer [Lundin and Evans, 1985; Lundin et al. 1990]. In the latter case, however, we note that while the teardrop shape of the quiet-time auroral oval can be accounted for by the expansion of the LLBL away from the dayside cleft, it seems unlikely that arcs deep within the nightside polar cap can be topologically attributed to this source. To date, the authors are unaware of an extended (statistical) study of ionospheric convection in the region between sun-aligned arcs and the nearby auroral oval using satellite data. As demonstrated in this paper, such a study may help evaluate competing models of polar cap arc formation and thus determine the source region(s) of these arcs.

Very weak but highly correlated electric and magnetic field perturbations made aboard the Polar ARCS instrumented rocket indicate that the weak, F-layer precipitation events crossed by the rocket are associated with small-scale, paired, field-aligned current sheets. The correlation of δB_y and E_x imply uniform Σ_p and provides a measure of that quantity, in this case $\sim 0.4 - 0.5$ mho, values consistent with that calculated from the Langmuir probe measurements. The current density in each event was calculated using the magnetic field (Ampere's Law), electric field (current divergence plus Ohm's law), and particle precipitation measurements, yielding well correlated field-aligned currents of densities between $1-2 \mu A/m^2$. The upward and downward current regions can be associated with velocity shears (higher and lower speed streams) embedded in a region of anti-sunward flow. Such mesoscale shear flows in association with polar cap arcs have been confirmed by many observations [Carlson et al., 1984; Hoffman et al., 1985; Mende et al., 1988; Weber et al., 1989 Valladares and Carlson, 1991]. These velocity shears appear to be of magnetospheric origin since the Poynting flux is predominately downward in the vicinity of the arcs. If the weak, sun-aligned arcs formed on open field lines in a bifurcated tail geometry, the velocity shears map to regions of the magnetosheath where nonuniform flow may be easily accounted for. If the arcs map to the LLBL, the velocity shears may result from finger-like injections of magnetosheath plasma onto closed LLBL field lines, or, if they map to a highly skewed plasma sheet, the velocity shears may originate as bursty flows in the tail. In all cases, the visual emissions are produced in the upward current regions by precipitating electrons carrying the outgoing current from the electric field divergence.

Acknowledgments. The authors would like to acknowledge the Danish Commission for Scientific Research in Greenland for permission to conduct the Polar ARCS experiments. We also thank Jim Vickrey of SRI, Bob Robinson of LPARL, Rudy Frahm of SwRI, and the two referees for their help in improving and evaluating this paper. Information critical to the analysis of the magnetometer and electron spectrometer data was supplied by Poul Jensen, Carl Bargainer, John Scherrer, and Nick Eaker of SwRI. We thank DuWayne Bostow of the

Geophysical Institute for managing the high explosive shaped charges and machining the barium metal cones, and Gale Weeding of the Denver Research Institute for fabricating the high explosive Octol charges. We would also like to thank the personnel of NASA Wallops Flight Facility, and in particular Jay Brown, the payload manager for payload fabrication and launch support. This research was supported at Southwest Research Institute under Phillips Laboratory grant AFOSR-87-0203, at Rice University by NASA under grant NAGW 1655 and by the National Science Foundation under grant ATM-91-03440, at Phillips Laboratory by AFOSR task 2310G9, and at the University of Alaska at Fairbanks by NASA under grant NAG6-1.

REFERENCES

- Axford, W. I., and C. O. Hines, A unifying theory of high-latitude geophysical phenomena and geomagnetic storms, *Can. J. Phys.*, **39**, 1433, 1961.
- Birn, J., E. W. Hones, Jr., J. D. Craven, L. A. Frank, R. D. Elphinstone, and D. P. Stern, On open and closed field line regions in Tsyganenko's field model and their possible associations with horse collar auroras, *J. Geophys. Res.*, **96**, 3811, 1991.
- Burch, J. L., P. H. Reiff, M. Sugiura, Upward electron beams measured by DE-1: A primary source of dayside region-1 Birkeland currents, *Geophys. Res. Lett.*, **10**, 753, 1983.
- Burke, W. J., M. C. Kelley, R. C. Sagalyn, M. Smiddy, and S. T. Lai, Polar cap electric field structures with a northward interplanetary magnetic field, *Geophys. Res. Lett.*, **6**, 21, 1979.
- Burke, W. J., M. S. Gussenhoven, M. C. Kelley, D. A. Hardy, and F. J. Rich, Electric and magnetic field characteristics and discrete arcs in the polar cap, *J. Geophys. Res.*, **87**, 2431, 1982.
- Bythrow, P. F., T. A. Potemra, W. B. Hanson, L. J. Zanetti, C.-I. Meng, R. E. Huffman, F. J. Rich, and D. A. Hardy, Earthward directed high-density Birkeland currents observed by HILAT, *J. Geophys. Res.*, **89**, 9114, 1984.
- Carlson, H. C., V. B. Wickwar, E. J. Weber, J. Buchau, J. G. Moore, and W. Whiting, Plasma characteristics of polar-cap F-layer arcs, *Geophys. Res. Lett.*, **9**, 895, 1984.
- Chiu, Y. T., Formation of polar cap arcs, *Geophys. Res. Lett.*, **16**, 125, 1989.
- Chiu, Y. T., and D. J. Gorney, Eddy intrusion of hot plasma into the polar cap and formation of polar cap arcs, *J. Geophys. Res.*, **85**, 543, 1980.
- Chiu, Y. T., and D. J. Gorney, Eddy intrusion of hot plasma into the polar cap and formation of polar cap arcs, *Geophys. Res. Lett.*, **10**, 463, 1983.
- Chiu, Y. T., N. U. Crooker, and D. J. Gorney, Model of oval and polar cap arc configurations, *J. Geophys. Res.*, **90**, 5153, 1985.
- Eastman, T. E., E. W. Hones, Jr., S. J. Bame, and J. R. Asbridge, The magnetospheric boundary layer: site of plasma, momentum and energy transfer from the magnetosheath into the magnetosphere, *Geophys. Res. Lett.*, **3**, 685, 1976.
- Eliasson, L., R. Lundin, and J. S. Murphree, Polar cap arcs observed by the Viking satellite, *Geophys. Res. Lett.*, **14**, 451, 1987.
- Elphinstone, R. D., K. Jankowska, J. S. Murphree, and L. L. Cogger, The configuration of the auroral distribution for interplanetary magnetic field B_z northward: 1. IMF B_x and B_y dependencies as observed by the Viking satellite, *J. Geophys. Res.*, **95**, 5791, 1990.
- Elphinstone, R. D., D. Hearn, J. S. Murphree, and L. L. Cogger, Mapping using the Tsyganenko long magnetospheric model and its relationship to Viking Auroral Images, *J. Geophys. Res.*, **96**, 1467, 1991.
- Frank, L. A., J. D. Craven, J. L. Burch, and J. D. Winningham, Polar views of the Earth's aurora with Dynamics Explorer, *Geophys. Res. Lett.*, **9**, 1001, 1982.
- Frank, L. A., J. D. Craven, D. A. Gurnett, S. D. Shawhan, D. R. Weimer, J. L. Burch, J. D. Winningham, C. R. Chappell, J. H. Waite, R. A. Heelis, N. C. Maynard, M. Sugiura, W. K. Peterson, and E. G. Shelley, The theta aurora, *J. Geophys. Res.*, **91**, 3177, 1986.
- Frank, L. A., and J. D. Craven, Imaging results from Dynamics Explorer 1, *Rev. Geophys.*, **26**, 249, 1988.

- Gussenhoven, M. S., and E. G. Mullen, Simultaneous relativistic electron and auroral particle access to the polar caps during interplanetary magnetic field B_z northward: A scenario for an open field line source of auroral particles, *J. Geophys. Res.*, **94**, 17,121, 1989.
- Hardy, D. A., W. J. Burke, and M. S. Gussenhoven, DMSP optical and electron measurements in the vicinity of polar cap arcs, *J. Geophys. Res.*, **87**, 2413, 1982.
- Hardy, D. A., Intense fluxes of low-energy electrons at geomagnetic latitudes above 85° , *J. Geophys. Res.*, **89**, 3883, 1984.
- Heelis, R. A., J. D. Winningham, W. B. Hanson, and J. L. Burch, The relationships between high-latitude convection reversals and the energetic particle morphology observed by Atmospheric Explorer, *J. Geophys. Res.*, **85**, 3315, 1980.
- Hoffman, R. A., R. A. Heelis, and J. S. Prasad, A sun-aligned arc observed by DMSP and AE-C, *J. Geophys. Res.*, **90**, 9697, 1985.
- Hones, E. W., Jr., J. D. Craven, L. A. Frank, D. S. Evans, and P. T. Newell, The horse-collar aurora: A frequent pattern of the aurora in quiet times, *Geophys. Res. Lett.*, **16**, 37, 1989.
- Huang, C. Y., L. A. Frank, W. K. Peterson, D. J. Williams, W. Lennartsson, D. G. Mitchell, R. C. Elphic, and C. T. Russell, Filamentary structures in the magnetotail lobes, *J. Geophys. Res.*, **92**, 2349, 1987.
- Huang, C. Y., L. A. Frank, J. D. Craven, Simultaneous observations of a theta aurora and associated magnetotail plasmas, *J. Geophys. Res.*, **94**, 10137, 1989.
- Iijima, T., T. A. Potemra, L. J. Zanetti, and P. F. Bythrow, Large-scale Birkeland in the dayside polar region during strongly northward IMF: A new Birkeland current system, *J. Geophys. Res.*, **89**, 7441, 1984.
- Kan, J. R., and W. J. Burke, A theoretical model of polar cap auroral arcs, *J. Geophys. Res.*, **90**, 4171, 1985.
- Kelley, M. C., D. J. Knudsen, and J. F. Vickrey, Poynting flux measurements on a satellite: a diagnostic tool for space research, *J. Geophys. Res.*, **96**, 201, 1991.
- Lassen, K., and C. Danielsen, Quiet time pattern of auroral arcs for different directions of the interplanetary magnetic field in the Y-Z plane, *J. Geophys. Res.*, **83**, 5277, 1978.
- Lassen, K., and C. Danielsen, Distribution of auroral arcs during quiet geomagnetic conditions, *J. Geophys. Res.*, **94**, 2587, 1989.
- Lu, G., P. H. Reiff, J. L. Burch, and J. D. Winningham, On the auroral current-voltage relationship, *J. Geophys. Res.*, **96**, 3523, 1991.
- Lundin, R., and D. S. Evans, Boundary layer plasmas as a source for high-latitude, early afternoon, auroral arcs, *Planet. Space Sci.*, **32**, 1389, 1985.
- Lundin, R., L. Eliasson, J. S. Murphree, The quiet-time aurora and the magnetosphere configuration, in *Auroral Physics*, ed. C.-I. Meng, M. J. Rycroft, and L. A. Frank, p.159, Cambridge University Press, Cambridge, U.K., 1990.
- Lyons, L. R., Generation of large-scale regions of auroral currents, electric potentials, and precipitation by the divergence of the convection electric field, *J. Geophys. Res.*, **85**, 17, 1980.
- Makita, K., C.-I. Meng, and S.-I. Akasofu, Latitudinal electron precipitation patterns during large and small IMF magnitudes for northward IMF conditions, *J. Geophys. Res.*, **93**, 97, 1988.
- Makita, K., C.-I. Meng, and S.-I. Akasofu, Transpolar auroras, their particle precipitation and IMF B_y component, *J. Geophys. Res.*, **96**, 14085, 1991.
- Mende, S. B., J. H. Doolittle, R. M. Robinson, R. R. Vondrak, and F. J. Rich, Plasma drifts associated with a system of sun-aligned arcs in the polar cap, *J. Geophys. Res.*, **93**, 256, 1988.
- Meng, C.-I., Polar cap arcs and the plasma sheet, *Geophys. Res. Lett.*, **8**, 273, 1981.
- Meng, C.-I., Auroral oval configuration during the quiet condition, in *Electromagnetic Coupling in the Polar Clefts and Caps*, ed. R. E. Sandholt and A. Egeland, p.61, Kluwer Academic Publishers, Dordrecht, Netherlands, 1988.
- Mikkelsen, I. S., Drift of the Ba-jets released over Greenland on February 26 and March 5, 1987, *Progress Report for Grant AFOSR-87-0203*, Danish Meteorological Institute, Copenhagen, Denmark, 1987.
- Mitchell, D. G., F. Kutchko, D. J. Williams, T. E. Eastman, L. A. Frank, and C. T. Russell, An extended study of the low-latitude boundary layer on the dawn and dusk flanks of the magnetosphere, *J. Geophys. Res.*, **92**, 7394, 1987.
- Murphree, J. S., and L. L. Cogger, Observed connections between apparent polar cap features and the instantaneous diffuse auroral oval, *Planet. Space Sci.*, **29**, 1143, 1981.
- Murphree, J. S., C. D. Anger, and L. L. Cogger, The instantaneous relationship between polar cap and oval auroras at times of northern interplanetary magnetic field, *Can. J. Phys.*, **60**, 349, 1982.
- Newell, P. T., W. J. Burke, C.-I. Meng, E. R. Sanchez, and M. E. Greenspan, Identification and observations of the plasma mantle at low altitude, *J. Geophys. Res.*, **96**, 35, 1991.
- Newell, P. T., and C.-I. Meng, Mapping the dayside ionosphere to the magnetosphere according to particle precipitation characteristics, *Geophys. Res. Lett.*, **19**, 609, 1992.
- Nielsen, E., J. D. Craven, L. A. Frank, and R. A. Heelis, Ionospheric flows associated with a transpolar arc, *J. Geophys. Res.*, **95**, 21169, 1990.
- Peterson, W. K., and E. G. Shelley, Origin of the plasma in a cross-polar cap auroral feature (theta aurora), *J. Geophys. Res.*, **89**, 6729, 1984.
- Primdahl, F., The fluxgate magnetometer, *J. Phys. E: Sci. Instrum.*, **12**, 241, 1979.
- Primdahl, F. and G. Marklund, Birkeland currents correlated with direct-current electric fields observed during the CEN TAUR Black Brant X rocket experiment, *Can. J. Phys.*, **64**, 1412, 1986.
- Primdahl, F., G. Marklund, and I. Sandahl, Rocket observations of E-B field correlations showing up- and down-going Poynting flux during an auroral breakup event, *Planet. Space Sci.*, **35**, 1287, 1987.
- Reiff, P. H., J. L. Burch, and R. A. Heelis, Dayside auroral arcs and convection, *Geophys. Res. Lett.*, **5**, 391, 1978.
- Reiff, P. H. and J. L. Burch, IMF By-dependent plasma flow and Birkeland currents in the dayside magnetosphere 2. A global model for northward and southward IMF, *J. Geophys. Res.*, **90**, 1595, 1985.
- Reiff, P. H., F. R. Toffoletto, L. A. Weiss, and J. S. Murphree, A new model of polar cap convection and auroral arcs during northward IMF, *EOS, Transactions*, **73**, p.466, 1992.
- Rich, F. J., D. A. Hardy, R. H. Redus, and M. S. Gussenhoven, Northward IMF and patterns of high-latitude precipitation and field-aligned currents: The February 1986 Storm, *J. Geophys. Res.*, **95**, 9893, 1990.
- Roble, R. G., and M. H. Rees, Time-dependent studies of the aurora: effects of particle precipitation on the dynamic morphology of ionospheric and atmospheric properties, *Planet. Space Sci.*, **25**, 991, 1977.
- Sharber, J. R., J. D. Winningham, J. R. Scherrer, M. J. Sablik, C. A. Bargainer, P. A. Jensen, B. J. Mask, and N. Eaker, Angle resolving energy analyzer (AREA): A versatile "top-hat" instrument for space plasma measurement, *IEEE Transactions on Geosciences and Remote Sensing*, **474**, 1988.
- Smiddy, M., W. J. Burke, M. C. Kelley, N. A. Safflekos, M. S. Gussenhoven, D. A. Hardy, and F. J. Rich, Effects of high-latitude conductivity on observed convection electric fields and Birkeland currents, *J. Geophys. Res.*, **85**, 6811, 1980.
- Sonnerup, B. U. O., Theory of the low-latitude boundary layer, *J. Geophys. Res.*, **85**, 2017, 1980.
- Stasiewicz, K., A fluid finite ion larmor radius model of the magnetopause layer, *J. Geophys. Res.*, **94**, 8827, 1989.
- Sugiura, M., N. C. Maynard, W. H. Farthing, J. P. Heppner, and B. G. Ledley, Initial results on the correlation between the magnetic and electric fields observed from the DE-2 satellite in the field-aligned current regions, *Geophys. Res. Lett.*, **9**, 985, 1982.
- Sugiura, M., A fundamental magnetosphere-ionosphere coupling mode involving field-aligned currents as deduced from DE-2 observations, *Geophys. Res. Lett.*, **11**, 877, 1984.
- Toffoletto, F. R., and T. W. Hill, Magnetic field configuration of the theta aurora, *Geophys. Res. Lett.*, **17**, 595, 1990.
- Toffoletto, F. R., and T. W. Hill, A non-singular model of the open magnetosphere, accepted for publication, *J. Geophys. Res.*, Sept., 1992.

- Torbert, R. B., C. A. Cattell, F. S. Mozer, and C.-I. Meng, The boundary of the polar cap and its relation to electric fields, field-aligned currents, and auroral particle precipitation, in *Physics of Auroral Arc Formation, Geophys. Monogr. Ser.*, vol. 25, edited by S.-I. Akasofu and J. R. Kan, p.143, Washington D.C., AGU, 1981.
- Valladares, C. E., and H. C. Carlson, Jr., The electrodynamic, thermal, and energetic character of intense sun-aligned arcs in the polar cap, *J. Geophys. Res.*, 96, 1379, 1991.
- Vasyliunas, V. M., Interaction between the magnetospheric boundary layers and the ionosphere, in *Proceedings of Magnetospheric Boundary Layers Conference*, ESA SP-148, p.387, 1979.
- Vickrey, J. F., R. C. Livingston, N. B. Walker, T. A. Potemra, R. A. Heelis, M. C. Kelley, and F. J. Rich, On the current-voltage relationship on the magnetospheric generator at intermediate spatial scales, *Geophys. Res. Lett.*, 13, 495, 1986.
- Weber, E. J., and J. Buchau, Polar cap F layer auroras, *Geophys. Res. Lett.*, 8, 125, 1981.
- Weber, E. J., M. C. Kelley, J. O. Ballenthin, S. Basu, H. C. Carlson, J. R. Fleischman, D. A. Hardy, N. C. Maynard, R. F. Pfaff, P. Rodriguez, R. E. Sheehan, and M. Smiddy, Rocket measurements within a polar cap arc: Plasma, particle, and electric field circuit parameters, *J. Geophys. Res.*, 94, 6692, 1989.
- Weiss, L. A., A study of high-latitude auroral arcs using radar, optical, and *in situ* techniques, *Ph.D. Thesis*, Rice University, Houston, TX, October, 1991.
- Williams, D. J., D. G. Mitchell, T. E. Eastman, and L. A. Frank, Energetic particle observations in the low-latitude boundary layer, *J. Geophys. Res.*, 90, 5097, 1985.
- Winningham, J. D., and W. J. Heikkila, Polar cap auroral electron fluxes observed with ISIS 1, *J. Geophys. Res.*, 79, 949, 1974.
- Zanetti, T. A. Potemra, R. E. Erlandson, F. F. Bythrow, B. J. Anderson, J. S. Murphree, and G. T. Marklund, Polar region Birkeland current, convection, and aurora for northward interplanetary magnetic field, *J. Geophys. Res.*, 95, 5825, 1990.
- Zhu, L., J. J. Sojka, R. W. Schunk, and D. J. Crain, A time-dependent model of polar cap arcs, in press, *J. Geophys. Res.*, 1993.
- Zhu, X., and M. G. Kivelson, Analytic formulation and quantitative solutions of the coupled ULF wave problem, *J. Geophys. Res.*, 93, 8602, 1988.